

NOVEL SYNTHESIS AND CHARACTERIZATION OF SUPPORTED BIMETALLIC FILMS FOR HYDROGEN DETECTION

by

Keren Valentín-Esteves

A thesis submitted in partial fulfillment of the requirements for the degree of

MASTER OF SCIENCE
in
CHEMICAL ENGINEERING

UNIVERSITY OF PUERTO RICO
MAYAGÜEZ CAMPUS
2014

Approved by:

María M. Martínez-Iñesta, Ph.D.
President, Graduate Committee

Date

David Suleiman-Rosado, Ph.D.
Member, Graduate Committee

Date

Arturo J. Hernández-Maldonado, Ph.D.
Member, Graduate Committee

Date

Enrique Meléndez, Ph.D.
Graduate School Representative

Date

Aldo Acevedo-Rullán, Ph.D.
Chairperson of the Department

Date

COPYRIGHT © 2014

Keren Valentín-Esteves, MS Thesis, UPRM. All rights reserved

ABSTRACT

Continuous increase in energy demand and high levels of pollution generated by the existing energy sources have led researchers to explore other clean and renewable alternatives. Hydrogen gas (H_2) is an option that has been implemented in some parts of the country but there are still some challenges in its worldwide implementation. Hydrogen has a low explosion limit of 4% v/v (H_2 /air) at atmospheric pressure, high diffusivity and low liquefaction point. These characteristics demand small, sensitive, selective, economic and reliable gas sensors that can detect accurately and precisely H_2 gas at different concentrations. Palladium (Pd) has a high sensitivity and selectivity towards hydrogen that is used in resistance based sensors. However, pure Pd undergoes large internal stresses when it goes through α to β phase transition that significantly affect its response deeming necessary the design of more reliable materials as hydrogen sensors.

The approach of this work was to synthesize Pd_{90}/Ag_{10} , Pd_{90}/Pt_{10} , Pd_{90}/Ni_{10} and Pd_{90}/Cr_{10} bimetallic materials using a modified Solid State Reduction method (SSR) method developed in our laboratory to delay the α to β phase transition to higher concentrations. The crystalline phase, the films' morphology, metal distribution, and the metals' oxidation state were characterized by X-ray Diffraction (XRD), Scanning Electron Microscopy (SEM), Energy Dispersive X-Ray Spectroscopy (EDS) and X-Ray Photoelectron Spectroscopy (XPS), respectively. Results of the Pd_{90}/Ag_{10} films suggest an alloy type interaction between the two metals. Results also show that the Pd_{90}/Ni_{10} films were not formed presumably because the hydrated salts used as precursors

can't be reduced by our synthesis method and because Ni has a negative standard reduction potential. Pd₉₀/Cr₁₀ films were presumably not formed for the same reasons as Pd₉₀/Ni₁₀.

Sensing results show that Pd₉₀/Ag₁₀ and Pd₉₀/Pt₁₀ bimetallic materials can detect H₂ with precision. Pd₉₀/Pt₁₀ delayed the α to β phase transition to 1.5% v/v and could detect at least 10% v/v H₂/N₂ before failure. Pd₉₀/Ag₁₀ did not delay the phase transition but could detect up to 4% v/v H₂/N₂. Results suggest that the bimetallic materials have an alloy interaction which constricts the structure expansion thus reducing the mechanical stresses during the phase transition. The results of both samples also showed that the sensitivity normalized by the response time (S/t_r) have two linear relationships with $[H_2]^{1/2}$, before and after the phase transition. The mentioned relation allows the implementation of our bimetallic films as sensing materials for H₂ detection.

In conclusion, the modified SSR yielded bimetallic films that can sense hydrogen, but it is limited to the use of anhydrous salts as precursors and the use of metals with a positive standard reduction potential such as Pd, Pt and Ag.

RESUMEN

El crecimiento continuo en la demanda energética y los altos niveles de contaminación causados por las fuentes de energía actuales han llevado a los investigadores a explorar otras alternativas más limpias y renovables. El gas de hidrógeno (H_2) es una opción que actualmente se está implementando en algunas partes de los Estados Unidos, pero aún existen algunos retos con su implementación a nivel global. El hidrógeno tiene un bajo límite de explosión de 4% v/v (H_2 /aire), a presión atmosférica, alta difusividad y bajo punto de licuefacción. Estas características demandan el uso de sensores pequeños, sensitivos, selectivos, económicos y seguros, para detectar, con alta precisión y exactitud, diferentes concentraciones del gas de H_2 . Paladio (Pd) tiene una alta sensibilidad y selectividad al hidrógeno las cuales son utilizadas en sensores basados en resistividad. Sin embargo, Pd puro sufre considerable estrés interno cuando pasa a través de la transición de fase α a β , el cual afecta significativamente su respuesta generando la necesidad de diseñar materiales más seguros como sensores de hidrógenos.

El enfoque de esta investigación era sintetizar materiales bimetálicos de Pd_{90}/Ag_{10} , Pd_{90}/Pt_{10} , Pd_{90}/Ni_{10} y Pd_{90}/Cr_{10} usando una modificación del método de Reducción en Estado Sólido (RES) desarrollado en nuestro laboratorio para retrasar la transición de fase de α a β a concentraciones mayores. La fase cristalina, morfología de las películas, distribución y estado de oxidación de los metales fueron caracterizadas por Difracción de Rayos-X (XRD, en inglés), Microscopía Electrónica de Barrido (SEM, en inglés), Espectroscopía de Rayos-X por Dispersión de Luz (EDS, en inglés), y Espectroscopía de Fotoelectrones de Rayos-X (XPS, en inglés). Resultados obtenidos con películas de Pd_{90}/Ag_{10} sugieren una interacción de tipo de

aleación entre los dos metales. Los resultados también muestran que las películas de Pd₉₀/Ni₁₀ films no se formaron probablemente porque la sal hidratada usada no se pudo reducir usando nuestro método de síntesis porque Ni tiene un potencial estándar de reducción negativo. Las películas de Pd₉₀/Cr₁₀ probablemente tampoco se formaron por las mismas razones de Pd₉₀/Ni₁₀.

Los resultados de detección muestran que los materiales bimetalicos de Pd₉₀/Ag₁₀ y Pd₉₀/Pt₁₀ pueden detectar H₂ con precisión. Pd₉₀/Pt₁₀ retrasó la transición de fase α a β a 1/5% v/v y pudo detectar concentraciones al menos de 10% v/v H₂/N₂. Resultados sugieren que los materiales bimetalicos tienen interacción de aleaciones el cual constriñe la expansión estructural reduciendo el estrés mecánico durante la transición de fase. Los resultados de ambas muestras también mostraron que la sensibilidad normalizada por el tiempo de respuesta tiene dos relaciones lineales con respecto $[H_2]^{1/2}$, antes y después de la transición de fase. La relación mencionada permite la implementación de nuestras películas bimetalicas como materiales de detección de hidrógeno.

En conclusión, el modificado RES produce películas bimetalicas que pueden detectar hidrógeno, pero esto está condicionado al uso de sales anhidras como los precursores y el uso de metales con un potencial de reducción estándar positivo tales como Pd, Pt y Ag.

DEDICATED

To God for providing health, support, strength and the required wisdom to achieve another goal, and opening new doors. To my lovely mom Irma Esteves-Gonzalez, who works very hard every single day to enjoy her children's happiness and success, and who also taught me that everything is possible with faith. To my brothers Emanuel Valentín-Esteves and Natanael Valentín-Esteves for always giving me unconditional love and support when needed and who always protect me as their little super-sister. To my brave grandmother Liduvina Gonzalez, who taught me to always fight for our dreams and to be strong on the road. Finally, I also dedicate this work to my nephew Michael Battle and nieces Caroline Battle and Angelisse Torres, for always motivating me with their innocent love and complete admiration to be a better professional and a more successful person every single day.

Keren

ACKNOWLEDGMENTS

First, I have to thank God because without him it would not be possible. I am really grateful for each one of his beautiful blessings. In addition, I want to express my gratitude to my advisor, Dr. María Martínez-Iñesta for giving me the opportunity to work under her guidance and in her research group during the last two years. I really appreciate her advice, supervision and guidance during this journey which contributed significantly to my professional and personal development. Thanks for making me a better professional and show me that I can do even more than what I can imagine.

Thanks to my labmates, Héctor Méndez and Lilliana Gámez for several things, but especially for the reliefs when we were full of stress. Héctor thanks because, despite the fact that in the beginning understanding each other required a lot of effort, you helped me several times. Thanks for all that you selflessly taught me, for allowing me to use your chamber to perform the hydrogen sensing tests, for your assistance with the XRD experiments, and obviously for your masculine strength when you saw me trying to do what obviously I could not. Lilly thanks for always being outstanding in helping me decipher the stressed mysteries that all research has in the beginning. Thanks to the trips to the Annual SHPE Conference (2013) and to Arizona from which a beautiful friendship emerged.

I want to thank my committee members Dr. David Suleiman and Dr. Arturo Hernández for their selfless help during this process. Thanks Dr. Hernández for your meticulous corrections of my writings because I recognize that you spend much time in it despite your busy agenda. Thanks Dr. Suleiman because you are one of the reasons for the more significant improvements in my personal and professional skills. In addition to allowing me to work in your lab as an undergraduate and meet

wonderful people, you recommended me to stay and complete graduate school, and thanks to that, several unexpected doors were opened and my professional life found their own way.

I extend my gratitude to José R. Almodóvar and Boris Renteria for their assistance in the XRD and SEM characterizations. I also want to emphasize my gratitude to Dr. Arturo Hernández for the use of the XRD, but especially for the confidence in allowing me to use the XPS equipment. This was not possible without the help of your graduate student Jennifer Guerrero to whom I want to thank in a special way all the time dedicated in that cold room. Jennifer, thanks for staying when you did not need to selflessly helping me during some of the most difficult days of that semester. Also, I want to thank Dr. José Cortés, my advance inorganic chemistry course professor, because he gave me the key to solve something very important in one of the most crucial moments of my graduate studies.

Special thanks to National Aeronautics and Space Administration (NASA) Grant and the Puerto Rico NASA Space Grant Fellowship for providing the financial support to develop this research.

Finally I would like to acknowledge the beautiful people who appreciate and love me sincerely: my family and friends. My deepest gratitude to my beautiful and lovely mom, Irma Esteves, who gave me daily the strongest support and the bigger unconditional and sincere love. Thanks for teaching me the importance of the education, moral values and the need to continually fight for our dream. Thanks to my father Cecilio Valentín for reminding me that I can always count with him. My brothers, Emanuel Valentín and Natanael Valentín, who always talk about me proudly and make me feel the most special super-sister in the world. Thank you, because your admiration is my energy to continue when I don't have enough strength. Thanks in a special way to my friends and sisters: Mercedes Ocasio, Carmen Rivas, and Wilmary Rivas for more than a decade of true friendship and for been the best sisters in the world. Thanks for always making me feel special and

for been there when I needed, in my tears and joys. I don't imagine how my life would be without you girls!

In addition, I had to thanks a very special family, Adrian Torres, Juanita Aviles, Janet Torres and my princesses Angelisse and Angelica for their love, help, support and all these powerful prays on my behalf. You are also my family.

I also want to extend my thanks to my two guardian angels in the Chemical Engineering Department, my beautiful and sincere friends Sonia Avilés and Maritza Pérez. Thanks for always being there as my "Chapulín Colorado". I'll be always grateful. You are very special people, a beautiful gift of God.

I am genuinely grateful to a special man who said present at a very difficult time of my life, who dedicated many hours in medical offices, who was always attentive to my health and thanks to him I earned a few pounds because he always was pending to my foods and rest. God definitely sent you in the perfect moment. Thanks Jean Caminero for the good and bad moments and for working very hard to get the best of both out. Definitively you made this process easier and happier.

Finally, I like to thank my friends: Michelle Acevedo, Jennifer Acevedo, Natalia Vázquez, Mariel Santiago, Noelia Lasanta, Angélica Román, Miguel Florian, David Mota, Eduardo Ruiz, Christian Rivera, Stephany Herrera, Ariangelis Ortíz, Daniel Mateo, Karem Court, Edward Guerrero, Camilo Mora and Paul Meza for their friendship and all the unforgettable moments that we lived together.

TABLE OF CONTENTS

CHAPTER 1	1
INTRODUCTION	1
1.1 JUSTIFICATION	1
1.2 LITERARY REVIEW.....	3
1.2.1 <i>Desired Hydrogen Gas Sensor Properties</i>	3
1.2.2 <i>Hydrogen sensing technologies</i>	4
1.2.3 <i>Palladium</i>	6
1.2.4 <i>Palladium Nanostructured Alloys and Bimetallic Mixtures</i>	11
1.2.4.1 <i>Pd/Ag</i>	11
1.2.4.2 <i>Pd/Ni</i>	14
1.2.4.3 <i>Pd/Pt</i>	15
1.2.4.4 <i>Pd/Cr</i>	15
1.2.5 <i>Synthesis of Palladium and Palladium bimetallic films</i>	16
1.3 GOALS AND SPECIFIC MAIN AIMS.....	17
1.4 CHAPTER DESCRIPTION.....	18
CHAPTER 2	19
MODIFICATION OF THE SOLID STATE REDUCTION (SSR) METHOD TO SYNTHESIZED NANOSTRUCTURED PALLADIUM BIMETALLIC MEMBRANES.	19
ABSTRACT	19
2.1 INTRODUCTION	19
2.2 EXPERIMENTAL METHODS	24
2.2.1 <i>Materials</i>	24
2.2.2 <i>Methodology Modifications</i>	25
2.3 RESULTS AND DISCUSSION.....	26
2.4 CONCLUSIONS.....	33

CHAPTER 3	34
------------------------	-----------

PALLADIUM BIMETALLIC FILMS CHARACTERIZATION 34

ABSTRACT	34
3.1 INTRODUCTION	34
3.2 EXPERIMENTAL METHODS.....	35
3.2.1 <i>Materials</i>	35
3.2.2 <i>Methodology</i>	36
3.3 RESULTS AND DISCUSSION.....	38
3.3.1 <i>Scanning Electron Microscopy Results</i>	38
3.3.2 <i>X-Ray Diffraction Results</i>	40
3.3.3 <i>Energy Dispersive X-Ray Results</i>	43
3.3.4 <i>Elemental Analysis with X-Ray Photoelectron Spectroscopy</i>	45
3.3.5 <i>Chemical states analysis using X-Ray Photoelectron Spectroscopy</i>	46
3.5 CONCLUSIONS.....	53

CHAPTER 4	55
------------------------	-----------

**HYDROGEN SENSING TEST USING BIMETALLIC NANOSTRUCTURED FILMS
SYNTHESIZED BY THE SOLID STATE REDUCTION METHOD AS A SENSING
MATERIAL..... 55**

ABSTRACT	55
4.1 INTRODUCTION	55
4.2 EXPERIMENTAL METHODS.....	57
4.3 RESULTS AND DISCUSSION.....	58
4.3.1 <i>Pure Palladium Film</i>	59
4.3.2 <i>Palladium/Platinum Bimetallic Films</i>	63
4.3.3 <i>Palladium/Silver Bimetallic Films</i>	73
4.3.4 <i>Palladium/Nickel Bimetallic Films</i>	78
4.3.5 <i>Palladium/Chromium Bimetallic Films</i>	79

4.4 BIMETALLIC AND PURE PALLADIUM COMPARISON	81
4.5 CONCLUSIONS	82
CHAPTER 5	84
CONCLUSIONS AND RECOMMENDATIONS.....	84
5.1 BIMETALLIC FILM SYNTHESIZED BY THE MODIFIED SSR METHOD.....	84
5.2 BIMETALLIC FILMS AS A SENSING MATERIAL FOR HYDROGEN DETECTION	86
APPENDIX	89
APPENDIX A.....	89
<i>Elements identification by XPS Technique</i>	<i>89</i>
APPENDIX B.....	92
<i>Metal Elemental Analysis obtained with CasaXPS Software</i>	<i>92</i>
APPENDIX C.....	102
<i>Analysis of the Metal Oxidation States obtained with CasaXPS Software.....</i>	<i>102</i>
APPENDIX D.....	110
<i>Sensitivity and Response Time Calculations and Additional Sensing Results.....</i>	<i>110</i>
REFERENCES.....	122

LIST OF FIGURES

Figure 1. 1 Number of publications related to the palladium use in hydrogen detection and separations applications.	6
Figure 1. 2 Sorption and Desorption Mechanism from E. David and J. Kopac ²⁶	7
Figure 1. 3 Lattice constant expansion as a consequence of the α to β phase transition	7
Figure 1. 4 Hysteresis effect on sensitivity upon phase transition during absorption and desorption of hydrogen in Pd films.....	9
Figure 1. 5 Hysteresis effect in the Pd films thickness reported by Lee <i>et al.</i>	10
Figure 2.1 SEM micrographs of Pd ₉₀ Ni ₁₀ bimetallic membrane obtained after different methodology modifications..	27
Figure 2. 2 Pd films formed by the adding the precursor by wet impregnation and adding 2uL water during reduction	28
Figure 2. 3 Water added in each side of the AAM membrane during the synthesis by SSR.	30
Figure 2. 4 SEM images of Pd ₉₀ Ni ₁₀ NWs	31
Figure 2. 5 SEM image of Pd ₉₀ Pt ₁₀ NWs.....	32
Figure 2. 6 SEM image of Pd ₉₀ Ag ₁₀ NWs	32
Figure 3. 1 Bimetallic membrane synthesis using a modification of the Solid State Reduction method.....	37
Figure 3.2 SEM micrographs of (A) Pd ₉₀ Ag ₁₀ , (B) Pd ₉₀ Pt ₁₀ and (C) Pd ₉₀ Ni ₁₀ films.....	39
Figure 3.3 SEM micrographs of Pd ₉₀ Cr ₁₀ sample (A) impregnation and (B) reduction sides.	39
Figure 3. 4 XRD results of the Pd ₉₀ Ag ₁₀ (A), Pd ₉₀ Pt ₁₀ (B) and Pd ₉₀ Ni ₁₀ (C) films.....	42
Figure 3. 5 Metals distribution in Pd ₉₀ Ag ₁₀ obtained with EDS.	43
Figure 3. 6 Metals distribution in Pd ₉₀ Pt ₁₀ obtained with EDS.....	44
Figure 3. 7 Metals distribution in Pd ₉₀ Ni ₁₀ obtained with EDS.....	44

Figure 3. 8 Metals peaks obtained in the chemical state analysis of Pd ₉₀ /Ag ₁₀ films.....	50
Figure 3. 9 Metals peaks obtained in the chemical state analysis of Pd ₉₀ /Pt ₁₀ films.....	52
Figure 4. 1 System Diagram for Hydrogen Test.....	57
Figure 4. 2 Pd film pretreatment with Hydrogen.....	60
Figure 4. 3 Sensing Response to H ₂ detection using pure Pd film synthesized by SSR.....	61
Figure 4. 4 Sensitivity (%) vs. hydrogen concentration detected by the pure Pd film.	62
Figure 4. 5 Response time (t _r , min) vs. hydrogen concentration detected by pure Pd film.....	62
Figure 4. 6 Sensitivity (%) vs. [H ₂] ^{1/2} detected by pure Pd film.....	63
Figure 4. 7 Current Sensing Response to Hydrogen detection using Pd ₉₀ /Pt ₁₀ (first run).....	64
Figure 4. 8 Sensing Response to Hydrogen detection obtained from the first run using the second Pd ₉₀ /Pt ₁₀ film synthesized by SSR Method (A. First 11 cycles, B. Last 11 cycles).	65
Figure 4. 9 In situ XRD of Pd ₉₀ /Pt ₁₀ at different [H ₂]	66
Figure 4. 10 Sensitivity (%) vs. [H ₂] detected by Pd ₉₀ /Pt ₁₀ bimetallic film (first run)	68
Figure 4. 11 Response time (t _r) vs. [H ₂] detected by Pd ₉₀ /Pt ₁₀ bimetallic film (first run)	68
Figure 4. 12 Sensitivity vs. [H ₂] ^{1/2} obtained using Pd ₉₀ /Pt ₁₀ bimetallic film (first run).....	69
Figure 4. 13 Sensitivity/response time vs. [H ₂] ^{1/2} obtained by Pd ₉₀ /Pt ₁₀ bimetallic film (first run)	70
Figure 4. 14 Sensitivity (%) vs. hydrogen concentration detected by the reused Pd ₉₀ /Pt ₁₀ bimetallic film (2nd and 3 rd Runs).....	71
Figure 4. 15 Response time (min) vs. [H ₂] detected by the reused Pd ₉₀ /Pt ₁₀ bimetallic film (2nd and 3 rd Runs).....	72
Figure 4. 16 Sensitivity/Response time (S/t _r) vs. [H ₂] ^{1/2} by the reused Pd ₉₀ /Pt ₁₀ bimetallic film (2nd and 3 rd Runs).....	72
Figure 4. 17 Sensing Response to Hydrogen detection using the first Pd ₉₀ /Ag ₁₀ film synthesized by SSR (A. First 10 cycles, B. Last 7 cycles).....	74

Figure 4. 18 In situ XRD patterns of Pd ₉₀ /Ag ₁₀ at different [H ₂]	75
Figure 4. 19 Sensitivity (%) vs. [H ₂] detected by Pd ₉₀ /Ag ₁₀ bimetallic film	76
Figure 4. 20 Response time (min) vs. [H ₂] detected by Pd ₉₀ /Ag ₁₀ bimetallic film.....	76
Figure 4. 21 Sensitivity vs. [H ₂] ^{1/2} detected by Pd ₉₀ /Ag ₁₀ bimetallic film.....	77
Figure 4. 22 Sensitivity/Response time (S/tr) vs. [H ₂] ^{1/2} detected by Pd ₉₀ /Ag ₁₀ bimetallic film.	77
Figure 4. 23 Sensing Response to Hydrogen detection using the second Pd ₉₀ /Ni ₁₀ membrane synthesized by SSR Method.	78
Figure 4. 24 Example of the sensing response obtained for the other synthesized Pd ₉₀ /Ni ₁₀ membranes.	79
Figure 4. 25 Sensing response results using Pd ₉₀ /Cr ₁₀ membrane synthesized by the SSR Method.	80
Figure 4. 26 Sensing Response using other Pd ₉₀ /Cr ₁₀ membrane synthesized by the SSR Method.	80
Figure A. 1 XPS spectra of Pd ₉₀ /Ag ₁₀ Impregnation Side	89
Figure A. 2 XPS spectra of Pd ₉₀ /Ag ₁₀ Reduction Side	90
Figure A. 3 XPS spectra of Pd ₉₀ /Pt ₁₀ Impregnation Side.....	90
Figure A. 4 XPS spectra of Pd ₉₀ /Pt ₁₀ Reduction Side.....	91
Figure A. 5 XPS spectra of Pd ₉₀ /Ni ₁₀ Impregnation Side	91
Figure A. 6 XPS spectra of Pd ₉₀ /Ni ₁₀ Reduction Side	92
Figure B. 1 Impregnation side of Pd ₉₀ /Ag ₁₀ (Sample 1).....	93
Figure B. 2 Impregnation side of Pd ₉₀ /Ag ₁₀ (Sample 2).....	93
Figure B. 3 Impregnation side of Pd ₉₀ /Ag ₁₀ (Sample 3).....	94
Figure B. 4 Reduction side of Pd ₉₀ /Ag ₁₀ (Sample 1).....	94

Figure B. 5 Reduction side of Pd ₉₀ /Ag ₁₀ (Sample 2).....	95
Figure B. 6 Reduction side of Pd ₉₀ /Ag ₁₀ (Sample 3).....	95
Figure B. 7 Impregnation side of Pd ₉₀ /Pt ₁₀ (Sample 1)	96
Figure B. 8 Impregnation side of Pd ₉₀ /Pt ₁₀ (Sample 2)	96
Figure B. 9 Impregnation side of Pd ₉₀ /Pt ₁₀ (Sample 3)	97
Figure B. 10 Reduction side of Pd ₉₀ /Pt ₁₀ (Sample 1).....	97
Figure B. 11 Reduction side of Pd ₉₀ /Pt ₁₀ (Sample 2).....	98
Figure B. 12 Reduction side of Pd ₉₀ /Pt ₁₀ (Sample 3).....	98
Figure B. 13 Impregnation side of Pd ₉₀ /Ni ₁₀ (Sample 1).....	99
Figure B. 14 Impregnation side of Pd ₉₀ /Ni ₁₀ (Sample 2).....	99
Figure B. 15 Impregnation side of Pd ₉₀ /Ni ₁₀ (Sample 3).....	100
Figure B. 16 Reduction side of Pd ₉₀ /Ni ₁₀ (Sample 1).....	100
Figure B. 17 Reduction side of Pd ₉₀ /Ni ₁₀ (Sample 2).....	101
Figure B. 18 Reduction side of Pd ₉₀ /Ni ₁₀ (Sample 3).....	101
Figure C. 1 Peaks deconvolution of Pd's 3d orbitals in Pd ₉₀ /Ag ₁₀ bimetallic film formed in the impregnation side. (A: sample 1, B: sample 2, C: sample 3).....	102
Figure C. 2 Peaks deconvolution of Ag's 3d orbitals in Pd ₉₀ /Ag ₁₀ bimetallic film formed in the impregnation side. (A: sample 1, B: sample 2, C: sample 3).....	103
Figure C. 3 Peaks deconvolution of Pd's 3d orbitals in Pd ₉₀ /Ag ₁₀ bimetallic film formed in the reduction side. (A: sample 1, B: sample 2, and C: sample 3)	103
Figure C. 4 Peaks deconvolution of Ag's 3d orbitals in Pd ₉₀ /Ag ₁₀ bimetallic film formed in the reduction side. (A: sample 1, B: sample 2, and C: sample 3).....	103
Figure C. 5 Peaks deconvolution of Pd's 3d orbitals in Pd ₉₀ /Pt ₁₀ bimetallic film formed in the impregnation side. (A: sample 1, B: sample 2, and C: sample 3)	104

Figure C. 6 Peaks deconvolution of Pt's 4f orbitals in Pd ₉₀ /Pt ₁₀ bimetallic film formed in the impregnation side. (A: sample 1, B: sample 2, and C: sample 3)	104
Figure C. 7 Peaks deconvolution of Pd's 3d orbitals in Pd ₉₀ /Pt ₁₀ bimetallic film formed in the reduction side. Pd was not detected in sample 2. (A: sample 1, B: sample 2, and C: sample 3)	104
Figure C. 8 Peaks deconvolution of Pt's 4f orbitals in Pd ₉₀ /Pt ₁₀ bimetallic film formed in the reduction side. Pt was not detected in Sample 2. (A: sample 1, B: sample 2, and C: sample 3)	105
Figure C. 9 Peaks deconvolution of Pd's 3d orbitals in Pd ₉₀ /Ni ₁₀ bimetallic film formed in the impregnation side. (A: sample 1, B: sample 2, and C: sample 3)	105
Figure C. 10 Peaks deconvolution of Ni's 2p orbitals in Pd ₉₀ /Ni ₁₀ bimetallic film formed in the impregnation side. Ni can't be differentiable in the analyzed area presented in C. (A: sample 1, B: sample 2, and C: sample 3).....	105
Figure C. 11 Peaks deconvolution of Pd's 3d orbitals in Pd ₉₀ /Ni ₁₀ bimetallic film formed in the reduction side. Pd was not detected in sample 3. (A: sample 1, B: sample 2, and C: sample 3)	106
Figure C. 12 Peaks deconvolution of Ni's 2p orbitals in Pd ₉₀ /Ni ₁₀ bimetallic film formed in the reduction side. Ni can't be differentiable in the analyzed areas presented in A and C. A: sample 1, B: sample 2, and C: sample 3).....	106
Figure D. 1 Sensitivity and Response Time Determination	110
Figure D. 2 Sensing Response to Hydrogen detection using the second Pd ₉₀ /Pt ₁₀ film synthesized by SSR Method (second run). The first run was presented in Figure 4.10.....	113
Figure D. 3 Sensing Response to Hydrogen detection using the second Pd ₉₀ /Pt ₁₀ film synthesized by SSR Method (third run). The first run was presented in Figure 4.10 and the second run in Figure D.2.....	114
Figure D. 4 Sensing Response to Hydrogen detection using the second Pd ₉₀ /Ag ₁₀ membrane synthesized by SSR Method (first run)	116
Figure D. 5 Sensitivity (%) vs. hydrogen concentration detected by Pd ₉₀ /Ag ₁₀ bimetallic film. Run presented in Figure D.4.	117
Figure D. 6 Response time (t _r) vs. hydrogen concentration detected by Pd ₉₀ /Ag ₁₀ bimetallic film. Run presented in Figure D.4.	117

Figure D. 7 Sensitivity/Response time (S/t_r) vs. hydrogen concentration detected by Pd ₉₀ /Ag ₁₀ bimetallic film. Run presented in Figure D.4.	118
Figure D. 8 Sensing Response to Hydrogen detection using the second Pd ₉₀ /Ag ₁₀ membrane synthesized by SSR Method (second run)	118
Figure D. 9 Sensitivity (%) vs. hydrogen concentration detected by the reused Pd ₉₀ /Ag ₁₀ bimetallic film. Run presented in Figure D.8.....	119
Figure D. 10 Response Time (min) vs. hydrogen concentration detected by the reused Pd ₉₀ /Ag ₁₀ bimetallic film. Run presented in Figure D.8.....	120
Figure D. 11 Sensitivity/Response Time (S/t_r) vs. hydrogen concentration detected by the reused Pd ₉₀ /Ag ₁₀ bimetallic film. Run presented in Figure D.8.	120

LIST OF TABLES

Table 1. 1 Flammable range for different fuels obtained from [27]	4
Table 3. 1 Palladium Bimetallic Films Elemental Analysis	46
Table 3.2 Standard Reduction Potentials	46
Table 3. 3 XPS results of Pd ₉₀ /Ag ₁₀ after peaks deconvolution using CASA-XPS	49
Table 3. 4 XPS results of Pd ₉₀ /Pt ₁₀ after peak deconvolution.....	51
Table 3. 5 XPS results of Pd ₉₀ /Ni ₁₀ after peaks deconvolution using CASA-XPS	53
Table 4. 1 Results summary.....	81
Table C. 1 XPS results of Pd ₉₀ /Ag ₁₀ after peaks deconvolution using CASA-XPS.....	107
Table C. 2 XPS results of Pd ₉₀ /Pt ₁₀ after peaks deconvolution using CASA-XPS	108
Table C. 3 XPS results of Pd ₉₀ /Ni ₁₀ after peaks deconvolution using CASA-XPS.....	109
Table D. 1 Sensitivity and Sensor Response Time using Pure Palladium Film (Figure 4.3).....	111
Table D. 2 Sensitivity and Sensor Response Time of the run presented in Figure 4.8 using Pd ₉₀ /Pt ₁₀ Film (first run).....	112
Table D. 3 Sensitivity and Sensor Response Time of the run presented in Figure D.2 using Pd ₉₀ /Pt ₁₀ Film (second film – second run)	113
Table D. 4 Sensitivity and Sensor Response Time of the run presented in Figure D.3 using Pd ₉₀ /Pt ₁₀ Film (second film – third run).....	114
Table D. 5 Sensitivity and Sensor Response Time of the run presented in Figure 4.17 using Pd ₉₀ /Ag ₁₀ Membrane (first membrane).....	115
Table D. 6 Sensitivity and Sensor Response Time of the run presented in Figure D.4 using Pd ₉₀ /Ag ₁₀ Membrane (second membrane - first run)	116
Table D. 7 Sensitivity and Sensor Response Time of the run presented in Figure D.8 using Pd ₉₀ /Ag ₁₀ Membrane (second membrane - second run).....	119
Table D. 8 Sensitivity and Sensor Response Time of the run presented in Figure 4.23 using Pd ₉₀ /Ni ₁₀ Membrane	121

Chapter 1

INTRODUCTION

1.1 Justification

Continuous increase in energy demand and high levels of pollution, generated by the use of existing energy sources, has led researchers to explore other clean and renewable energy alternatives. Hydrogen gas (H_2) is an alternate option. Hydrogen gas is one of the most useful gases in many industries (such as chemical, food and semiconductor industries) and transportation (as fuel in fuel cells and rockets for space shuttle).¹⁻³ However, H_2 is a highly flammable gas in the concentration range above 4% by volume in air and its low mass, high diffusivity and low liquefaction point cause difficulties for its storage.^{1,4,5} As a result, the detection of hydrogen below the lower explosion limit is an important safety concern^{5,6} which warrants the need for sensitive, selective, economic and reliable hydrogen gas sensors for its worldwide implementation as an alternative energy source.^{1,2,5,7-10}

According to transportation industries, the first experimental hydrogen gas fueled vehicle concept was designed by Isaac de Rivaz in 1807.¹¹ In 2003, President George W. Bush announced a hydrogen-fuel initiative to develop commercial fuel-cell vehicles (FCV) by 2020.^{11,12} Nowadays, FCV, also known as “eco-cars”, are been designed as a promising solution to the energy and emissions problems by different car manufacturers such as Daimler, Ford, General Motors, Honda, Hyundai, Kia, Renault, Nissan and Toyota.¹² The first commercial models were designed in 2013, and a higher production is expected of these hydrogen-powered cars for 2015.^{11,13-17} There are ten hydrogen stations in the state of California, one in South

Carolina and the most recent one in Connecticut that make more accessible the use of these eco-friendly vehicles in the United States.¹⁷ With this expected increase in the production of hydrogen powered cars, it is also expected that the number of hydrogen station increases around the United States.

NASA uses H₂ for the propulsion of space shuttles. For NASA, hydrogen leak detection is a vital issue. The detection of explosive conditions in aerospace applications is important for safety and economic reasons.^{2,9,10} Thus, NASA is always looking for ways to improve hydrogen sensors.² The limited resources available in outerspace missions naturally generate an interest in the reduction of size, weight, and power consumption of the sensors and one alternative is using nanostructured sensors.

The hydrogen gas is also used in different industries such as the chemical industry for the production of methanol, chloride acid, ammonia, hydrogen peroxide and fertilizers,^{1,18,19} the pharmaceutical industry for the manufacture of vitamins,^{18,19} the petrochemical industry for crude oil refinements,^{18,19} the food industry to make hydrogenated vegetable oils such as margarine and butter,^{1,18,19} and in the semiconductor industry as a carrier gas in the manufacture of the semi-conducting layers in integrated circuits.^{1,18,19}

Palladium was classified as a highly hydrogen permeable material in the 19th-century.^{20,21} An important characteristic of this metal is its selectivity to the adsorption and dissociation of hydrogen gas into its atoms, when compared to other materials.^{2,8-10,20,22,23} Other characteristics that make it a desired hydrogen sensing material are its temperature stability and corrosion resistance.^{1,7,20,24,25}

Nevertheless, pure palladium exhibits an alpha (α) to beta (β) structural phase transition upon hydrogen adsorption at temperatures below 294°C and hydrogen pressures under 2000 kPa.²⁰ The transition causes an increase in the unit cell volume, which can cause mechanical strains, physical distortions and possible failure of Pd as sensing material.^{10,20}

Palladium bimetals and palladium alloys have been observed to delay or inhibit this transition and other significant limitations.^{1,2,7,9,10,26,27} The approach of this research is to design a nanostructured self-supporting bimetallic film for hydrogen sensing applications using a modification of the Solid State Reduction Method (SSR) that was developed in our research group. This project was designed in collaboration with Dr. Gary Hunter, Technical Lead of the Chemical Species Gas Sensors Division at the NASA Glenn Research Center.

1.2 Literary Review

1.2.1 Desired Hydrogen Gas Sensor Properties

Despite the fact that hydrogen gas is one of the least flammable materials having a low explosion limit of 4% (a higher concentration than other common flammable compounds), it has a large flammability range of 4 – 75 % (Table 1.1). This fact and its tendency to leak when it is stored -as a consequence of its light weight and small size- are some of the challenges that limit the widespread use of hydrogen.^{28,29}

Table 1. 1 Flammable range for different fuels obtained from [27]

Fuel	Low explosion limit percent (LEL %)	Upper explosion limit percent (UEL %)
Gasoline	1.4	7.6
Propane	2.1	10.1
Ethane	3.0	12.4
Hydrogen	4.0	75.0
Methane	5.0	15.1
Propylene	2.0	11.1

There are some important parameters considered in hydrogen sensors. A hydrogen sensor must be able to detect hydrogen at concentrations below the lower explosive limit of 4% v/v (H₂/air) and be able to survive exposure to 100% hydrogen concentration avoiding damage or change in calibration.² The sensor must have a high sensitivity and selectivity towards hydrogen, a fast response time to allow a real time monitoring of gas, avoid hysteresis (evidenced in changes in calibration after desorption of the hydrogen), a fast recovery time, and low cost.^{1,2,9,10} In addition sensors must have a high durability, a well-defined replacement, maintenance, and low operational cost associated with them. Also they should have minimal signal drifts.²⁹

For NASA and transportation applications, the size, weight, and power consumption are also significant concerns.^{2,9}

1.2.2 Hydrogen sensing technologies

Hydrogen is often detected in the industry using gas chromatography (GC), mass spectrometry (MS) or GS-MS combined systems.^{26,29,30} These technologies are very expensive

techniques and require bulky equipments, extensive sample systems and a continuous bypass flow of gases.²⁹ GC also has slow response times and requires a carrier gas. Despite these disadvantages, this technology has as advantages the detection of hydrogen when present in a mixture of gases.

Hydrogen can be also detected using electrolytic reactions in systems called electrochemical sensors in which H₂ is oxidized at the surface of a sensing electrode.²⁸ This oxidation increases the potential difference allowing the detection of the mentioned gas. These sensors are highly sensitive and do not have a high power consumption, but the deterioration of the electrode decreases the sensitivity as function of time.^{28,29} Other often used sensors are the solid-state technologies, *i.e.* catalytic bead, electrochemical-based sensors, surface acoustic wave, microresonance-based sensors, and semiconducting metal oxide, but some of this technology require high temperature (approx. 500°C) and the presence of oxygen. Other sensing mechanism often used in industry is based on thermal conductivity. These sensors can detect concentrations up to 100% v H₂ and avoid poison, but are the less sensitive technology used for this application.^{28,29} On the other hand, several sensors operate under the presence of oxygen which promotes the grain boundary formation in the metal oxide sensor and electron transfer in the electrochemical sensors.²⁹

NASA uses two different hydrogen detection approaches: Schottky diode and resistor sensors.³¹ The Schottky Diode is used to detect low concentrations of hydrogen and it does not require oxygen to be operated. The resistor is used to detect concentrations up to 100% in which the resistance is dependent on the H₂ concentration. But this technology requires a temperature

detector and a heater which are incorporated in the same chip. In addition, it shows damage at high concentrations.³¹

Despite the use of several technologies, there are not very efficient and cost-effective.³⁰ Researchers are studying the way to improve the properties of hydrogen sensors. Some research has been focused in the use of Palladium for this application and Figure 1.1 shows the increment in the number of research publications and patents related to the use of palladium in hydrogen separation and detection.²⁵

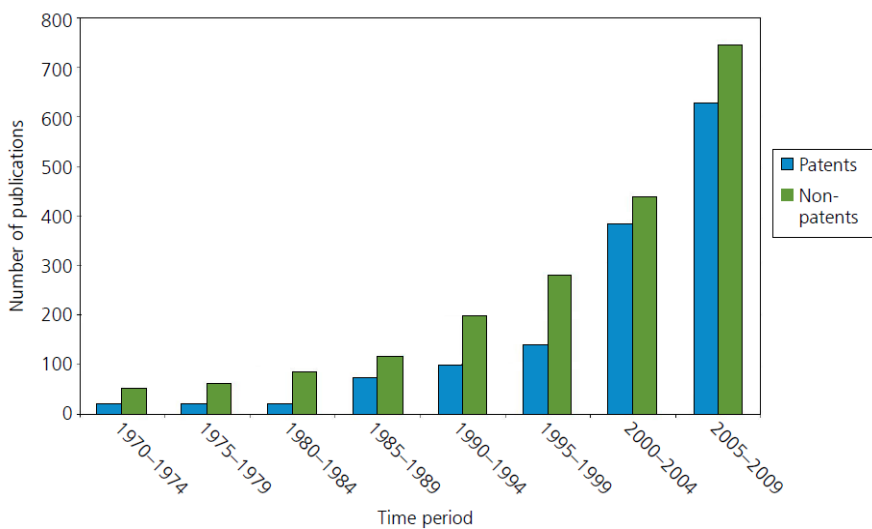


Figure 1. 1 Number of publications related to the palladium use in hydrogen detection and separations applications. Data obtained from [23]

1.2.3 Palladium

Palladium is a noble metal with a cubic close packed crystalline structure (FCC) which forms many compounds and several complex salts. Palladium has been studied as the active phase of hydrogen sensor due to its great capacity to adsorb hydrogen.^{2,8-10,20,22,23} Palladium-based sensors are divided in (1) palladium resistors, (2) palladium capacitors or field-effect

transistors (FETs), and (3) optical sensors. The most studied are the palladium resistors in which conductivity changes are detected as a result of the phase transition in palladium.

All Pd based sensors use the fact that its properties - such as mass, volume and electrical resistance- change when it interacts with hydrogen.¹ Figure 1.2 shows a schematic of the hydrogen sorption, dissociation, migration and desorption mechanism that occurs in Pd.^{1,10,20,27} The dissociation facilitates diffusion and dissolution of hydrogen atoms into a Pd layer which then migrate into the interior of the metal.^{5,10,20,26} This migration produces an increase in the electrical resistance that is proportional to the amount of hydrogen adsorbed by the metal phase enabling the use of Pd in resistor-based sensors.^{1,7,10,24,27} However, the lattice expansion and contraction that occurs during this process can provoke Pd mechanical and topographical instability.³²

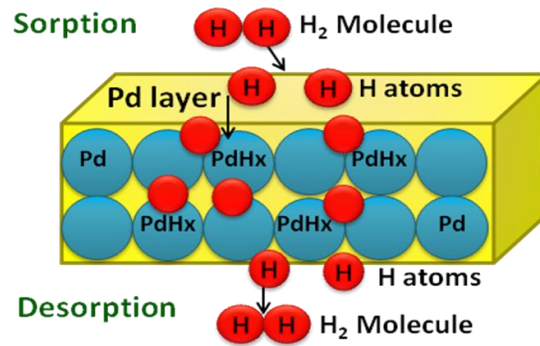


Figure 1. 2 Sorption and Desorption Mechanism from E. David and J. Kopac²⁶

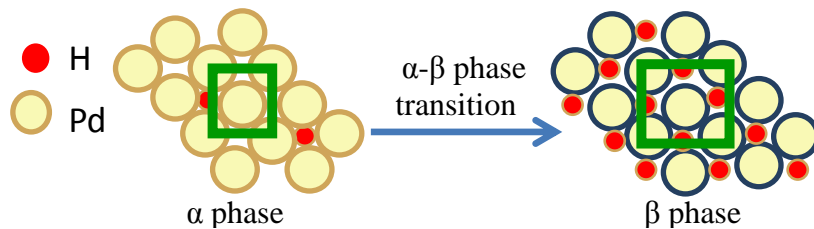


Figure 1. 3 Lattice constant expansion as a consequence of the α to β phase transition

The adsorption of hydrogen by palladium produces two different phases at different hydrogen concentrations. The α phase appears at low concentrations with a lattice constant similar to pure Pd. The lattice increases from 3.889 Å, which corresponds to pure Pd, to 3.893 Å.^{7,26,33,34} In this phase the interaction between the metal and hydrogen atoms produces a solid solution of Pd and H.³⁵ The β phase appears at higher H₂ concentrations when more hydrogen atoms occupy the interstitial positions of the Pd lattice. This causes a significant lattice constant expansion, in which metal hydride is formed (Figure 1.3).^{2,9,35,36} The palladium lattice parameter in the β phase is approximately 4.023 Å.^{7,26,33,34} The transition typically occurs at hydrogen concentrations between 0.1% - 2% v/v, but it depends on the Pd film thickness, presence of an alloying element and concentration.^{7,37} This transition occurs when the amount of incorporated hydrogen atoms exceeds the limit of H solid solubility in the palladium film.³⁵

Phase transitions can lead to physical distortions and changes in the sensor response, such as embrittlement, hysteresis, or film damage.^{9,10} Embrittlement causes macroscopic damage in the metals' films when it is submitted to a significant stress.³⁸ Brittle fractures are mechanical deformations characterized by the complete absence or small presence of plastic deformation prior to failure. Brittle fractures typically occur in glasses, ceramics, metals and some polymeric materials.³⁹

On the other hand, a hysteresis effect can be observed on a Pd resistor based hydrogen sensor on the electrical resistance. When Pd adsorbs hydrogen and goes through the phase transition to the beta phase it has a resistivity value that is different at the same concentration when hydrogen is desorbed.³⁵ This occurs because in the β phase the Pd and the H have strong interactions. Therefore, to overcome this interaction in order to return to the alpha phase the

sample requires high activation energy. In addition, a significant concentration gradient between the palladium hydride in the beta phase and the Pd surface exposed to environment is needed in order to obtain the require driving force to remove the hydrogen atoms and decrease the expansion in the unit cell volume.³⁵ This process yields a change in sensitivity during absorption and desorption as shown in Figure 1.4. Here, and elsewhere in this thesis sensitivity (S) is defined as:

$$S = \frac{|I_j - I_o|}{I_o} \quad \text{Equation 1.1}$$

where I_j represents the plateau value of the current under H_2 exposure and I_o represents the current plateau value under N_2 exposure.

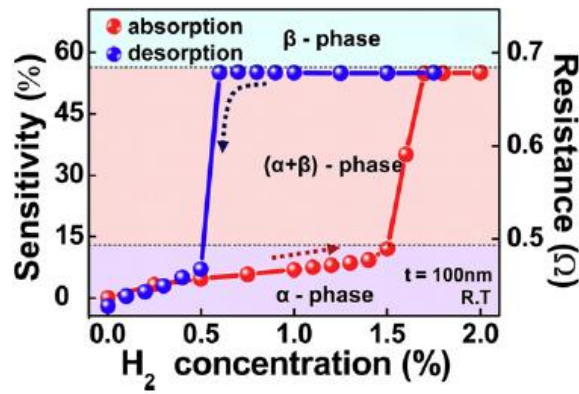


Figure 1. 4 Hysteresis effect on sensitivity upon phase transition during absorption and desorption of hydrogen in Pd films. Figure taken from [33]

Reported studies have evidenced the hysteresis effects in thin-film Pd based sensors at high temperatures²⁹ but *Lee et al.* studied the effect at room temperature.³⁵ These results, shown in Figure 1.5, evidenced that the difference between the sensitivity to hydrogen concentrations in the absorption and desorption process increases proportional to the Pd films' thickness. They

repressed this effect using 20 nm Pd films and in 5nm thin films the transition to the beta phase was suppressed. They conclude that as the film thickness decreases, the palladium thin films were confined to the substrate strongly and further absorption of the H atoms and the lattice expansion was restricted.³⁵This effect was called a clamping effect.

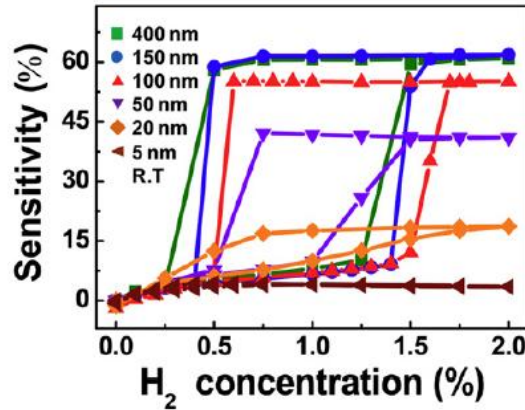


Figure 1. 5 Hysteresis effect in the Pd films thickness reported by Lee *et al.* Figure taken from [33]

Film buckling and delamination is another effect observed in Pd film based sensors. It is caused by a compressive stress in the interface between the film and the substrate due to the increase in the volume during the phase transition.^{35,36,40} This is observed in bulk Pd and thick Pd films. Detachment of the film occurs as a consequence of a mechanical deformation to release the mentioned stress. In this case the structural change in the film is irreversible allowing an unchanged deformed structure even after the desorption process in which all the H atoms are removed from the system.^{35,40} The mentioned deformation limits the film reusability. As stated before, if the film is thin the beta phase can be suppressed or reduced and the film buckling is minimized.

The material instabilities, resulting from the large volume changes that occur during the Pd-H α to β phase transition, limit the durability and reliability of pure Pd thin film sensors. One way to circumvent or delay this transition is through the use of Pd bimetallic materials and these will be discussed next.

1.2.4 Palladium Nanostructured Alloys and Bimetallic Mixtures

Palladium bimetallic and palladium alloyed membranes are also suitable for hydrogen detection by the sorption and desorption mechanism.²⁶ The use of nanostructured Pd alloys reduces the damage to the film and has been demonstrated to be an alternative to surpass the mentioned α to β phase transition and others limitations.^{1,2,7,9,10,37,41} Pd alloys also show an expansion of the crystal structure lattice that leads to faster kinetics for hydrogen absorption and desorption.³⁶

Considering the reasons mentioned in the section above, several bimetallic structures are studied in order to enhance the palladium sensing properties. Some of the most studied are Pd/Pt, Pd/Ni, Pd/Ag, and Pd/Cr being the last two the most studied by NASA for aerospace applications. This section summarizes reported results of the use of palladium bimetallic materials as hydrogen sensors.

1.2.4.1 Pd/Ag

In the chemical industry, Pd/Ag alloys are used as catalysts and for hydrogen extraction due to their complete miscibility and the increase in rate and selectivity of reactions when Ag is

added.^{3,22,42} Pd/Ag membranes have been successfully employed in different reaction processes, *i.e.* methanol synthesis and in the water gas shift reaction (WGSR) for H₂ production.^{43–45}

The use of Pd/Ag as a sensing material for hydrogen detection was pioneered by Hughes.⁹ Hughes et al. studied the differences between Pd/Ag and Pd thin films with different ratios and preparation procedures in order to analyze the rate of response to H₂.⁴² After a series of experiments they concluded that alloys with Ag content of 15%, 21 % and over 40% (molar percent) show poor sensitivity. However, an Ag content of 10% (molar) exhibited a faster response and signal than pure Pd. The poor performance at high Ag concentrations is a consequence of its low H₂ solubility and adsorption rate, and the significant reduction of the Pd concentration.

Previous works have reported that the presence of O₂ affects the response of Pd based devices because it reduces the signal from a given H₂ partial pressure due to competitive adsorption.⁴² Hughes also demonstrated that the presence of oxygen causes less significant changes in the response when using an Pd/Ag alloy with 33% of Ag compared to pure Pd.

Chen et al. also synthesized Pd/Ag nanostructures and demonstrated that the addition of Ag greatly increases the hydrogen sorption capacity and diminishes the α to β phase transition. The Pd₈₀/Ag₂₀ (Pd 80% molar) alloy presented the highest capacity for the α phase hydrogen sorption at -225 mV, over 4 times higher than the pure Pd.³⁶ In addition, the time required to achieve the hydrogen saturation for the nanoporous Pd/Ag was significantly less than for the nanoporous Pd electrodes. Other experiments demonstrated that 23wt % Ag Pd alloys have higher hydrogen permeability at temperatures above 200 °C and pressure of 1 atm.²²

Tasaltin et al. studied nanoporous Pd/Ag (15 wt. % Ag) and Pd/Cu (15 wt. % Cu) alloys films supported on alumina substrate (AAO). Results showed the alloys hydrogen sensing properties at different temperatures (in a range of 25 °C and 100 °C), and different hydrogen/nitrogen concentrations (between 250 and 5000 ppm).¹ The results evidenced an increase in hydrogen sensitivity, a decrease in recovery time, and a faster response time from the nanoporous Pd/Ag and Pd/Cu films on the AAO template when compared to the traditional unsupported Pd/Ag and Pd/Cu thin film sensors.¹ They also demonstrated that the resistance changes were proportional to the hydrogen concentration for both nanoporous Pd/Ag and Pd/Cu alloy sensors at room temperature. Moreover, the sensor response decreased with increasing temperature for all desired H₂ concentrations. The operation of both alloy sensors was totally reversible and the limit of detection (LOD) of the sensors was 250 ppm at room temperature. However, the nanoporous Pd/Cu sensor response and sensitivity to H₂ was always lower than the Pd/Ag sensor response at all temperatures and hydrogen concentrations. The maximum sensor responses were obtained at room temperature for both alloys avoiding the need to energy to improve the responses.

In internal studies by NASA, Pd/Ag alloys showed resistance to damage from exposure to high hydrogen concentrations. In addition, their sensitivity is high and the response is fast and reproducible.^{2,9} Results show that the 13% mol Ag is considered the optimum concentration⁹ and had a faster response time than pure Pd.² The presence of oxygen decreases the sensor response but the sensor is still sensitive to low concentrations of hydrogen. A small amount of H₂ produces a large signal with a fast return to the baseline when is used in oxygen containing environments.⁹ The Pd/Ag sensor responds to hydrogen through a wide concentration range with

a signal and response time that is temperature dependent.² Despite this, the Pd/Ag sensor calibration changed when exposed to higher concentrations and higher temperatures. These changes led the sensor to failure. EDAX results suggested that at these conditions the material suffered damages and was removed from the substrate surface.

1.2.4.2 Pd/Ni

Pd/Ni alloys are one of the most studied materials for hydrogen sensing.¹ Similar to Pd and Pd/Ag, the electrical resistance of Pd/Ni thin films is a function of the adsorbed hydrogen.⁴⁶ Pd/Ni alloys were also studied by Hughes et al and showed that a Ni concentration of 8% and 15% (molar) in Pd/Ni thin films resulted in H₂ sensors that responded rapidly and reversibly at room temperature and pressure of 1 atm.²³ No response to H₂ in films with 56 % (atomic) Ni was observed. The addition of Ni suppressed the phase transition observed in pure Pd under the same conditions. Accurate H₂ concentrations measurements were obtained near the H₂ lower explosion limit.

Cheng and coworkers analyzed different concentrations of Pd/Ni thin films deposited on Al₂O₃ substrates.⁴⁶ XRD results showed a systematic shift of the Pd <111> peak position to a higher angle when the nickel concentration was increased. This behavior was explained by a contraction of the face-centered-cubic (fcc) palladium lattice with nickel additions as a result of isomorphous substitution of palladium atoms by the smaller atomic radius of nickel atoms.⁴⁶ This lattice contraction is believed to suppress the phase transition from α - to β -hydride phase.⁴⁶ The results also showed that the sensor sensitivity decreases with increasing temperature, rendering the sensor insensitive above 100 °C.

1.2.4.3 Pd/Pt

Kumar et al. studied the response and recovery of hydrogen sensing in Pd/Pt nanoparticles dispersed onto graphene layers at temperatures from -110 to 100°C.³² The poor hydrogen sensitivity of graphene towards H₂ was increased by functionalizing it with catalytically active metals such as Pd and Pt, which form hydrides (PdH_x, PtH_x) after the dissociation of H₂ molecules on their surface. The hydrogen sensing response was studied by measuring the electrical resistance changes when the material was exposed to 2% H₂/ 98% Ar. Results demonstrated a maximum sensitivity and fast response time at 20–40 °C, which is consistent with the variation of physisorption and chemisorption processes with temperature. In this study they concluded that graphene–Pd/Pt nanoparticle based hydrogen sensors have a faster response and recovery times than the pure palladium thin film.

1.2.4.4 Pd/Cr

Another metal combination that has been studied at NASA is Pd/Cr. This sensor responds well to 100% hydrogen at 100°C and is much more stable than the Pd/Ag sensor under these conditions avoiding the calibration changes. The results of these tests and other testing suggest that Pd/Cr is better for applications where the sensor is exposed to higher hydrogen concentrations while Pd/Ag can be used for lower hydrogen concentration applications.²

Zeng et al. designed a H₂ sensor based on Pd/Cr nanowires sputter-deposited on a commercial alumina membrane.⁵ A thin layer of Pd was deposited on the top of a thin layer of Cr, previously deposited onto the alumina membrane, and created networks of Pd/Cr nanowires. Results show a faster response for Pd/Cr than for pure palladium and, unlike pure Pd NWs, can

differentiate H₂ concentrations higher than 3%. Similar to the NASA results, this sensor can detect H₂ up to 100%.

1.2.5 Synthesis of Palladium and Palladium bimetallic films

As evidenced in some of the works described above, nanosized materials have a large surface area and others characteristics that can improve the sensor performance.^{1,5,45,47,48} Nanoalloys can be generated in a variety of ways. Some are in gas phase in a solution, supported on a substrate, or in a matrix. Some techniques can be applied to synthesize both nanoalloys and monometallic nanostructures.⁴⁹ For example, monometallic and nanoalloy clusters can be synthesized by molecular beam deposition, ion implantation and electrochemical synthesis.^{49,50} They can also be synthesized by chemical reduction methods such as a co-reduction, successive or sequential reduction and reduction of co-complexes.^{49,51} In co-reduction the bimetallic colloids are synthesized by reducing a solution of the metal salts. In sequential reduction, also called seeded growth, one metal is deposited and reduced on the surface of a cluster metal. Lastly in reduction of co-complexes complexes with both metals are reduced to form bimetallic particles.

Palladium and bimetallic films can be also synthesized by several methods, including some mentioned above. They can also be synthesized by electroless deposition on Al₂O₃ support,⁵² sputtering^{4,53}, thermal evaporation⁵⁴, electron beam evaporation⁵⁵, chemical vapor deposition⁵⁶, atomic layer deposition⁵⁷, and electrodeposition⁵⁸.

In order to reduce the negative environmental impact and reduce cost several researchers are studying the use of green or eco-friendly synthesis. Some examples of these methods are described in Chapter 2.

1.3 Goals and Specific Main Aims

The need to develop an enhanced hydrogen sensor requires the further study of Pd bimetallic materials. To achieve this purpose, AAM films with different Pd bimetallic combinations was synthesized using a modification of the SSR method, in order to obtain the desired properties without compromising the palladium sensing properties. The studied metals were silver (Ag), nickel (Ni), platinum (Pt) and Chrome (Cr).

The specific objectives of this research project were:

1. Modify the Solid State Reduction (SSR) method to determine its feasibility in obtaining bimetallic nanostructures
 - a. Synthesize Pd/Ag, Pd/Ni, Pd/Pt, and Pd/Cr films in porous alumina membranes using the SSR.
 - b. Characterize the morphology and composition of the films
 - i. X-ray Diffraction to study the crystalline phases that are formed of each bimetallic mixtures (Pd/Ag, Pd/Ni, Pd/Pt and Pd/Cr).
 - ii. X-ray Photoelectron Spectroscopy to study the metal oxidation states of the metals after synthesis using our SSR Method.
 - iii. Scanning Electron Microscopy to observe material's morphology of bimetallic films and nanowires.

- iv. Energy Dispersive X-ray Spectroscopy to study the metals distribution in the bimetallic films.
2. Study the effect of the bimetallic/alumina materials on Hydrogen sensing
 - a. X-ray Diffraction to study the effect on the α to β phase transition.
 - b. Determine the sensitivity, response times, and reproducibility of the Pd/Ag, Pd/Ni, Pd/Pt and Pd/Cr ensembles compared to pure palladium.

1.4 Chapter Description

Feliciano *et al.* demonstrated the synthesis of monometallic Ag, Cu, and Pd nanowires by the Solid State Reduction (SSR) Method, a technique that was developed in our research group^{59,60} This method does not require the use of organic solvents, high temperature, current or voltage changes which makes it compliant with several of the principles of green chemistry. Chapter 2 of this thesis discusses modifications done to the SSR method to obtain homogeneously distributed bimetallic films supported on AAM. Chapter 3 includes the results of the characterization of our bimetallic materials by SEM, EDS, XRD and XPS. In Chapter 4 the results of the hydrogen sensing tests are presented. Finally Chapter 5 has general conclusions and recommendations followed by an appendix with additional results.

Chapter 2

MODIFICATION OF THE SOLID STATE REDUCTION (SSR) METHOD TO SYNTHESIZED NANOSTRUCTURED PALLADIUM BIMETALLIC MEMBRANES

Abstract

Recent research studies are focusing in the development of green syntheses, so that the society demands are satisfied by using more economic resources while at the same time avoiding the negative environmental impact. Achieving a green synthesis for nanomaterials while maintaining particle size control is a challenge. The Solid State Reduction (SSR) method designed in our research group to synthesize monometallic nanowires complies with various green synthesis criteria such as operation at room temperature and no excess solvent used. Our approach in this Chapter was to modify the SSR method to synthesize bimetallic films that are suitable for hydrogen sensors such as metal homogeneity and surface roughness.

2.1 Introduction

Nanotechnology is one of the most studied research topics in the past decades but the study of the properties and structures of small particles has attracted the interest of investigations for more than a century.^{21,61} Their particular properties (like quantum effect, small size effect, surface effect, tunneling effect, electronic and thermal properties, magnetic properties, etc.) allow its use in many applications. Some applied fields are energy devices, electrochemistry,

electrocatalysis, optics, electronics, analytical devices, space technology, aeronautic industry automotive engineering, construction industry, and others.^{45,48,61,62}

Metallic nanostructures are of great significance for electrochemistry, catalysis, optoelectronics, energy devices, and sensing applications.^{45,61} They are also used in biochemical, pharmaceutical, clinical (drug release)^{63,64} and environmental field for separation and pollution analysis⁴⁸ and water purification,^{65,66}

Nanostructures of Pd and bimetallic Pd are studied for sensing applications, particularly for the detection of hydrogen. As stated in Chapter 1, palladium has been studied as the active phase of hydrogen sensor due to its great capacity to adsorb hydrogen.^{2,8-10,20,22,23} Palladium-based sensors are divided in (1) palladium resistors, (2) palladium capacitors or field-effect transistors (FETs), and (3) optical sensors. Pd bimetallic nanostructures are synthesized in order to enhance the palladium sensing properties in order to overpass some limitations such as the alpha phase transition.^{1,2,5,9,22,32,36,42,43,46} Reported results show that the use of nanostructured Pd alloys reduces the damage to the film and has been demonstrated to be an alternative to surpass the mentioned α to β phase transition and others limitations.^{1,2,7,9,10,37,41} Pd alloys show an expansion of the crystal structure lattice that leads to faster kinetics for hydrogen absorption and desorption.³⁶

Bimetallic nanoparticles are also studied because they can reduce costs by minimizing the amount of noble metals by replacement or addition of other inexpensive metals.⁶⁷

Many procedures and synthesis have been developed in order to obtain highly defined bimetallic structures.⁶⁸ Some of the desired nanostructure shapes are wires (rods), core-shell, sheets, clusters, branched particles, and thin films.⁶⁸

In recent years, the need to use eco-friendly syntheses for reducing the negative environmental effects and threats has stimulated research and industrial interest.⁶⁹ Most of the methods reported in literature to synthesize nanostructures are expensive and involve the use of toxic and hazardous chemicals as the stabilizers.⁷⁰ These chemicals can be potential environmental and biological risks. Many companies have adopted green chemistry as one of their main approaches in the design of new products and processes under sustainable conditions. The principal objective behind the green chemistry, also known as sustainable chemistry, is reducing the consumption and generation of hazardous substances. There are some environmentally friendly conditions that are considered in the twelve green chemistry principles, which include operating at ambient temperature and atmospheric pressure, reducing the amount of reagents, organic solvents, and derivatives, among others. Industries also look for easier and cost-effective processes that enhance not only their productivity, but that also satisfy these green principles.

Many of the nanomaterials synthesis methods are not considered environmentally friendly, something that limits their use in large-scale applications regardless of their unique properties. This is why the development of environmental-friendly and cost-effective procedures is highly desirable for the synthesis of this type of nanomaterials.^{69, 45, 67} However, to achieve a reduction in the number of the reagents and the elimination of organic solvents while obtaining metal nanocrystals with specific shapes is a challenge.⁷¹

Zhao et al. developed a new strategy for the electrodeposition of Au/Pt alloy nanowires onto a pair of gold microelectrodes for H₂O₂ detection.^{48, 68} Their method didn't require the use of a stabilizer surfactant and pretreatment as involved in conventional wet chemical synthesis. This

method also allowed the control of the growth by changing voltage, current or frequency without changing the constituents.^{48,68} The final products were dendritic bimetallic nanowires, a crystal that develops as multi-branching tree. In their method they used two additives (in addition to the precursors) and an external voltage.

Koenigsmann et al. synthesized segmented Pd/Pt and Pd/Au nanowires, combining distinctive characteristics of each metal in a single nanostructure, under ambient, surfactantless and template-base conditions.⁴⁵ Their main focus was the need of new techniques that facilitated the electroless reduction process to replace the commonly used electrochemical and chemical reduction processes. The NWs were prepared under environmental double-diffusion conditions avoiding the use of toxic chemicals or expensive instrumentations. The used U-tube double-diffusion device has two glass half-cells separated by a polycarbonate membrane used as a template. One half-cell has the precursor solution and in the other the reducing agent solution (NaBH_4) which enters the template pores by diffusion. The nanowires were synthesized by the metals reduction that occurred when the diffusion fronts interact. They classified the one-dimensional pores as a spatially confined reaction chamber. Previous works allowed them to conclude that the rate of diffusion and reducing agent solution into the template pores depended on the pore diameters, solutions concentrations and temperature.

Other groups of researchers have synthesized bimetallic nanowires by wet-chemical methods. Fu et al. prepared Ag/Au nanowires by first adding a AgNO_3 solution into a suspension containing V_2O_3 particles where Ag nanostructures precipitated.⁶⁷ The Ag/Au nanostructures were obtained by adding an $\text{HAuCl}_4 \cdot 7\text{H}_2\text{O}$ aqueous solution in the silver suspension. The product was sonicated to form Ag-Au nanowires on the surface of the V_2O_3

particles. Ag/Au bimetallic porous nanowires were also synthesized by Shi et al.⁷² After synthesizing Ag nanowires, by a polyvinylpyrrolidone-assisted reaction in ethylene glycol, the Ag nanowires were washed in acetone and then dispersed in ethanol allowing the use of organic solvents. Chloroauric acid (HAuCl₄) was added drop-wise to the Ag NWs dispersion and based on a galvanic replacement reaction the Au-Ag bimetallic porous nanowires were synthesized. Both procedures allowed the formation of Au-Ag bimetallic porous nanowires varying the metals molar ratio by controlling the addition of HAuCl₄. These results show the formation of highly defined suspended nanowires with facile techniques in which many steps are required during the procedure.

Palladium (Pd) and palladium alloys (Pd/M) films have become materials of great interest due to their high hydrogen (H₂) adsorption capacity. Pd and Pd/M films and membranes are used for different applications such as: sensing elements^{23,30,53,54,73}, H₂ separation membranes⁷⁴, membrane reactors for hydrogenation and dehydrogenation reactions^{75,76}, among others⁷⁷⁻⁷⁹. Some palladium and palladium bimetallic films are synthesized by different techniques. The commonly used way to produce metals films is by sputtering, in which films of different thicknesses can be obtained easily. Other techniques include thermal evaporation⁵⁴, electron beam evaporation⁵⁵, chemical vapor deposition⁵⁶, atomic layer deposition⁵⁷, and electrodeposition⁵⁸.

Few green synthesizes of metallic films are actually published. One of them was reported by Zoya, who synthesized tiny silver nanoparticles at ambient room temperature. These particles showed the ability to self-assemble into films after several days.⁷⁰ They used Cetyltrimethylammonium bromide (CTAB) as stabilizing agent, silver nitrate (AgNO₃) as the

oxidant and oxalic acid ($C_2H_2O_4 \cdot 2H_2O$) as the reducer. In the report, the importance of the selection of a non harmful solvent medium, environmentally benign reducing agent and nontoxic substances for the nanoparticle stability were mentioned as key steps to achieve green chemistry.

Dinh and coworkers synthesized silver nanoparticle-reduced graphene oxide composites films. They used graphene as a building material because of its ability to hybridize with other materials, such as polymers, organic molecules and metal/metal oxides. They used water as a solvent and vitamin C as a non toxic and non hazardous reducing agent. This procedure, however, required the use high temperatures and many hours.⁸⁰

Feliciano and Quiñones showed that by the Solid State Reduction (SSR) Method, a technique that was developed in our research group, defined monometallic nanowires can be obtained.^{59,60} This method does not require the use of organic solvents, high temperature, current or voltage changes which makes it compliant with several of the principles of green chemistry.

This Chapter includes results showing that through a modification of the SSR method bimetallic films are formed on both sides of the AAM template used as a support, in addition to the nanowires inside its pores. The results presented here show that SSR is as an easy, cost effective and eco-friendly way to synthesize nanowires and films. The final morphology makes it useful for different applications such as hydrogen sensing, as will be discussed in following chapters.

2.2 Experimental Methods

2.2.1 Materials

Palladium (II) nitrate [$Pd(NO_3)_2 \cdot xH_2O$, 99.9% metal basis Alfa Aesar],

tetraammineplatinum(II) nitrate [Pt(NH)₄(NO₃)₂, Sigma Aldrich], nickel (II) nitrate hexaydrate [Ni(NO₃)₂•6H₂O, 99% metal basis Alfa Aesar], silver nitrate [AgNO₃, 99.9% metal basis Alfa Aesar] and chromium (III) nitrate nonahydrate [Cr(NO₃)₃•9H₂O, 99% Fisher Scientific], were used as the metal precursors while commercial anodic alumina membranes (AAM) [Whatman Anodisc inorganic filter membranes, 25mm, 0.02µm pores size, Sigma Aldrich] were used as a support. Deionized water was used as solvent and Sodium Borohydride as reducing agent.

2.2.2 Methodology Modifications

Pure palladium films on AAM templates were previously synthesized in our research group using the SSR method by incorporating the precursor in powder form. However, as it was developed, the method had limitations to obtain a homogeneous distribution of more than one metal. Understanding this, the first modification was to incorporate the metals using aqueous precursor solutions.

Specific quantities of Pd and a second metal (M = Pt, Ag, Ni, Cr) precursors salts were dissolved in 30 µL of deionized water to obtain a total metal loading of 5% wt and a relative molar concentration of Pd₉₀M₁₀. After sonication of the resulting solutions for five minutes they were added to one side of the AAM using incipient wetness impregnation. The materials were then dried in air. Metal reduction was attained by spreading a small pellet of approximately (~0.006 g) of solid sodium borohydride (NaBH₄). NaBH₄ and remaining solid products were removed by dipping the membranes in cold deionized water three times for 30 minutes.

In order to study the effect of the reduction conditions on the morphology of the films different operational conditions were considered as detailed in the discussion.

To study the formation of nanowires inside the pores of the AAM support, the support was dissolved in a 1.0 M aqueous sodium hydroxide solution (NaOH) during a period of 24 hours.

2.3 Results and Discussion

Figure 2.1 shows the SEM images of the Pd₉₀Ni₁₀ bimetallic films using different modifications of the SSR method. These modifications were performed with the objective to study their effect on the morphology of the resulting films. The images on the left column (1) correspond to the films formed on the impregnation side and the images on the right column (2) correspond to the films formed on the reduction side. In each case, the precursors in the membrane changed to a dark color when the NaBH₄ was spread suggesting that the metals were reduced and was also observed by Feliciano⁵⁹ when using the method to synthesize monometallic nanowires.

Through all the modifications to obtain bimetallic films on either side of the AAM were formed. A rougher film was observed in the impregnation side when compared to the reduction side. This was also observed for a pure palladium sample with the precursor salt incorporated by wet impregnation as observed in Figure 2.2. Observations, however, are based solely on the SEM images as attempts to quantify the roughness of each film proved difficult with the use of atomic force microscopy and a profilometer due to the unevenness of the films' surface.

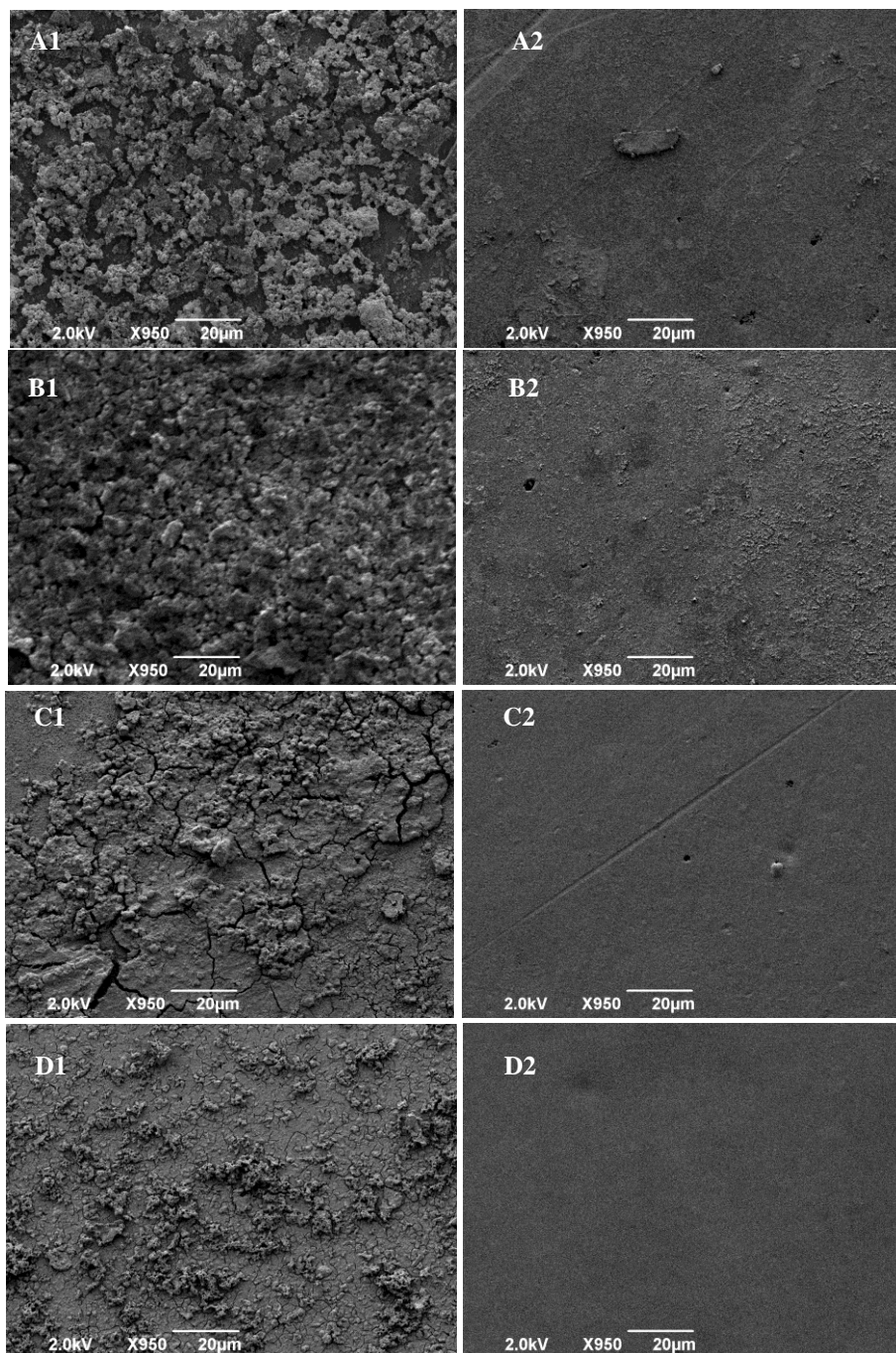


Figure 2.1 SEM images of Pd₉₀Ni₁₀ films obtained after different synthesis modifications (left: impregnation side, right: reduction side). A-without adding 2μL of DI water during reduction and air dried, B- adding 2μL of DI water during reduction and air dried, C- adding 2μL of DI water during reduction and oven dried at 50°C for 15 min, and D- adding 2μL of DI water, dried in air and treated under H₂ flow (100ccm) in an oven at 130°C for 3 hours.

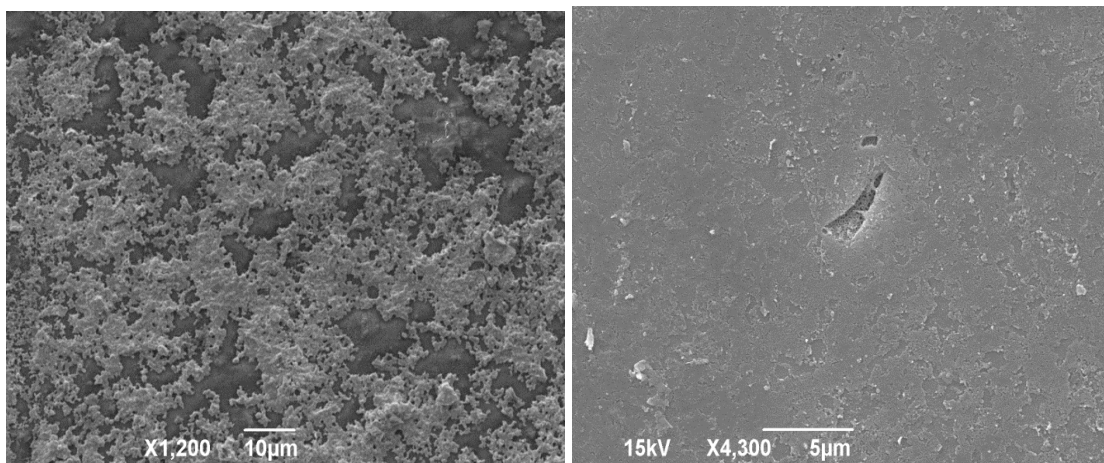
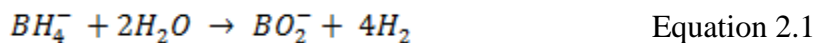


Figure 2.2 Pd films formed by the adding the precursor by wet impregnation and adding 2uL water during reduction [left-the precursor side, right- reduction side]

Sample A in Figure 2.1 was reduced with the typical SSR method, using a NaBH₄ pellet for reduction without adding water, whereas sample B was synthesized with the addition of 2 μL of deionized water during the reduction process. Both were dried in air at room temperature. The addition of water promoted the formation of a rougher uniform film on the precursor side as observed in Figure B1.

The difference observed between these two modifications can be explained by looking at the reaction of water reacts with the borohydride ion to produce hydrogen gas (as presented below) which enables the metals reduction.⁸¹



In the first reduction method the sodium borohydride reacts with water that has been absorbed from the ambient in the sample, either in the pores of the AAM or due to the hydrophilicity of the palladium salt. The fact that the reaction takes place shows that there is water present in the sample. However, when water is added to the sample it ensures that an

excess amount of water is present so that all the sodium borohydrate reacts. These results suggest that when an excess amount of water is present, the kinetics of the reaction are faster and a rougher film is formed. It also suggests that using water the complete reduction of the metal is promoted. X-ray photoelectron studies are presented in Chapter 3 studying the oxidation state of the metals after synthesis.

Sample C was synthesized adding 2 μ L of deionized water in the reduction process and dried in a furnace at 50°C for 15 minutes. Comparing both, the oven dried sample yielded a smoother bimetallic film but with significant cracks on the precursor side (C1) as a result of some stress.^{9,10,38,39} These stress can be attributed to the sudden desorption of internal water from the material with temperature.

Figures D1 and 2 show the films of the membrane synthesized through the SSR method with the addition of 2 μ L of deionized water, dried in air, and treated under hydrogen flow (100ccm) in an oven heating in a rate of 5°C/min up to 130°C for 3 hours to improve the metals reduction. Small cracks were detected and a smoother film was obtained. The temperature provokes some internal stress which can cause the small cracks but, in contrast to the sample in Figure C, the sample should not suffer an abrupt desorption of water due to the slow temperature ramp used. In addition, the use of hydrogen as reducing agent promotes the complete metal reduction. The smoothness of the films can be as a result of a complete metal reduction and an annealing process.

These results suggest that the addition of 2 μ L of deionized water and air drying yield a rougher uniform film without cracks on the impregnation side. Previous work in our research group, using monometallic palladium film, demonstrated that the rougher film exhibited a more

stable sensor response. A possible explanation is that the increased surface area allows a better contact with the electrodes and also probably enhances the hydrogen adsorption process. Therefore, this is the synthesis method that was chosen for the synthesis of other bimetallic materials in Chapter 3.

The morphology of these films are the inverse to what was observed when the precursors were incorporated in solid form where the rougher film is formed on the reduction side. This difference is presumably due to the location with highest water concentration. In wet impregnation there is a greater amount of water on the side on the impregnation side whereas in solid impregnation there is a higher water concentration on the reduction side (Figure 2.3). These results suggest that the reduction is more abrupt where more water is present through reaction 2.1.

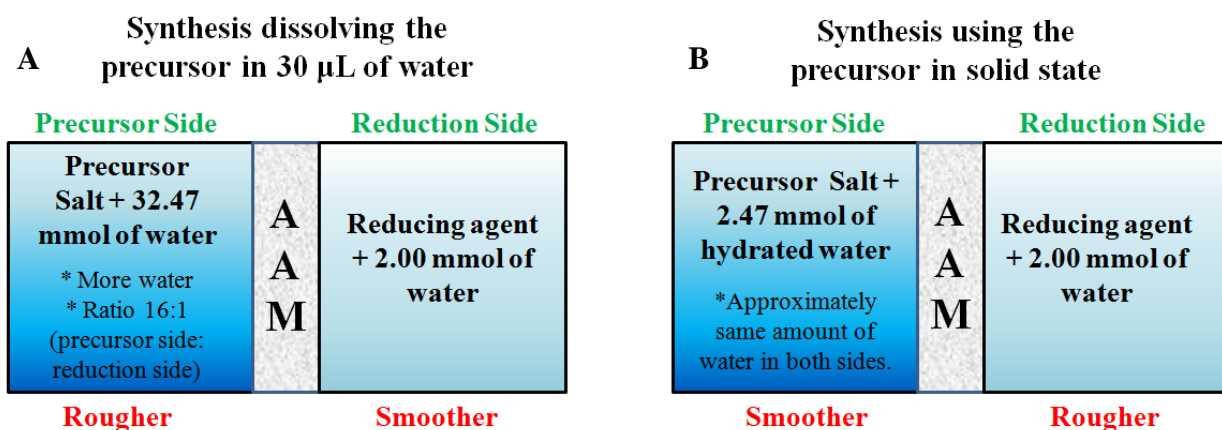


Figure 2. 3 Water added in each side of the AAM membrane during the synthesis by SSR. (A) Using the precursors dissolved in 30 µL of water, and (B) the solid precursor salt without dissolved it in water

In addition to the bimetallic films, the SSR synthesis method also yielded bimetallic nanowires in the pores of the AAM. Figure 2.4 shows the formation of Pd₉₀Ni₁₀ nanowires (NWs). Nanowires show variations in diameter. These variations in diameter occur along the

same nanowire and between each of them. The variations in the same nanowire show the tapering of the NW diameters near the middle of it. Feliciano and Martínez⁵⁹ also observed this phenomenon. Comparing all Pd₉₀Ni₁₀ nanowires, the diameters ranged between 149 and 204 nm with relative standard deviations (standard deviation divided by the sample average value) of 8% and 2%, respectively. Some of the observed variations between the nanowires diameters are caused because not all of them can be observed at the same depth on the SEM images. Also, there is a gradient in the pore size along the alumina membrane, in where the smallest pore size of 0.02μm corresponds to the side that has the polypropylene support ring, to 0.2μm in the opposite side which contributes to the tapering.⁸² The precursor solutions were added on the side of 0.2μm pores. Considering the 0.2μm AAM pores size, the SEM results corroborate the formation of the nanowires inside the AAM pores ($d_{nanowires} < d_{AAM-pores}$).

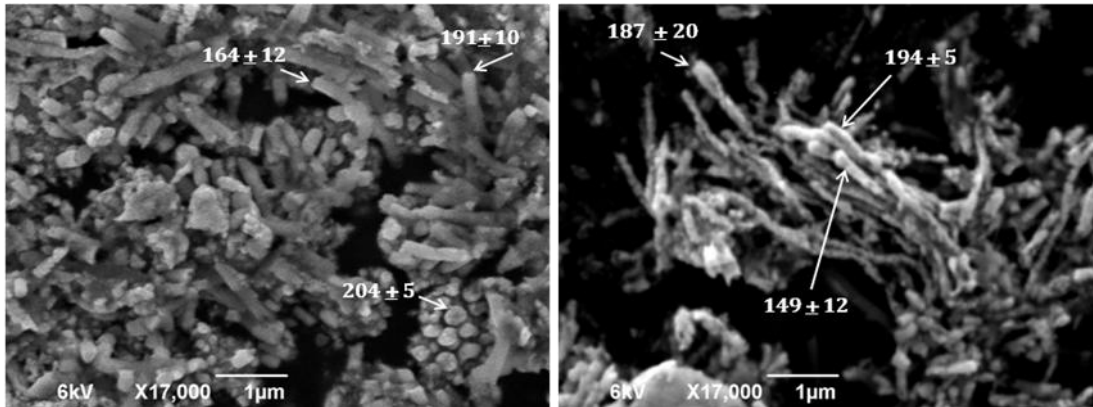


Figure 2.4 SEM images of Pd₉₀Ni₁₀ NWs

The SEM micrographs in Figures 2.5 and 2.6 show that the formation of nanowires also occurs for Pd₉₀Pt₁₀ and Pd₉₀Ag₁₀. Similar to the Pd₉₀Ni₁₀ nanowires, Pd₉₀Pt₁₀ and Pd₉₀Ag₁₀ nanowires also show variations in diameters. Their diameters ranged from 124 to 171 nm and

from 118 to 175 nm, respectively. The former had a relative standard deviation (RSD) of 15%, while the latter was 20%. The differences in diameter sizes suggest that the nanowires have a greater diameter at their ends, where the nanowires formation is presumed to be easier, and decreases as it goes into the middle of the nanowires.

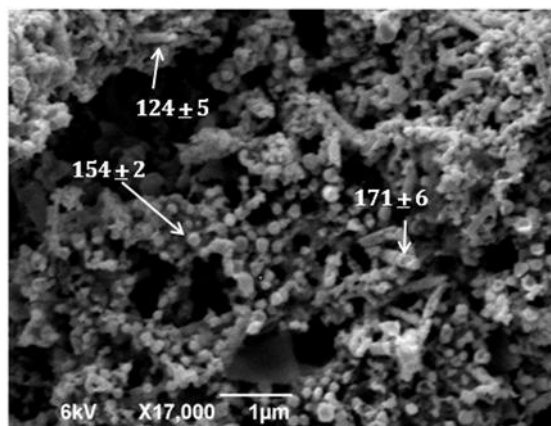


Figure 2. 5 SEM image of Pd₉₀Pt₁₀ NWs

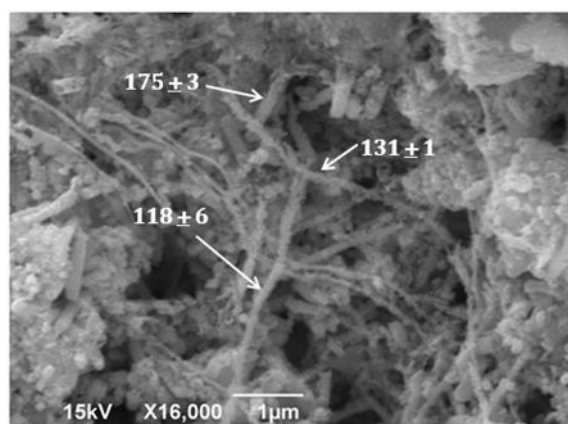


Figure 2. 6 SEM image of Pd₉₀Ag₁₀ NWs

2.4 Conclusions

The modification of the published SSR method by adding bimetallic precursor salts in solution to obtain films and nanowires supported on AAM was successful. The method complies several of the principles of green chemistry as it does not need organic solvents, high temperature, current or voltage changes.

In addition SEM results showed that by slight post modifications of the SSR method it is possible to change the final morphology of the films. Smoother films are obtained when the metal sample is post treated with hydrogen. In addition some cracks were detected when the membrane was dried at 50°C as a result of the sudden desorption of water from the film. For the application in hydrogen sensing presented in following chapters rougher films are desired and the optimal synthesis conditions are the addition of 2 μL of deionized water during the reduction process and drying in air at room temperature. This allows to obtained rougher films avoiding cracks in the films' surfaces.

Chapter 3

PALLADIUM BIMETALLIC FILMS CHARACTERIZATION

Abstract

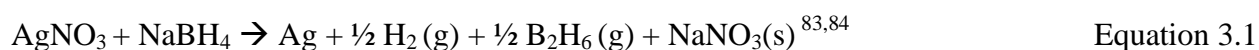
In order to understand the applicability of bimetallic Pd/Pt, Pd/Ag, Pd/Ni and Pd/Cr films synthesized via the modified SSR method as hydrogen sensors they needed to be further characterized and the results are presented in this Chapter. Scanning Electron Microscopy (SEM) and Energy Dispersive X-Ray analysis (EDAX-EDS) were used to study their morphology and metal distribution. X-Ray Diffraction (XRD) patterns were used to determine the crystallinity of the metals in the films, relative concentration of the metals and the effect of the second metal on the Pd phase transition. Finally X-Ray Photoelectron Spectroscopy (XPS) was used to study the oxidation state of the metals and to verify the absence of impurities that might remain after synthesis.

3.1 Introduction

As explained in Chapter 1, palladium is being studied as a hydrogen sensing material for its strong interactions with it through adsorption, absorption, migration and desorption mechanisms.^{2,8-10,20,22,23} However, mechanical stresses related to its alpha to beta phase transition at high hydrogen concentrations and other limitations warrant the need for sturdier materials.²⁰ Pd bimetallic nanostructures have demonstrated to circumvent some of these limitations and are thus a promising alternative in the hydrogen sensing field.^{1,2,7,9,10,26,27}

These limitations were observed in our research group in pure palladium films synthesized by the SSR method which was a motivation to study Pd bimetallic films. The synthesis of these bimetallic films was done by the modified SSR method described in Chapter 2, although this chapter includes more details. In order to study the morphology, metal homogeneity distribution, the crystalline phases and the oxidation states of our bimetallic films several characterization techniques were used and the results are presented in this chapter.

To understand the results it is important to consider the reduction reactions of the precursors salts used with NaBH₄:



The products of these reactions are the desired metallic species, gaseous species (H₂, H₂O, NO₂, B₂H₆) and white crystalline powders (NaNO₃ and NaBO₂) that are soluble in water.^{86,87} The reducing agent (NaBH₄) is also soluble in water.⁸⁸ Therefore the washing process in a cold bath can remove the byproducts and unreacted reducing agent. Considering the ligands bounded to the metals in Pd(NO₃)₂•H₂O and Pt(NH₃)₄ (NO₃)₂ similar byproducts are expected to be obtained in their respective reduction reactions.

3.2 Experimental Methods

3.2.1 Materials

Palladium (II) nitrate [Pd(NO₃)₂xH₂O, 99.9% metal basis Alfa Aesar], tetraammineplatinum(II) nitrate [Pt(NH₃)₄(NO₃)₂, Sigma Aldrich], nickel (II) nitrate hexaydrate

[$\text{Ni}_2\text{NiO}_6 \cdot 6\text{H}_2\text{O}$, 99% metal basis Alfa Aesar], silver nitrate [AgNO_3 , 99.9% metal basis Alfa Aesar] and chromium (III) nitrate nonahydrate [$\text{Cr}(\text{NO}_3)_3 \cdot 9\text{H}_2\text{O}$, 99% Fisher Scientific], were used as the metal precursors while commercial anodic alumina membranes (AAM) [Whatman Anodisc inorganic filter membranes, 25mm, 0.2 μm pores size, Sigma Aldrich] were used as a support. Deionized water was used as solvent and sodium borohydride as reducing agent.

3.2.2 Methodology

Considering the literature cited in Chapter 1, bimetallic films with a $\text{Pd}_{90}\text{M}_{10}$ concentration were synthesized where M= Pt, Ni, Ag, and Cr. The materials were obtained via the modified SSR Method studied in Chapter 2. For each combination the metal precursors were first dissolved in 30 μL of deionized water and added by incipient wetness impregnation in quantities such that a total metal loading of 5%wt was maintained. For the $\text{Pd}_{90}\text{Pt}_{10}$ film 0.8 mg of Tetraammineplatinum(II) nitrate [$\text{Pt}(\text{NH}_3)_4(\text{NO}_3)_2$, Sigma Aldrich] was mixed with 4.4 mg of [$\text{Pd}(\text{NO}_3)_2 \cdot \text{H}_2\text{O}$ Alfa-Aesar]. For the $\text{Pd}_{90}\text{Ni}_{10}$ sample 0.7 mg of nickel (II) nitrate hexahydrate [$\text{Ni}(\text{NO}_3)_2 \cdot 6\text{H}_2\text{O}$, Alfa Aesar] was mixed with 5.2 mg of $\text{Pd}(\text{NO}_3)_2 \cdot \text{H}_2\text{O}$. For the $\text{Pd}_{90}\text{Ag}_{10}$ sample 0.4 mg of silver nitrate [AgNO_3 , Alfa Aesar] was mixed with 4.9 mg of $\text{Pd}(\text{NO}_3)_2 \cdot \text{H}_2\text{O}$. Finally, for $\text{Pd}_{90}\text{Cr}_{10}$ a 0.9 mg of Chromium(III) nitrate nonahydrate [$\text{Cr}(\text{NO}_3)_3 \cdot 9\text{H}_2\text{O}$, Fisher] was mixed with 4.6mg of the palladium precursor salt. The solutions were sonicated for 5 minutes and then added by impregnation to the Anodisc membrane. The materials were then dried in air. Metal reduction was attained by spreading a small pellet (~ 6mg) of solid sodium borohydrate (NaBH_4) with 2 μL of deionized water on the opposite side of the membrane. In each case a small amount of NaBH_4 remains suggesting that the quantity used was in excess.

This excess, along with any solid product, was removed by dipping the membranes in cold deionized water three times for 30 minutes. Figure 3.1 shows a schematic of the modified SSR synthesis process.

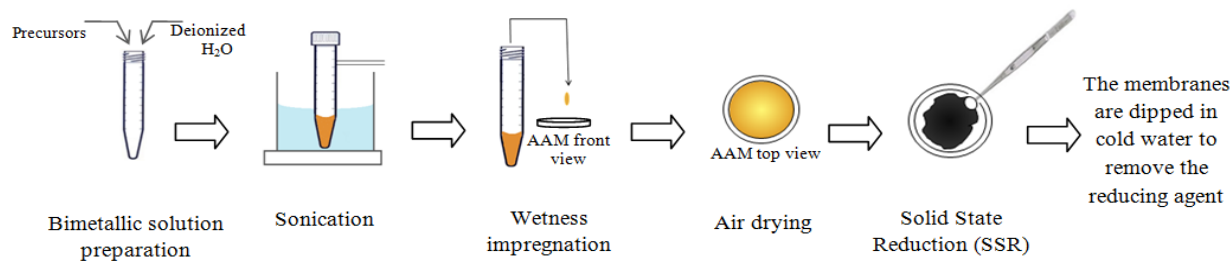


Figure 3. 1 Bimetallic membrane synthesis using a modification of the Solid State Reduction method.

The morphology, composition, and homogeneity of the bimetallic films and nanowires were characterized by Scanning Electron Microscopy (SEM) in a JEOL JSM – 6390 equipped with an Energy Dispersive Analysis with X-Ray (EDS) detector. To study the films obtained in both sides of the AAM template a piece of each of the Pd/M/AAM was placed in the sample holder using carbon tape and an acceleration voltage of 2.0 kV was used.

The XRD analyzes was performed using a Siemens D500 X-Ray Diffractometer, with a CuK α radiation operating at 40 kV and 40 mA. The synthesized Pd/M/AAMs were positioned in the center of the sample holder assuring a flat surface. The analysis was performed at a scanning speed of 0.002 °/sec and small step sizes (0.01°) to reduce the XRD background effect. A two theta (2θ) interval from 5° to 90°, which is enough for the identification of the samples characteristic peaks, was used to obtain the XRD patterns.

XPS experiments were performed using a PHI 5000 VersaProbe. The analysis was performed using a monochromatic Al K α X-ray Source operated at 23.98W. The full energy range scans were done at a pass energy of 187.85 eV and 0.800eV step size. These scans are

done to verify the presence of the metals and the elimination of the reducing agent. Specific element scans were done at a pass energy of 29.35eV and 0.125V step size for chemical states analysis. The binding energy was calibrated by palladium 3d_{5/2} binding energy at 335.2 eV which also shifted the C 1s binding energy to acceptable values as described in Phi Handbook of X-ray Photoelectron Spectroscopy⁸⁹ and NIST X-Ray Photoelectron Spectroscopy Database⁹⁰. Three testing points were studied for each sample and for the films formed on each side of the AAM to determine reproducibility and homogeneity.

Peak deconvolution of the element peaks and qualitative elemental analysis were done in the Casa XPS Software.^{91,92}

3.3 Results and Discussion

3.3.1 Scanning Electron Microscopy Results

Using the determined optimal synthesis conditions, nanostructured bimetallic membranes with compositions Pd₉₀Ag₁₀, Pd₉₀Pt₁₀ and Pd₉₀Ni₁₀ were obtained. Consistent with the Pd/Ni results SEM micrographs presented in Chapter 2, the films obtained with Pd₉₀Ag₁₀, Pd₉₀Pt₁₀ had a rougher texture on the side where the precursors were added as seen in Figure 3.2. Figure 3.3 shows that for the Pd₉₀/Cr₁₀ sample a film was not formed on the reduction side. The Pd₉₀/Cr₁₀ films were analyzed only by SEM since hydrogen sensing results (presented in the Chapter 4) showed that this bimetallic material was not practical as a sensing material for hydrogen detection.

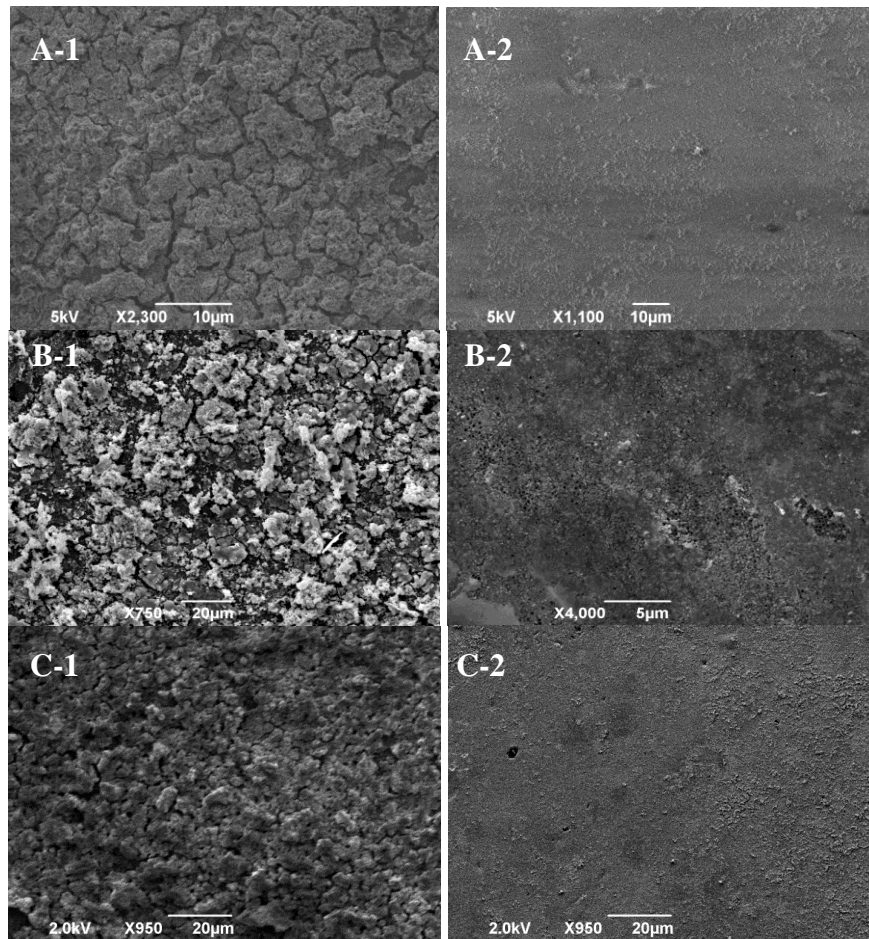


Figure 3.2 SEM micrographs of (A) Pd₉₀Ag₁₀, (B) Pd₉₀Pt₁₀ and (C) Pd₉₀Ni₁₀ films. Left and right side images show the impregnation and reduction side films, respectively.

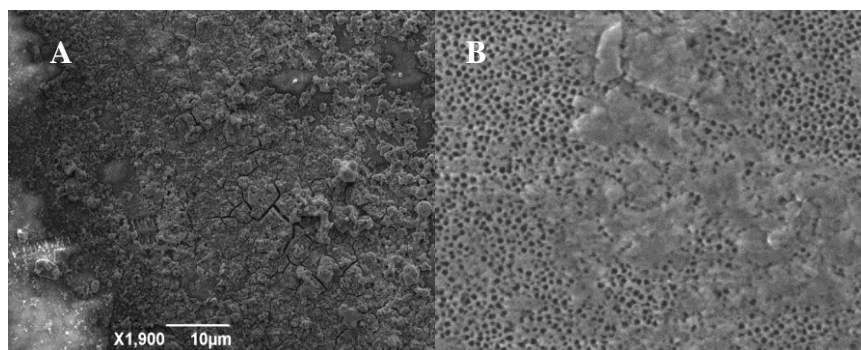


Figure 3.3 SEM micrographs of Pd₉₀Cr₁₀ sample (A) impregnation and (B) reduction sides.

3.3.2 X-Ray Diffraction Results

Figure 3.4 shows the XRD patterns of the bimetallic films. All the samples show the characteristic crystalline Pd peaks evidencing that it was at least partially reduced. For the Pd₉₀Ag₁₀ sample both Pd and Ag peaks are present concluding that both metals were at least partially reduced with the SSR method as shown in Figure 3.4 A. There is a shift, however, in the position of the characteristic Ag peak to higher angles suggesting that there is an alloy like interaction between both metals vs. a physical mixture.

Figure 3.4 B shows the XRD pattern of Pd₉₀Pt₁₀. It was not possible to differentiate the Pd and Pt peaks as they appear theoretically at very similar angles. This and the fact that the Pt is at a much lower concentration difficult the identification of its peaks. However there is an asymmetry in the Pd peak that suggests that the Pt is present in reduced state.

Figure 3.4 C shows that for the Pd₉₀Ni₁₀ sample, the Ni characteristic peaks are not present. Since the Ni peaks are at distinct positions, these results suggest that the synthesized Ni particles are either very small or not reduced. Similar results were observed by Chou et al. who studied the effect of NaBH₄ in the reduction of NiCl₂ to form Ni thick films.⁹³ They varied the NaBH₄:NiCl₂ to study the effect of the reducing agent on the Ni reduction. Only the smaller addition of NaBH₄ ([NaBH₄] / [NiCl₂] = 0.125) showed very Ni weak peaks in the XRD patterns suggesting that the reducing agent interfered with the crystallization of their Ni nanoparticles. Reported results also show that the Ni-B alloy was formed when the reduction process is carried out at room temperatures showing amorphous substances with complete absence of crystalline peaks in the XRD patterns.^{93,94} Therefore, an increase in temperature for the annealing process was required in order to promote the crystallization and at 300K began to appear several

characteristics peaks.^{93,94} The diffraction peaks of the Ni(111), Ni(200) and Ni(220) were fully developed at 703K. This partially explains the absence of Ni crystalline peaks in our XRD patterns and allows to conclude that at ambient temperature, Ni might not be reduced by the SSR method.

In addition, reported results suggest that the anhydrous precursors require a lower activation energy than the hydrated precursors to react.⁸⁵ The heat of reaction is lower in precursors that don't contain water of hydration or the water of hydration is lower.⁸⁵ Considering that the silver and platinum salts are anhydrous and palladium salt monohydrate, the fact that the used nickel salt is hexahydrated can be the reason for the limitations in the nickel reduction by SSR method. Also, the $\text{Cr}(\text{NO}_3)_3 \cdot 9\text{H}_2\text{O}$ salt used on the PdCr sample was the more hydrated salt used during our experiments and this suggests that in this sample the Cr was not reduced.

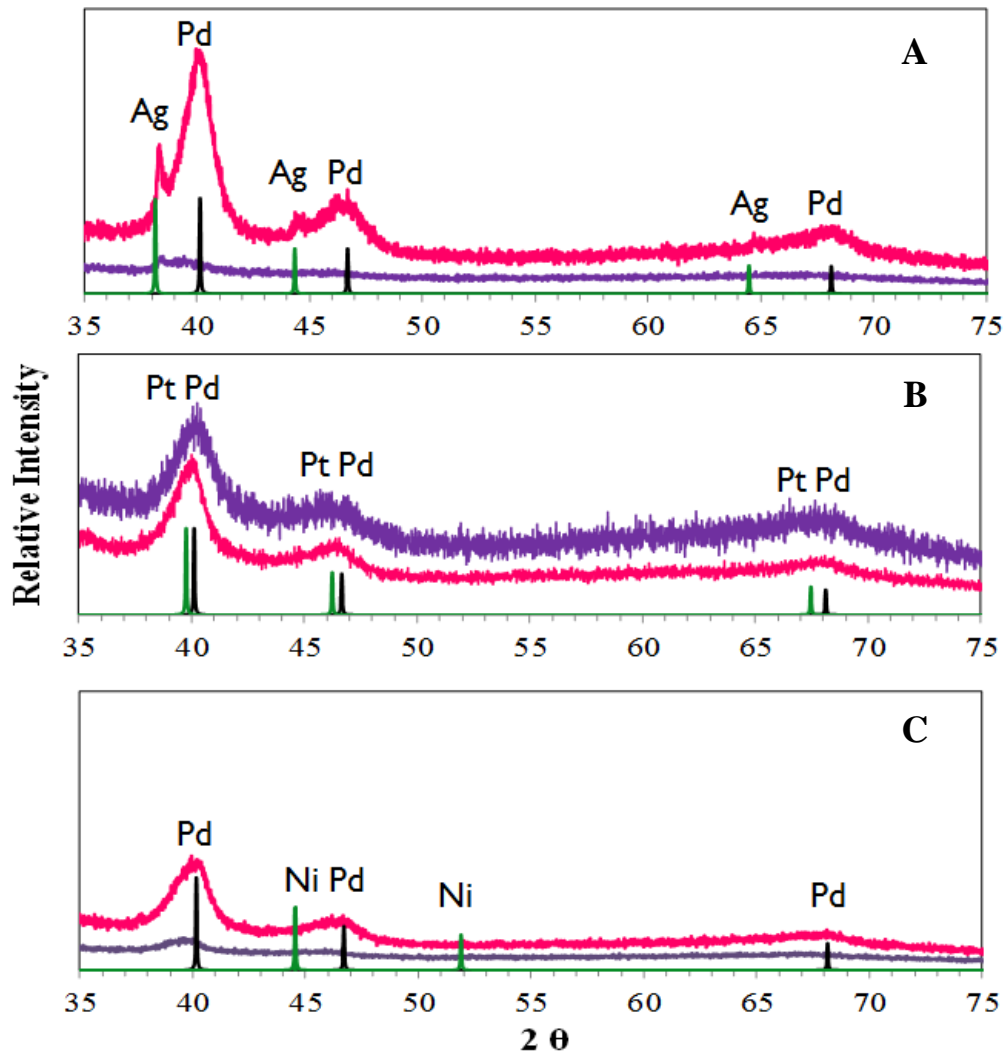


Figure 3. 4 XRD results of the Pd₉₀Ag₁₀ (A), Pd₉₀Pt₁₀ (B) and Pd₉₀Ni₁₀ (C) films

— Bimetallic film in the side where the NaBH_4 was spread, — Bimetallic film in the side where the precursors were added, — Pd theoretical , — M theoretical (Ag, Pt and Ni respectively)

3.3.3 Energy Dispersive X-Ray Results

Figures 3.5, 3.6 and 3.7 show the Energy Dispersive X-Ray results of both films formed on either side of the AAM for Pd/Ag, Pd/Pt and Pd/Ni, respectively. These results suggest that for all the metal combinations and for both films formed the metal distribution was homogeneous. Moreover, these mappings suggest that there is a higher metal concentration in the film formed on the impregnation side for all bimetallic mixtures as evidenced visually by the more intense colors.

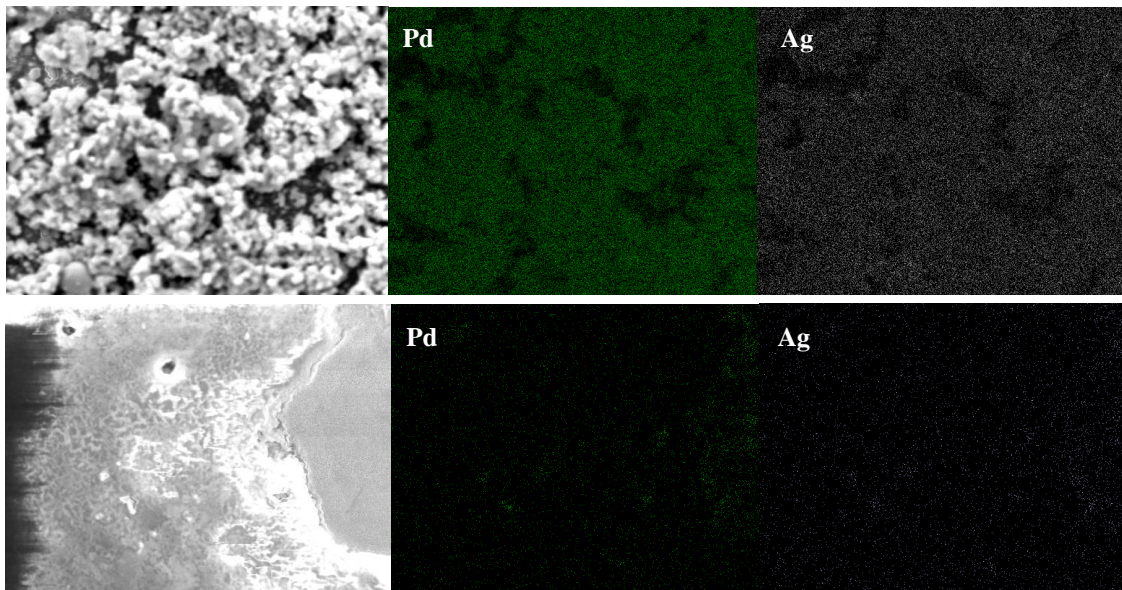


Figure 3. 5 Metals distribution in Pd₉₀Ag₁₀ obtained with EDS. First and second row correspond to the impregnation and reduction side, respectively.

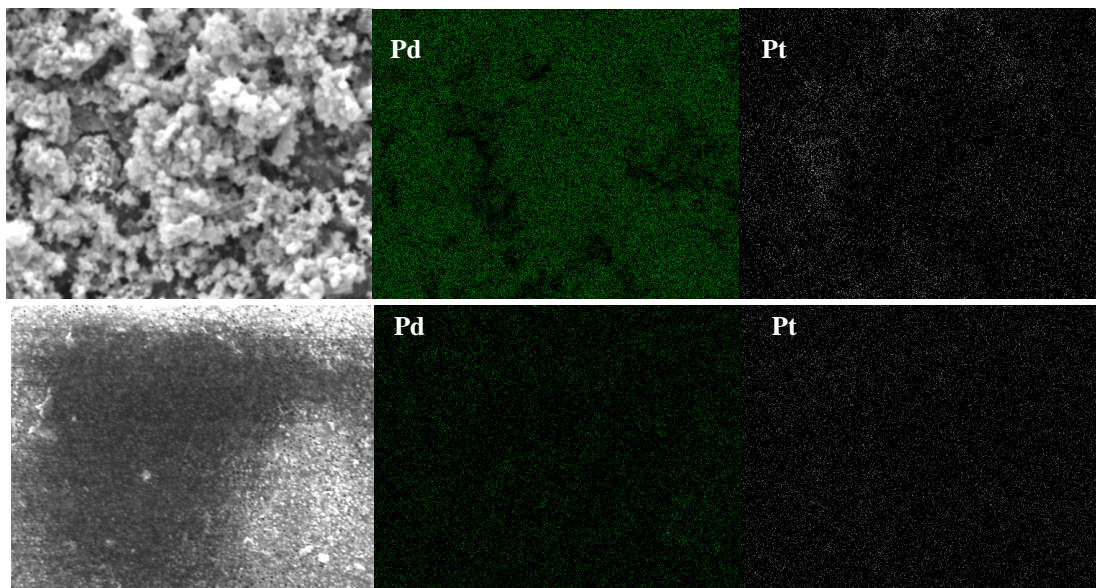


Figure 3. 6 Metals distribution in Pd₉₀Pt₁₀ obtained with EDS. First and second row correspond to the impregnation and reduction side, respectively.

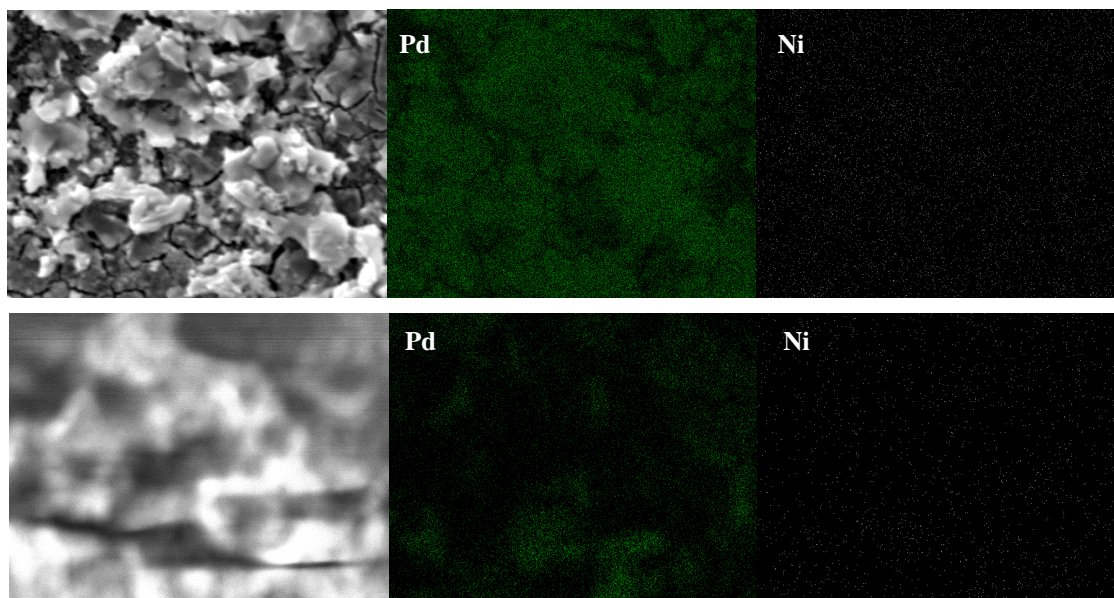


Figure 3. 7 Metals distribution in Pd₉₀Ni₁₀ obtained with EDS. First and second row correspond to the impregnation and reduction side, respectively.

3.3.4 Elemental Analysis with X-Ray Photoelectron Spectroscopy

The full scan XPS spectrums for all the samples are presented in Figures A1-A6 . Sodium and boron elements are not detected in 95% of our spectrums (17 out of 18) suggesting that the cleaning process after the reduction is efficient.

These spectrums were analyzed to obtain the surface elemental composition and the results are summarized in Table 3.1. The results show Pd concentrations for the Pd/Ag and the Pd/Pt surfaces lower than expected. For the Pd/Ag sample this might be due to a poor interaction between Ag with the AAM support compared to Pd. This weak Ag interaction with alumina was previously reported by Khan *et al.* in a Pd-Ag catalyst supported on alumina.⁹⁵ Their results showed the formation of Pd-Ag alloy particles with Ag segregated in the surface. No reported results were found to support the same segregation for Pt in Pd/Pt supported on AAM, but these results suggest a similar behavior.

The Pd₉₀/Ni₁₀ XPS results, on the other hand, show lower nickel concentrations than the expected 10% and in three sample points nickel was not detected. These results, combined with the XRD results suggest that SSR does not reduce the [Ni(NO₃)₂]•6H₂O salt. Moreover, the absence of Ni peaks in the XPS suggests that the salt was removed from the surface when the material was washed. This agrees with the Pd/Ni XRD results, the results obtained by Chou *et al* and the low reducibility of hydrated nickel salts discussed above. Table 3.2 shows the standard reduction potential of the studied metals in which it can be observed that the values for the Pd²⁺, Ag¹⁺, and Pt² are positive whereas for Ni²⁺ and Cr³⁺ they are negative.⁹⁶ Ni²⁺ and Cr³⁺ then prefer to be in oxidized states thus needing more energy to be reduced. The synthesis of Ni nanoparticles using water as the solvent is also unfavorable promoting the formation of oxidized

species.⁸⁵ This is evidenced in the analysis of the metals chemical states presented in the next section.

Table 3. 1 Palladium Bimetallic Films Elemental Analysis

<i>Bimetallic Membrane</i>		<i>Precursors side</i>		<i>Reduction Side</i>	
		<i>Pd Atomic %</i>	<i>M (Ag, Pt, Ni) Atomic %</i>	<i>Pd Atomic %</i>	<i>M (Ag, Pt, Ni) Atomic %</i>
<i>Pd90/Ag10</i>	<i>Sample 1</i>	89.89 %	10.11 %	82.19 %	17.81 %
	<i>Sample 2</i>	84.55 %	15.45 %	84.48 %	15.52 %
	<i>Sample 3</i>	81.21 %	18.79 %	72.89 %	27.11 %
<i>Pd90/Pt10</i>	<i>Sample 1</i>	81.87 %	18.13 %	88.13 %	11.87 %
	<i>Sample 2</i>	77.12 %	22.88 %	0.00 %	0.00 %
	<i>Sample 3</i>	77.35 %	22.65 %	82.71 %	17.29 %
<i>Pd90/Ni10</i>	<i>Sample 1</i>	97.09 %	2.91 %	100.00 %	0.00 %
	<i>Sample 2</i>	95.83 %	4.17 %	96.77 %	3.23 %
	<i>Sample 3</i>	100.00 %	0.00 %	0.00 %	0.00 %

Table 3. 2 Standard Reduction Potentials⁹⁶

<i>Precursor Salt</i>	<i>Metal Charge</i>	<i>Reduction Reaction</i>	<i>E° (volts)</i>
<i>Pd(NO₃)₂•H₂O</i>	2+	$Pd^{2+} + 2e^- \leftrightarrow Pd_{(s)}$	0.915
<i>AgNO₃</i>	1+	$Ag^{1+} + 1e^- \leftrightarrow Ag_{(s)}$	0.799
<i>Pt(NH₃)₄(NO₃)₂</i>	2+	$Pt^{2+} + 2e^- \leftrightarrow Pt_{(s)}$	1.180
<i>[Ni(NO₃)₂]•6H₂O</i>	2+	$Ni^{2+} + 2e^- \leftrightarrow Ni_{(s)}$	-0.236
<i>Cr(NO₃)₃•9H₂O</i>	3+	$Cr^{3+} + 3e^- \leftrightarrow Cr_{(s)}$	-0.740

3.3.5 Chemical states analysis using X-Ray Photoelectron Spectroscopy

Deconvolution of the peaks of the elemental XPS results was needed in order to determine the chemical environment and chemical state of the metals. This deconvolution is presented for all the samples in Figures C.1-C.12 of the Appendix but the results for all the samples is summarized in the tables below. Published reports, the NIST Database and the PHI

Handbook of X-ray Photoelectron Spectroscopy were used to identify the deconvoluted peaks.

57,89,90,95,97–103

The interpretation of XPS results poses unique difficulties when used for chemical states analysis.¹⁰¹ For example, the analysis of transition metal 2p spectrum has many complications as consequence of shake-up, plasmon loss structures, and multiplet splitting.¹⁰¹ Shake-up satellite lines occur frequently in paramagnetic compounds. Satellite peaks are formed if during the photoelectric process the ion left in an excited state with a few electron volts (eV) above the ground state which reduce the kinetic energy of the emitted photoelectron.⁸⁹ Therefore additional peaks can be formed at higher binding energies than the main peak (lower kinetic energy). The multiplet splitting occurs in the ionization of p levels. This effect increases the spin doublet separation in the first row of transition metals increasing the distance between $2p_{1/2}$ and $2p_{3/2}$.⁸⁹ It also generates more asymmetric peaks which makes difficult its characterization. This occurs when the emission of a core electron that has a spin, *i.e.* unpaired electron in valence levels, creates a vacancy. The unpaired electron that left the s-orbital can create an ion with other unpaired electron in the atom which allows many possible final configurations and many energies.⁸⁹ Energy can be lost as consequence of the interaction between the photoelectron and other electrons in the surface of the analyzed sample. This effect provokes plasmon loss structures. This effect in metals is more significant reflecting Auger lines at higher binding energy with lower intensities.⁸⁹ These and other effects make the analysis of the first row transition metals difficult.

The main objective of this section was to study the metals' oxidation state to determine the efficiency of our SSR method. Therefore, the possibility to detect the characteristic peaks of the reduced metals, oxidized species and the commercial salts was considered. The chemical environment was also considered, but it is not the main scope of this section.

The oxidation state of palladium, platinum and nickel shifts the peak from the peak of the reduced metal to higher binding energy (BE). Silver is a notable exception to other metals in that the peaks at an oxidized state are reported to shift to lower binding energies. In addition silver metal (Ag(0)) shifts an additional -0.7 eV when it interacts with palladium at a molar ratio of Pd₉₀/Ag₁₀, but palladium peaks do not shift when it interacts with silver.^{95,100}

Table 3.3 summarizes the XPS results obtained for the Pd and Ag peaks obtained for Pd₉₀/Ag₁₀ films at the three sample points and on the films formed on each side the Pd₉₀/Ag₁₀ films after deconvolution. The BE of the Ag metals were at 367.52 ± 0.02 eV with its respective spin-orbit splitting values. This value corresponds to reduced Ag when considering the mentioned shift of -0.7 eV observed when Ag interacts with Pd. These results show that the Ag is interacting with palladium and that it was reduced efficiently by the SSR. This interaction suggests the formation of Pd-Ag alloys. This agrees with results observed in XRD where the Ag peaks were observed to shift to higher values.

Table 3. 3 XPS results of Pd₉₀/Ag₁₀ after peaks deconvolution using CASA-XPS

Metal	Precursor Side		Reduction Side	
	Peak		Peak	Description
Pd	335.201 ±0.003 eV	Pd (0) ^A	335.201 + 0.004 eV	Pd (0) ^A
	336.5 ±0.3 eV	PdO ^B Pd(2+)	336.916 eV	PdO ^B Pd(2+)
Ag	367.9 + 0.5eV	Ag (0) ^C	367.4635 + 0.02eV	Ag (0) ^C
	367.51 + 0.01 eV	Ag (0) reacting with Pd(0) ^C	367.571 eV	Ag (0) reacting with Pd(0) ^C
Small additional contribution	369.847 eV	unknown 369.0 eV for Ag ₅ Al ₉₅ ^A	369.418 eV	unknown 369.0 eV for Ag ₅ Al ₉₅ ^A

A. Φ Handbook of X-Ray photoelectron Spectroscopy [⁸⁹]

B. Data obtained from [^{99,104}]

C. Data obtained from [^{95,100}]. Ag shifts -0.7 eV when interacts with Pd in a molar ratio of Pd₉₀:Ag₁₀

In sample point 2 of the precursor side a Ag peak at 368.32eV was detected. This BE corresponds to the energy for pure Ag without interaction with Pd. Also two other peaks appear at 369.6 ± 0.2 eV and 375.7 ± 0.5 , but they are in binding energies higher than pure Ag metal so they do not correspond to oxidized silver species. Ag peaks appears at 369.0 eV when interacts with Al at ratio of Ag₅Al₉₅ (as reported in Φ Handbook of X-Ray photoelectron Spectroscopy) thus these peaks suggest a possible interaction with the support.⁸⁹ Although contribution of the oxygen in the AAM should be considered in the mentioned BE shift.

The reduction of Pd(NO₃)₂•H₂O to Pd in Pd₉₀/Ag₁₀ by the SSR was also efficient as evidenced by the presence of the Pd metal peaks at 335.201 ±0.002 eV with its respective spin-orbit splitting values. A small presence of PdO (*i.e.* Pd 2+) was also detected in all samples points of the film on the precursor side and in one sample point on the reduction side. Comparing the reduction of Pd and Ag it can be concluded that the silver reduction was more efficient. This may occur because the Ag precursor is an anhydrous salt and the metal charge in the salt is 1+, compared to Pd which has a charge of 2+ in the monohydrate salt.

Figure 3.8 shows the Pd and Ag peaks obtained for Pd₉₀/Ag₁₀ films at the three sample points and on the films formed on each side. It shows a reduction in the peaks intensity in the Pd₉₀/Ag₁₀ films where the reducing agent was spread. The reduction in the peaks intensity validates the previous obtained by XRD and EDS techniques showing a high metal concentration on the side where the precursors were added. Considering the XPS and XRD peaks' intensities, the films synthesized in the AAM side where the reducing agent was spread can be described as the thinner film in comparison to the film formed in the AAM side where the precursors were added.

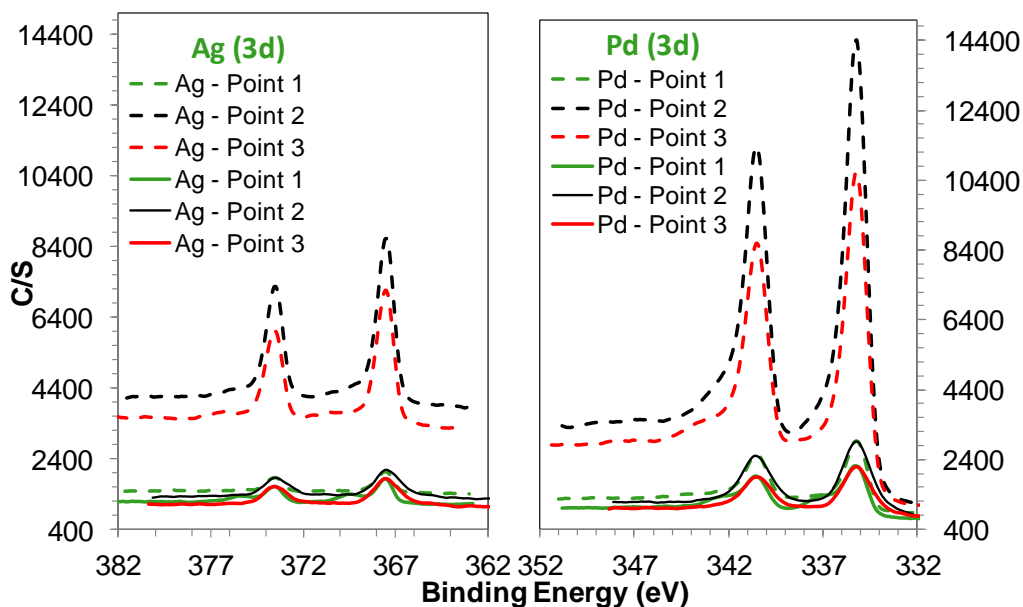


Figure 3. 8 Metals peaks obtained in the chemical state analysis of Pd₉₀/Ag₁₀ films.
(dashed lines: Precursors Impregnation side, solid lines: Reduction Side)

The results of the chemical states of the metals in Pd₉₀/Pt₁₀ films are shown in Table 3.4. Reported results by Corro *et al.*, suggest that Pd and Pt peaks do not shift to higher or lower binding energies with Pd-Pt interactions. Therefore only the effect of the support and oxidized states were considered.

Table 3. 4 XPS results of Pd₉₀/Pt₁₀ after peak deconvolution.

Metal	Precursors Side		Reduction Side	
	Peak		Peak	Description
Pd	335.22 ±0.03 eV	Pd (0) ^A	335.20 eV	Pd(0) ^A
	336.235 ±0.007 eV	PdO ^A Pd(2+)	337.75 ±0.22 eV	PdO ₂ ^A Pd(4+)
Pt	70.95 ± 0.06 eV	Pt (0) ^A	70.95 ± 0.01 eV	Pt (0) ^A
Al ₂ O ₃	-	-	73.85 ± 0.11 eV	Support
Small additional contribution	71.50 eV	Pt (δ+)	-	-
	72.38 eV	Pt (δ+)	-	-
	75.44 eV	Pt (δ+)	-	-
	75.75eV	Pt (δ+)	-	-

A. Φ Handbook of X-Ray photoelectron Spectroscopy [⁸⁹]

On the films formed on both sides Pd(NO₃)₂•H₂O oxidized species were identified. On the precursor side the Pd(0) peaks were detected at 335.22 ±0.03 eV and PdO (Pd 2+) peaks at 336.235 ±0.007 eV with its respective spin-orbit splitting values. Platinum was also reduced showing a high intensity peak at 70.95 ± 0.06 eV. Others platinum peak contributions were detected at 71.50 eV, 75.44 eV, 72.38 eV, and 75.75 eV, but these binding energies do not correspond to PtO, PtO₂, Al, Al₂O₃, or Al which appear at 72.4 - 73.8 eV, 74.6 – 75.0 eV, 72.8 eV, 73.7 - 74.3 eV and 74.65 eV, respectively.^{89,90} Dablemont *et al.* detected an additional platinum contribution at 72.1 eV which was not identified. They classified this peak as Pt (δ+) because this BE was higher than for Pt(0) concluding that platinum had a probable positive charge. The shift of Pt to high energy value may occur as consequence of interaction with elements present in the environment that were not identified.

In the Pd₉₀/Pt₁₀ sample oxidized species of palladium were detected on the reduction side at all three sample points at a high concentration relative to the reduced state. Pd and PdO₂ (*i.e.* Pd 4+) was detected in both samples at 335.2 eV and 337.75 ± 0.22 respectively. Reduced Pt (70.95 ± 0.01 eV) and Al₂O₃ (73.85 ± 0.11 eV) peaks were also detected. The presence of the

PdO₂ and the detection of the AAM support suggest that a thinner film was obtained in the side where the reducing agent was spread. Figure 3.9 shows a decrease in intensity of Pd's peaks in the reduction side.

Figures A3 and A4 (Appendix Section) show a significant increase in the peaks intensities of Al 2s and O 1s in the reduction side, even when compared with the other bimetallic samples, and a significant decrease in the intensity of the Pd 3d and Pt 4f peaks. Similar results are reported for palladium films deposited on Al₂O₃ surfaces, in which the thinner sample showed an increase in the characteristic peaks of Al 2p and O 1s and the detection of oxidized Pd.⁵⁷ They attributed the increase in oxidized palladium peaks to palladium bounded to the substrate oxygen as a consequence of the small film thickness.⁵⁷

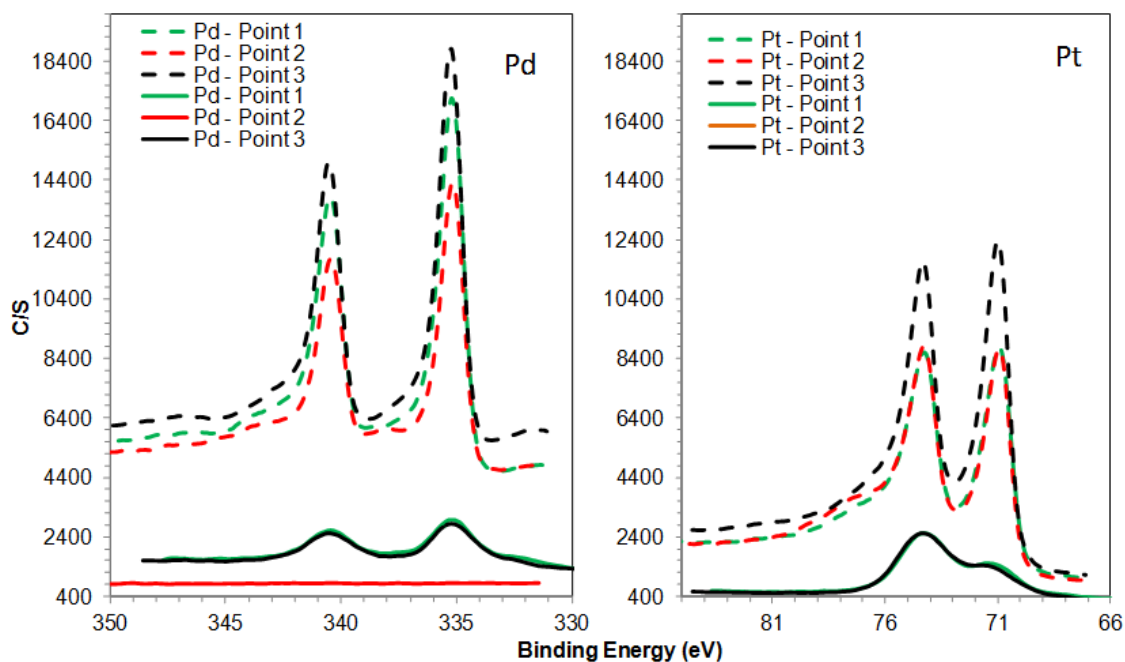


Figure 3. 9 Metals peaks obtained in the chemical state analysis of Pd₉₀/Pt₁₀ films. (dashed lines: Precursors Impregnation side, solid lines: Reduction Side)

Table 3. 5 XPS results of Pd₉₀/Ni₁₀ after peaks deconvolution using CASA-XPS

Metal	Precursors Side		Reduction Side	
	Peak	Description	Peak	Description
Pd	335.15 ±0.03 eV	Pd (0) ^A	335.15± 0.04 eV	Pd(0) ^A
	336.5 ±0.2 eV	PdO ^A Pd(2+)	336.46 ±0.17 eV	PdO ^A Pd(2+)
Ni and other small contributions onal contriubution	855.25 eV	<i>Not identified</i>	856.53	[Ni(NO ₃) ₂] ^A •6H ₂ O
	856.64 eV	[Ni(NO ₃) ₂] ^A •6H ₂ O	861.84	<i>Unidentified</i>
	857.87 eV	<i>Unidentified</i>	858.13	<i>Unidentified</i>
	859.00 eV	<i>Unidentified</i>	863.37	<i>Unidentified</i>
	860.26 eV	<i>Unidentified</i>	-	-
	861.01 eV	<i>Unidentified</i>	-	-
	862.27 eV	<i>Unidentified</i>	-	-
863.49 eV	<i>Unidentified</i>	-	-	

A. Φ Handbook of X-Ray photoelectron Spectroscopy [⁸⁹]

The results of the chemical states of the metals in Pd₉₀/Ni₁₀ films are shown in Table 3.5. Similar to others bimetallic films, the reduction of Pd(NO₃)₂•H₂O to Pd in the Pd90Ni10 sample by the SRR was partially efficient and PdO (*i.e.* Pd 2+) was also detected. Palladium peaks were detected at 335.15 ±0.03 eV and the PdO (Pd2+) at 336.5 ±0.2 eV with its respective spin-orbit splitting values. The theoretical BE for Ni and NiO are 852.7 eV and 854.3 eV respectively. The results show chemical states of nickel at BE higher than 854.51 eV evidencing that no nickel metal were present in the sample. The large quantity of Ni (the more intensive peak) appeared at 856.64 eV, 856.26 eV, and 856.53 with a peak contribution of 49.43%, 44.24%, and 50.86 % in each sample. The mentioned peaks correspond to [Ni(NO₃)₂]^A•6H₂O. These and the results discussed before lead us to conclude that the nickel salt was not reduced.⁸⁹

3.5 Conclusions

The results presented in this chapter show that the modified SSR Method using Anodic Alumina Membranes, is an efficient method to synthesize bimetallic films if anhydrous salts of metals with positive standard reduction potentials are used as precursors.

Specifically, results showed that hydrated salts are more difficult to reduce as evidenced with the Pd₉₀/Ni₁₀ and Pd₉₀/Cr₁₀ samples. In addition, the fact that these metals prefer to be in the oxidized state yield the SSR method inefficient to reduce them, especially because using water as the solvent can promote the formation of oxide species. This was evidenced by XRD and XPS results and they agreed.

Among the Ag, Pt and Pd precursors a difference in reducibility with the SSR method was also observed. In general the AgNO₃ and Pt(NH)₄(NO₃)₂ salts used were reduced readily with the SSR method while some of the Pd remained in an oxidized state. This is a combination effect of the hydration of the salts and the standard reduction potential of the metals. The fact that some of the Pd is in an oxidized state has implications on some of the results shown in Chapter 4.

XRD and XPS results also suggested that there was a significant difference in the films obtained on either side of the AAM. The films on the reduction side tended to have more oxidized species and XRD and Qualitative Elemental Analysis with XPS suggest that the films on this side were thinner. This has implications on the possible applications of each of these films.

Chapter 4

HYDROGEN SENSING TEST USING BIMETALLIC NANOSTRUCTURED FILMS SYNTHESIZED BY THE SOLID STATE REDUCTION METHOD AS A SENSING MATERIAL

Abstract

As reported before, the SSR method used to obtain bimetallic films on either side of Anodic Alumina membranes presumably connected by bimetallic nanowires. Previous sensing results showed that pure Pd film synthesized by SSR had limitations sensing hydrogen above 2% v/v. well below the hydrogen LEL (4% v/v). The incorporation of Pt and Ag enhanced the palladium properties delaying the phase transition to higher concentrations and detecting [H₂] over the LEL. The previous was evidenced by hydrogen sensing tests and by XRD in situ phase transition experiments. Pd/Pt showed better sensing response than other studied mixtures allowing the detection of higher concentrations and better response upon material reutilization.

However Pd₁₀/Ni₁₀ and Pd₉₀/Cr₁₀ films could not detect quantifiable hydrogen concentrations. Findings discussed in previous chapters suggest that these metals were not reduced by SSR.

4.1 Introduction

The use of several bimetallic mixtures in the literature has shown an enhancement of palladium sensing properties for different applications, being the detection of hydrogen one of the most studied as described in Chapter 1.

Those results motivated our interest to study the synthesis and characterization of bimetallic films using SSR, as described in previous chapters. This chapter is focused in the study of the hydrogen detection using our bimetallic materials.

Sievert's law was considered in order to study the relation between sensitivity and hydrogen concentrations. Sievert's law describes the interaction between H₂ and the metal as a result of the dissociation of H₂ into hydrogen atoms at low concentrations and its diffusion in the bulk³⁷ This law states that the amount of a diatomic gas dissolved in a metal is proportional to the square root of the partial pressure.³⁴ The interaction of H₂ with Pd allows the dissociation by chemisorption process can be described as³⁷



If diffusion (Eq. 4.2) is the rate limiting step then:

$$[\text{H}] (\text{adsorbed}) \propto [\text{H}_2](\text{gas})^{1/2}. \quad \text{Equation 4.3}$$

Sievert's law correlates sensitivity (S) with the square root of the hydrogen concentration as

$$S = K_s \sqrt{C_{H_2}} \quad \text{Equation 4.4}$$

where S is sensitivity, K_s is the Sievert's constant and c the hydrogen concentration. This equation is equivalent to Henry's law and apply only at low hydrogen concentrations.¹⁰⁵

Therefore, Equation 4.4 is true for [H₂] where Pd is in the alpha structure.

4.2 Experimental Methods

The hydrogen sensing tests were performed in a chamber designed in house. A 7 L chamber was made of a cylindrical poly(vinyl chloride) (PVC) tube with its respective caps. The system has one inlet, in where the nitrogen and hydrogen gases flow into the system, and one outlet to maintain the desired H_2 concentration at the chamber. Nitrogen was used as a carrier gas at a constant flow of 4000 SCCM. Two electrodes were connected to the rougher film using colloidal silver liquid. These electrodes were also connected to a detector, with alligator electrical connectors, to measure the current changes. A sketch of the hydrogen sensing system is shown in Figure 4.1

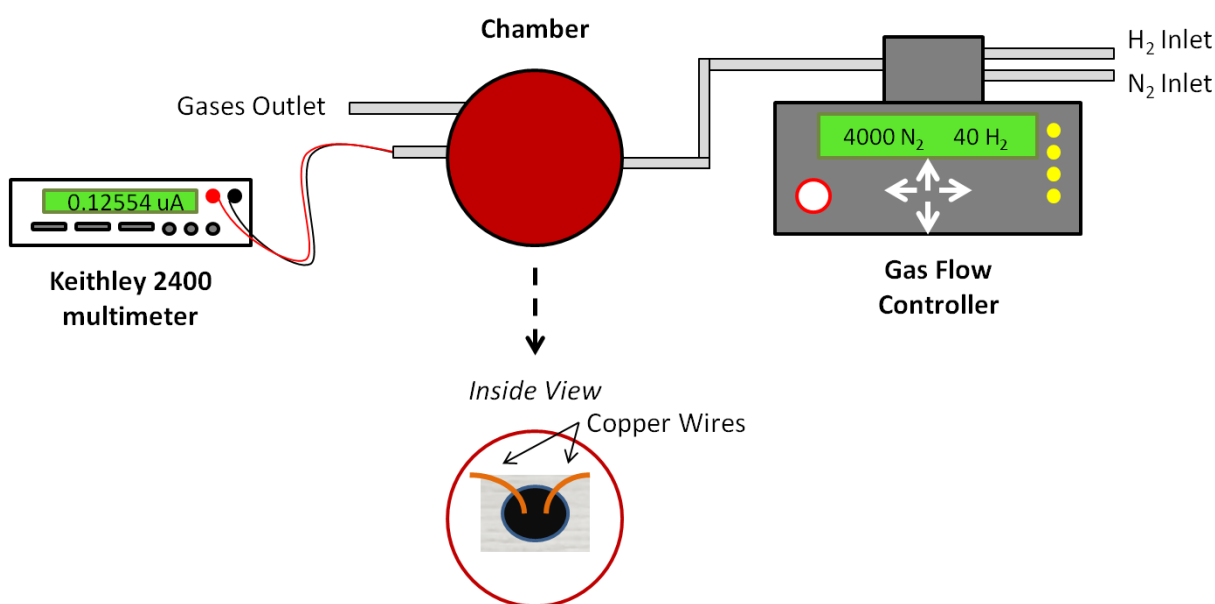


Figure 4. 1 System Diagram for Hydrogen Test

The flow of the gases entering in the chamber was controlled using MKS gas flow controllers. The current changes were recorded at different hydrogen concentrations using a

Keithley 2400 multimeter and recorded using Labview 2010. For these experiments, the electrical wires were connected to the films formed on the side where the precursors were added because, as discussed previously, this surface was rougher, thicker and with the largest concentration of reduced metals.

The study of the effect of hydrogen concentrations in the alpha to beta phase transition was performed using a Ultima III Diffractometer equipped with a Reactor X. The Reactor X was used as a chamber to maintain a constant hydrogen concentration in the system. The hydrogen concentration was varied from 0% to 3%. The used operational conditions include a scanning speed of 2.5 °/sec and sampling width of 0.02°. A two theta (2θ) interval from 30° to 55°, which is enough for the identification of both phases, was used to obtain the XRD patterns.

4.3 Results and Discussion

The sensing results at different H₂ concentrations for pure Pd and Pd bimetallic sensors are shown in Figures 4.2-4.26. The results are shown as current as a function of time. The sensitivity and response time was determined for all the samples using equations 1.1, D.1 and D.2 presented in Chapter 1 and Appendix D respectively. The response time (t_r) is obtained determining the time required to reach 90% of the maximum change in the electrical resistance for at specific [H₂].¹⁰⁶ The raw data of sensitivity and t_r are included in the Appendix. A pure Pd material synthesized via the modified SSR method was studied as a reference.

4.3.1 Pure Palladium Film

The pure palladium (Pd/AAM) sample was exposed to H₂ concentrations between 0.10% and 1.50% v/v in N₂. Contrary to what is expected, there is an increase in the current when the film was first exposed to H₂ as seen in Figure 4.2. This increase occurs as consequence of the presence of PdO as evidenced by XPS results in Chapter 3. Lee et al. also detected this behavior.¹⁰⁶ PdO and Pd films have different sensing mechanisms for hydrogen detection.¹⁰⁶ PdO-based sensors show a decrease in resistance (equivalent to an increase in current) when exposed to hydrogen but the reduced Pd films or sensors show an increase in resistance (decrease in current) when is exposed to H₂. During this process, the PdO is reduced to Pd by the reaction below:



This reaction can occur at room temperature because PdO is very unstable allowing the easy deoxidization process. Therefore considering that the reduction of PdO at room temperature is irreversible, the current increment when our material was exposed to H₂ the first time (Figure 4.2) occurs as a consequence of the reduction of the PdO presence in the sample. This increment did not occur again when the material was reused, evidencing that the PdO was reduced to Pd. Thus we called the first hydrogen exposition a pre-treatment in which the complete reduction was promoted.

Figure 4.3 shows that when the material was reused for second time only a small current increment in the initial signal was observed and it stabilizes fast. This is due to desorption of physisorbed ambient oxygen.

The presence of oxidized species of the second metal, as evidenced by XPS analysis, may also contribute to the change in signal observed when a sample is used for the first time. As they undergo reduction reactions similar to that of Pd the current will also increase. The fact that these oxidized species can be observed on the XPS spectra and the increase does not show up when a sample is reused supports the conclusion that it is due to a metal reduction and not due to an interaction between the metal and the substrate (AAM) or environmental oxygen adsorbed.

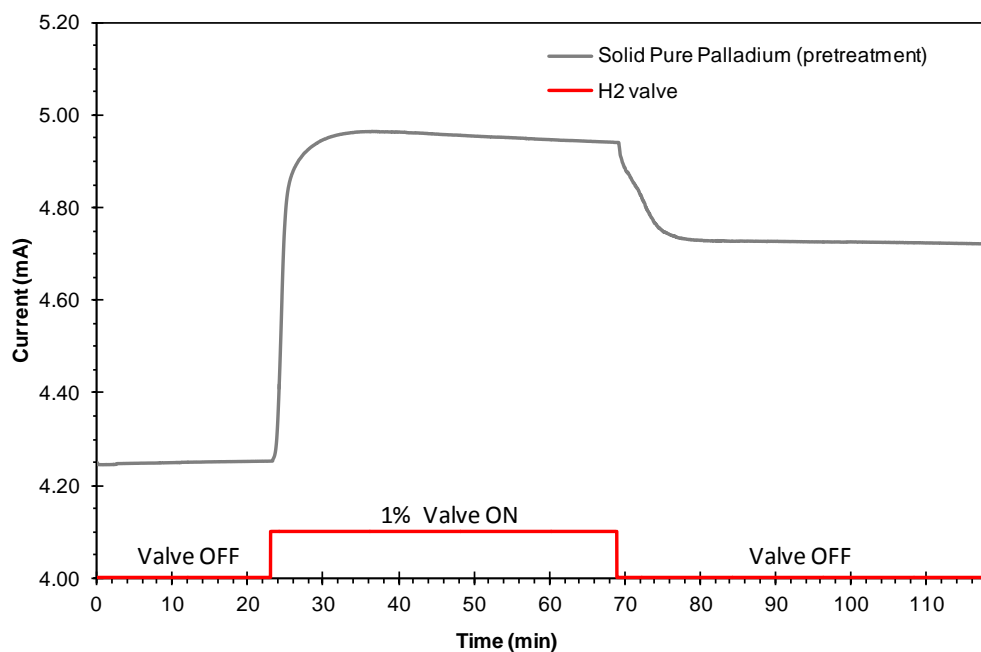


Figure 4. 2 Pd film pretreatment with Hydrogen

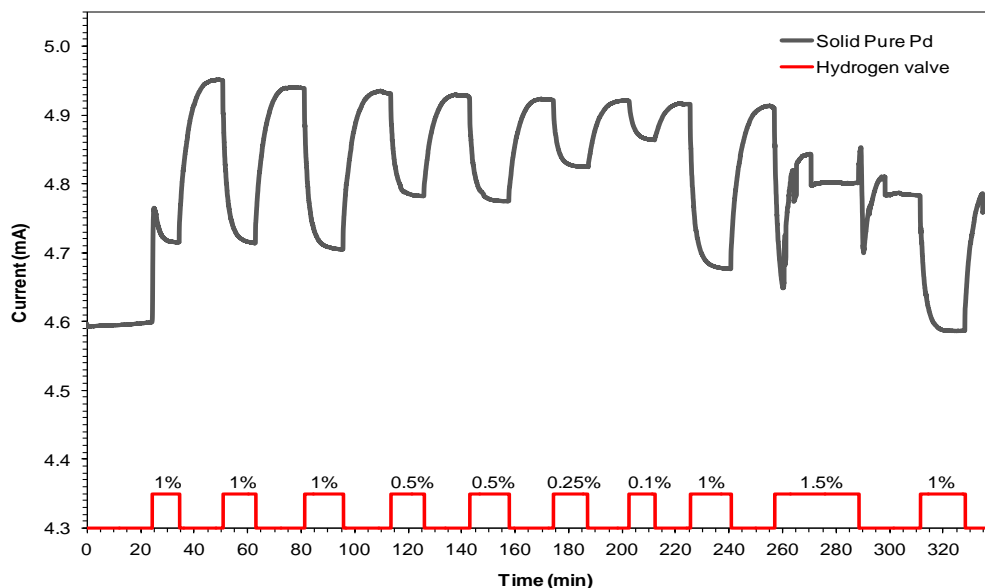


Figure 4. 3 Sensing Response to H₂ detection using pure Pd film synthesized by SSR

Figure 4.3 shows that after the first cycle, the current decreases when the film is exposed to hydrogen, and the current increases in the absence of hydrogen. This pure palladium film detects hydrogen with similar sensitivity at the same hydrogen concentration except at 1.5%v/v where the signal leaped and failed. As determined by previous work in our laboratory, XRD patterns of pure Pd samples with the same morphology showed an alpha to beta phase transition close to 1.5 % (v/v H₂/air). This can lead to physical distortions and changes in the response, hysteresis or film damage which affect its sensing properties as discussed in Chapter 1.^{2,9,36} Therefore the leaps observed in 1.5% can be as consequence of this α to β phase transition.

Figure 4.4 shows that the sensitivity is proportional to the hydrogen concentrations. The response time (t_r) does not show an identifiable relation with hydrogen concentrations, but for all concentrations it was approximately 4 minutes (Figure 4.5). Results also show that the sensor

recovers (including after the signal fails at 1.5 %) and that the interaction between H₂ and Pd is reversible, but a sensitivity reduction was observed for 1% after the signal leap at 1.5%. This reduction in sensitivity can suggest film damage.

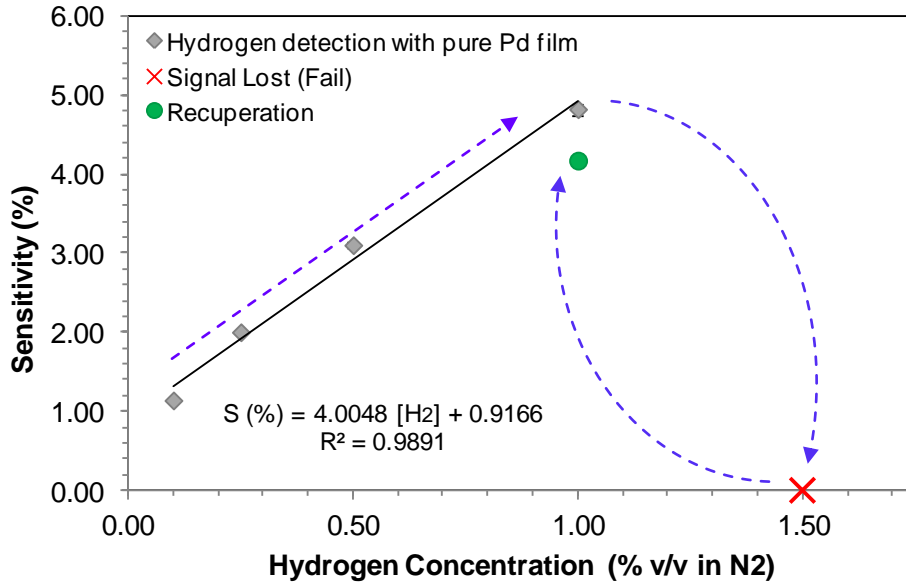


Figure 4. 4 Sensitivity (%) vs. hydrogen concentration detected by the pure Pd film.

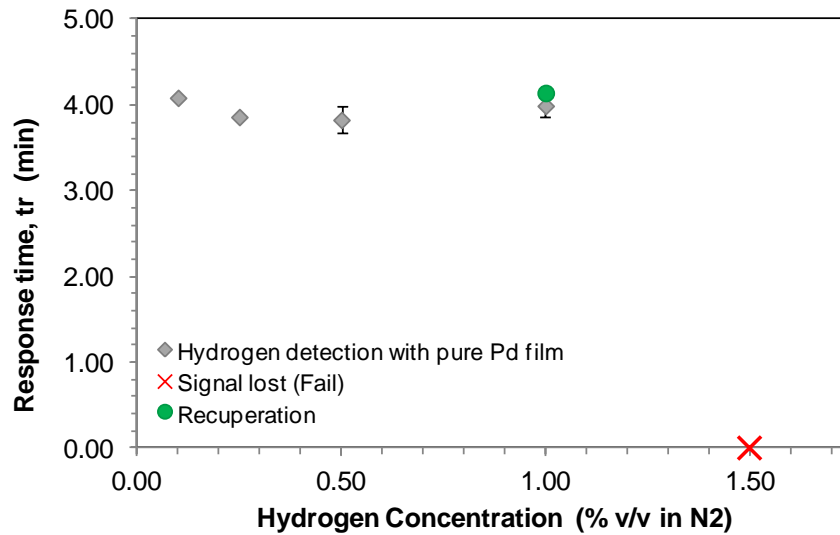


Figure 4. 5 Response time (t_r , min) vs. hydrogen concentration detected by pure Pd film

Figure 4.6 shows a linear relation between sensitivity and $[H_2]^{1/2}$ with a R^2 of 0.9891 which obeys Sievert's law. This was expected because pure Pd maintains an alpha structure at $[H_2] \leq 1.5\%$.

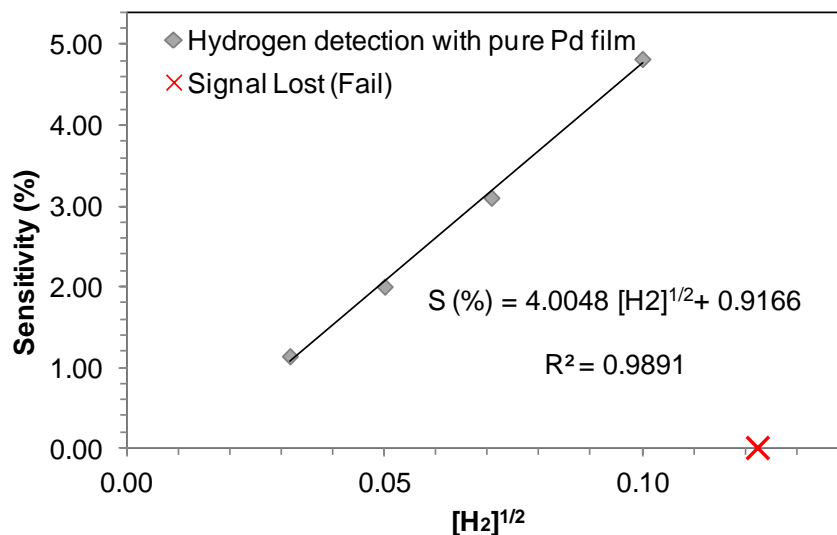


Figure 4. 6 Sensitivity (%) vs. $[H_2]^{1/2}$ detected by pure Pd film

In general, these and previous results obtained show that SSR method is an alternative synthesis method to obtain Pd films that can be used in different application such as H_2 detection. However at hydrogen concentrations over 1.5% v/v the signal loses stability. This limits the use of pure palladium, synthesized by SSR, for the detection of H_2 concentrations near and above the explosion limit (4% v/v in air).

4.3.2 Palladium/Platinum Bimetallic Films

Figures 4.7-4.16 show the sensing results for Pd_{90}/Pt_{10} bimetallic films. Results show that our Pd_{90}/Pt_{10} film can detect H_2 with precision (current changes are the same at the same concentration) but with a displacement in the baseline.

Similar to the pure palladium film response, there was an increase in current upon first exposure to hydrogen (Figure 4.7) but in the subsequent run (Figure 4.8) the increase was smaller upon the first exposition and in the following cycles the bimetallic film showed a decrease in current. As mentioned above for pure Pd film and reported by Lee *et al.*, this first increment shown in Figure 4.7 occurs as consequence of the reduction of PdO. In this case any remaining oxidized Pt is probably also reducing during this initial hydrogen exposure.

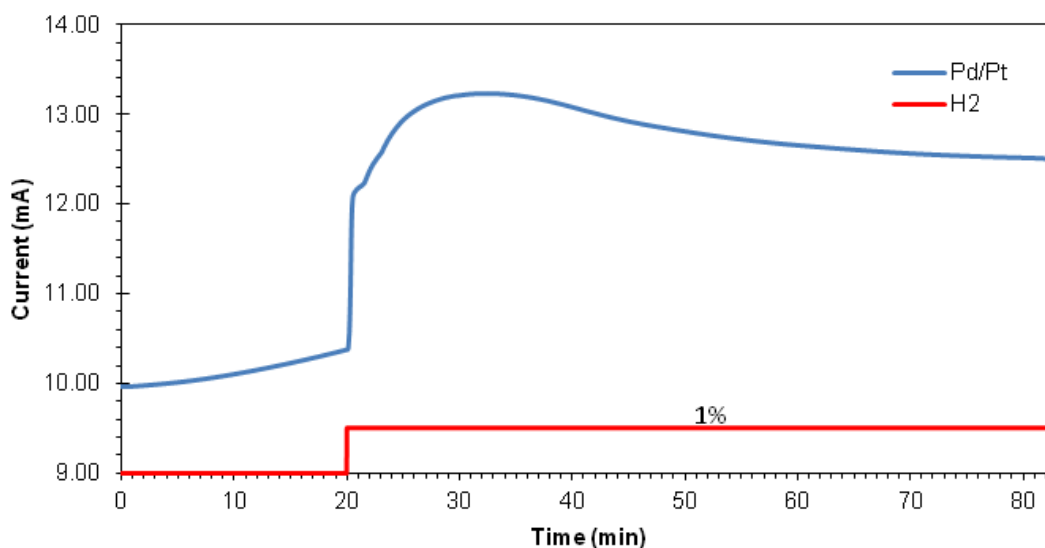


Figure 4. 7 Current Sensing Response to Hydrogen detection using Pd₉₀/Pt₁₀ (first run).

Figure 4.8 shows the sensing results for the Pd₉₀/Pt₁₀ bimetallic film after pretreatment with hydrogen. This film was exposed to H₂ concentrations between 0.10% and 10.0 % of H₂ volume in N₂ volume. After this concentration, the run was stopped to avoid experimental complications (*i.e.* possible H₂ leaks) but the results are enough to demonstrate that the incorporation of platinum enhance the palladium sensing properties. Similar to the pure Pd film,

there was a fast and small increase in current upon first exposure to hydrogen after pretreatment, which occurs as consequence of desorption of physisorbed oxygen. Results show that this sample can detect hydrogen concentrations up to 10% v/v without failure. This is significantly higher than the maximum concentration detected by pure Pd without failure (<1.5% v/v).

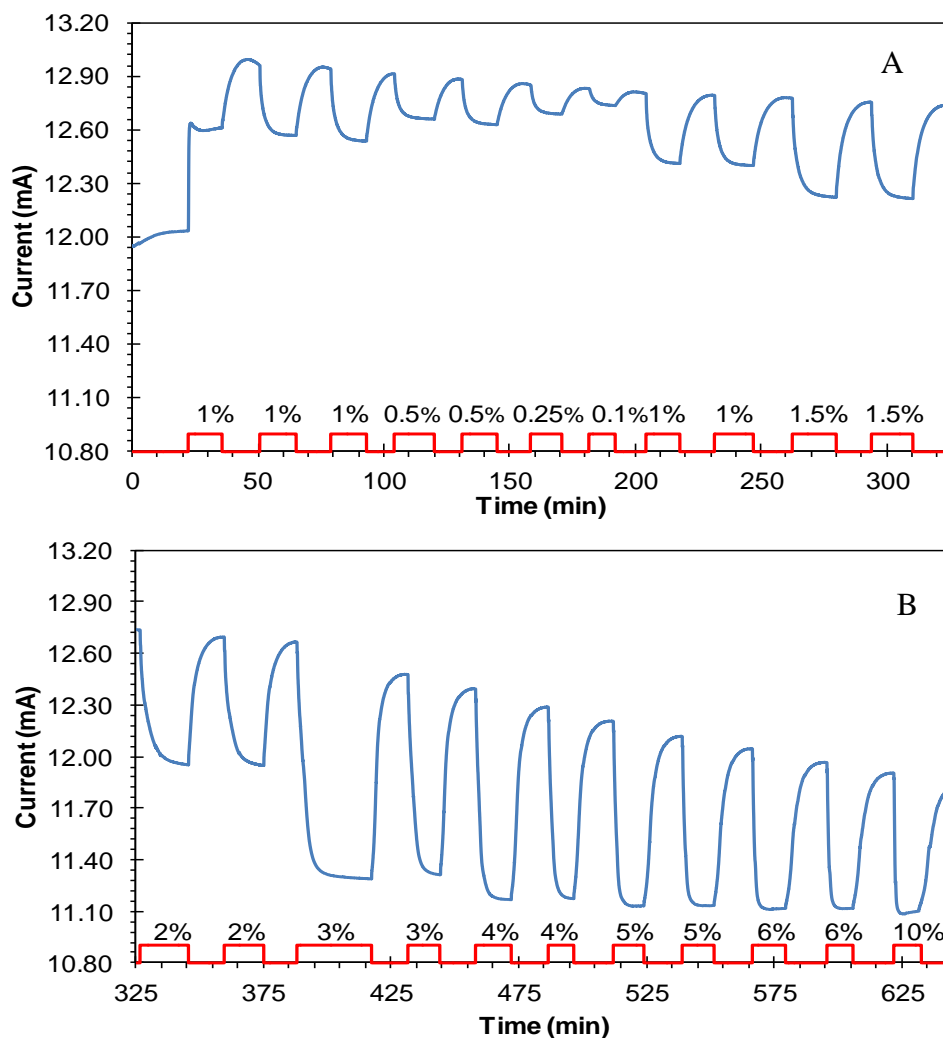


Figure 4. 8 Sensing Response to Hydrogen detection obtained from the first run using the second Pd₉₀/Pt₁₀ film synthesized by SSR Method (A. First 11 cycles, B. Last 11 cycles).

Figure 4.9 shows the in situ XRD results under different hydrogen concentrations to study the phase transition of Pd₉₀/Pt₁₀. The in situ XRD experiment was performed to study the effect of the incorporation of Pt in the Pd phase transition. Results show that phase transition has not started at 1.5% v/v H₂, whereas for pure palladium the phase transition to the beta structure was complete at this concentration. Therefore our Pd₉₀/Pt₁₀ bimetallic film delays the phase transition to higher concentrations. Results at hydrogen concentrations higher than 1.5% v/v H₂ showed a shift in the peak to lower angles and at 3% v/v H₂ the Pd peak hadn't reached the characteristic angle for the theoretical beta phase.

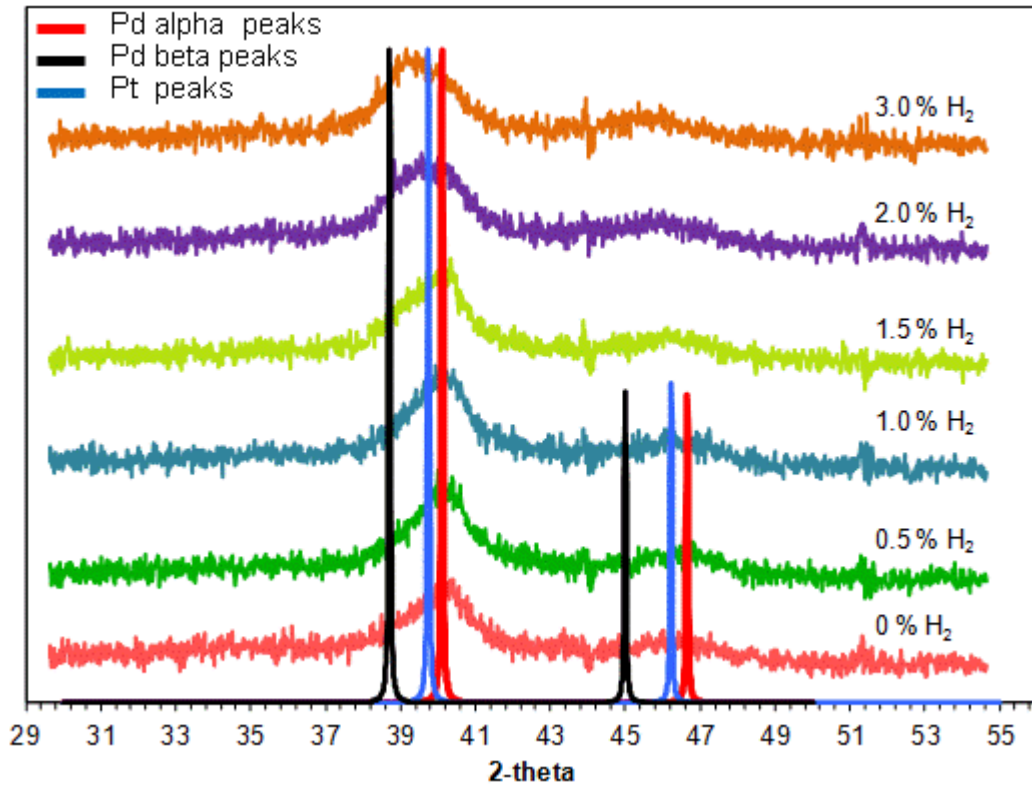


Figure 4. 9 In situ XRD of Pd₉₀/Pt₁₀ at different [H₂]

This behavior is contrary to what is observed in pure Pd where the characteristic Pd peak in the alpha phase disappears while the characteristic Pd peak in the beta phase appears. This difference could be artificial as the characteristic Pt peak is located at an angle midway between the alpha and beta peaks and the peak observed at 2% v/v H₂ could be a convolution of the alpha and beta Pd peaks in addition to the Pt peak. If that is the case, at 3% v/v the phase transition could have been completed. Nevertheless, these results suggest that the Pd₉₀/Pt₁₀ beta phase peak is located at a higher angle than in pure Pd suggesting a significant interaction between the Pd and Pt atoms.

Figures 4.10-4.11 show the relation between [H₂], sensitivity, and response time. The sensitivity increases linearly with a slope of 2.4629 between 0.1 % < [H₂] < 1.5% and then increases linearly with a higher slope of 3.8694 until 3%. Subsequently, a decrease in sensitivity was detected for concentrations higher than 3%. Comparing these results with the in situ XRD we can conclude that the first linear behavior (until 1.5%) occurs when PdPt have an alpha structure, the increase from 1.5% to 3% occurred as a result of the alpha to beta phase transition and the decrease in sensitivity occurs when the Pd/Pt have a beta structure.

Similar to the pure Pd results, the response time does not show significant changes in hydrogen concentrations under 2%. Despite this, a small reduction on the response time (tr) was detected when the material was first submitted to H₂ followed by a small increase until 1.5%. Then, a significant increase was detected when the structure experienced the first structure expansion at 2% [H₂]. After that, a decrease in tr was detected at concentrations where the Pd's structure approaches to the beta structure.

Previous reported results suggested that the sensitivity and response time changes depend of the material's structural changes,^{1,40} but is the first time that the effect in the S and tr caused by structure changes is demonstrated by in situ XRD.

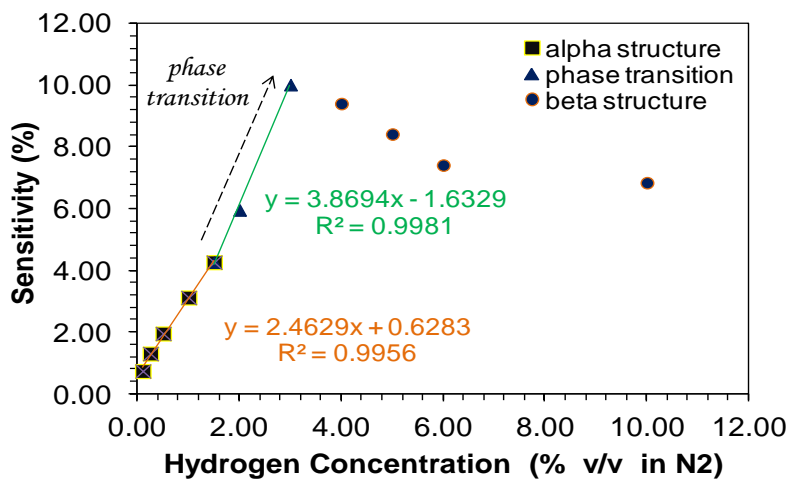


Figure 4. 10 Sensitivity (%) vs. [H₂] detected by Pd₉₀/Pt₁₀ bimetallic film (first run)

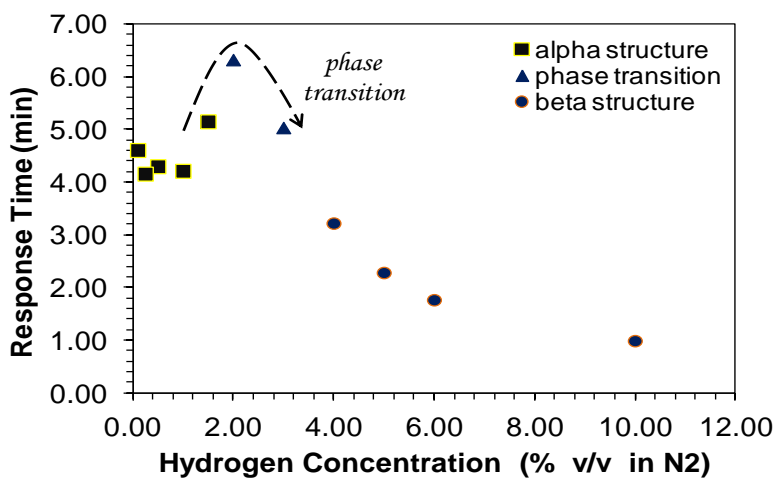


Figure 4. 11 Response time (t_r) vs. [H₂] detected by Pd₉₀/Pt₁₀ bimetallic film (first run)

Figure 4.12 shows S vs $[H_2]^{1/2}$ and, as expected, a linear relationship was obtained at hydrogen concentrations where the metal maintains an alpha structure. The mentioned behavior obeys the Sievert's law which is expected for the alpha phase. In the phase transition, a linear relation with a higher slope was also detected, but this linearity was lost when the material structure changed to beta structure. However, considering that the S and t_r change as a result of the phase changes, the sensitivity was normalized by the response time (S/t_r) and results demonstrated that this ratio shows two different linear relationships with $[H_2]^{1/2}$ (Figure 4.13). The first one at the α phase ($[H_2] \leq 1.5\%$) with a R^2 of 0.9876, and the other one started at concentrations that shows the loss of the alpha phase ($[H_2] > 1.5\%$) and survey to concentrations where the material structured achieved the beta phase with a R^2 of 0.9975. In our knowledge this behavior has not been previously reported.

These results demonstrate that the sensitivity and response time results can be related in order to quantify the hydrogen concentrations. This allows the efficient use of our Pd_{90}/Pt_{10} film as a sensing material for hydrogen detection at a wider range of concentrations.

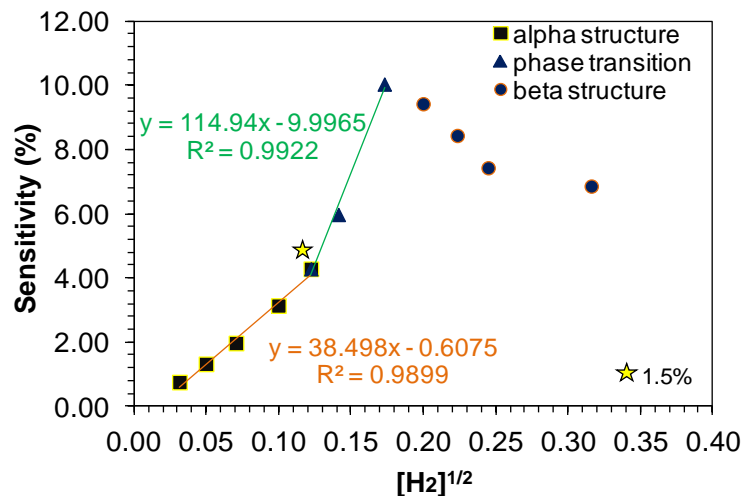


Figure 4. 12 Sensitivity vs. $[H_2]^{1/2}$ obtained using Pd_{90}/Pt_{10} bimetallic film (first run)

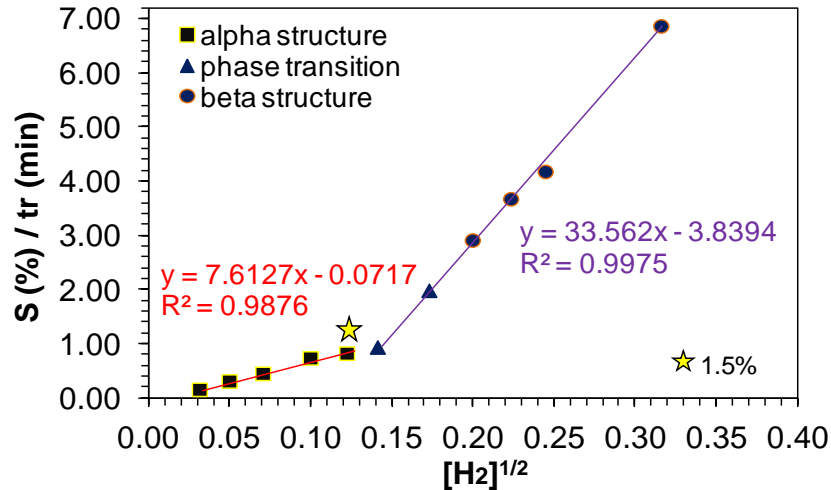


Figure 4. 13 Sensitivity/response time vs. $[H_2]^{1/2}$ obtained by Pd₉₀/Pt₁₀ bimetallic film (first run)

This film was studied three times after the pretreatment (the same film was analyzed three consecutive days using the same assembling to avoid problems such as sealing, connection of electrodes, possible break of the film, and others) to study the possibility of film damage and the reusability of the film. The sensing response curves of the repetitions are included in the Appendix but the sensitivities and response times are included in this Chapter.

The second time it was studied this film detected up to 6% v/v without failure and when it was reused the third time it detected up to 4% v/v without failure. Figure 4.14 shows that the sensitivity in both runs 1% and 2% v/v H₂ was similar but at 4% in run 3 it decreased probably due to the start of the signal instability. One important fact is that after the sensor's failure the sensitivity was recovered at a very similar value in both runs. This behavior suggest that desorption of hydrogen from the material doesn't present the hysteresis effect which has been observed in other reports after the transition to the beta phase (refer to Chapter 1 and Figures 1.4 and 1.5).

Figure 4.15 shows that, similar to previous results, the response time does not show an identifiable relationship with the hydrogen concentrations. However the response time achieves a maximum and then decreases. In addition, the response time required to stabilizing in the recuperation cycle at 1% (after signal leaps) was very similar.

Therefore reduction in the efficiency of Pd₉₀/Pt₁₀, as evidenced in both the sensitivity reduction at the same concentration and a lower maximum detection limit, suggests a possible film damage (provoked by hydrogen embrittlement) or saturation. The reason for the reduction in the film efficiency is probably due to morphological changes in our material.

Despite this, the sensitivity normalized by the response time (S/t_r) vs. $[H_2]^{1/2}$ was also studied and results follows a linear relationship in both repetitions (Figure 4.16) but a reduction in the R^2 was obtained. This was expected as a result of the possible film damage,.

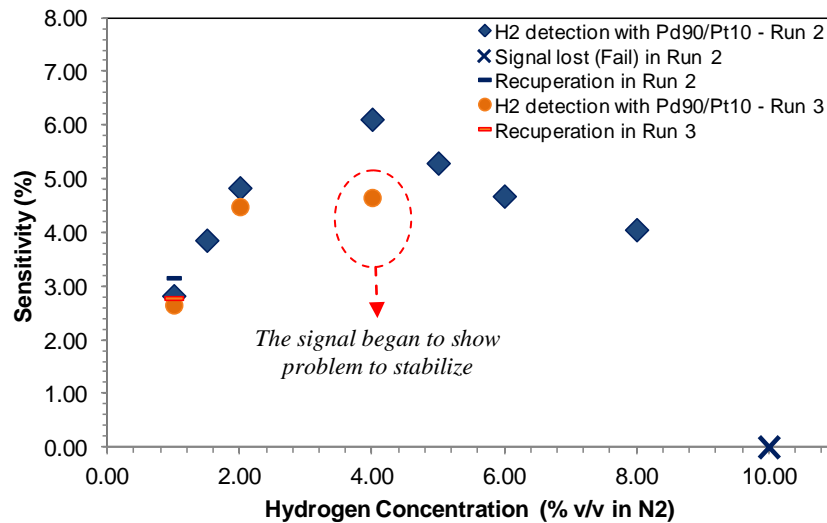


Figure 4. 14 Sensitivity (%) vs. hydrogen concentration detected by the reused Pd₉₀/Pt₁₀ bimetallic film (2nd and 3rd Runs)

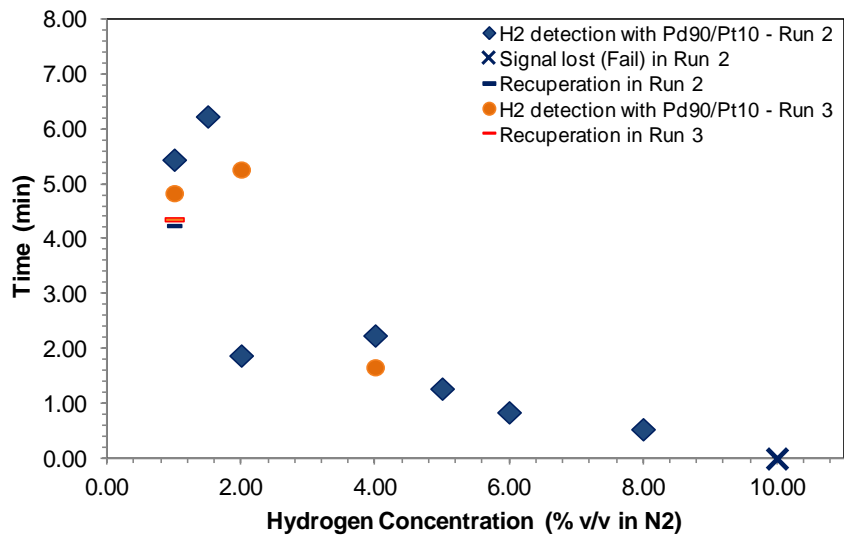


Figure 4. 15 Response time (min) vs. [H₂] detected by the reused Pd₉₀/Pt₁₀ bimetallic film (2nd and 3rd Runs)

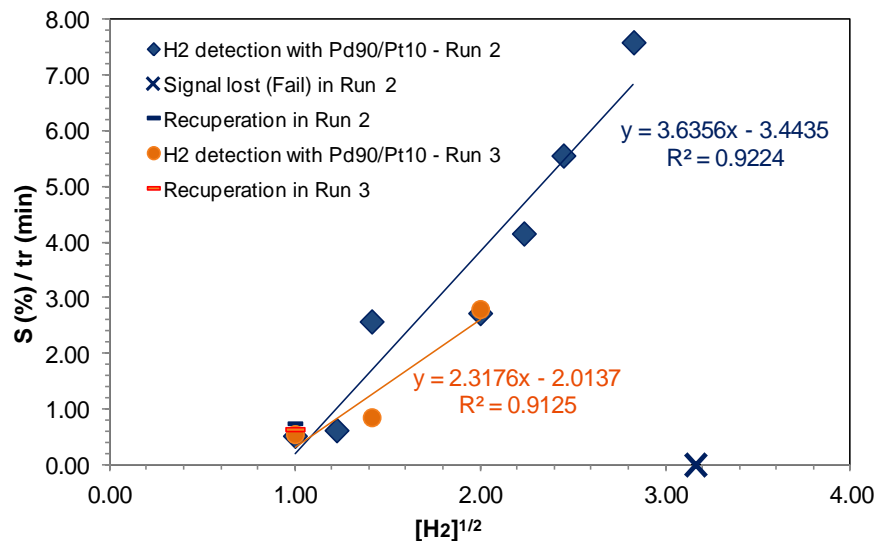


Figure 4. 16 Sensitivity/Response time (S/t_r) vs. [H₂]^{1/2} by the reused Pd₉₀/Pt₁₀ bimetallic film (2nd and 3rd Runs)

The XPS results discussed in Chapter 3 and the XRD results presented here suggest that the addition of the second metal occurred by isomorphous substitution⁴⁶ which allows Pd to maintain a fcc unit cell. Taşaltın *et al.* suggested that the incorporation of a second metal to the

palladium film supported on AAM template caused the material to possess two different interstitial sites with different activation energies required for the H atom to jump between the active sites of Pd and the other metal, after H-H bond dissociation.¹ These differences in activation energies inhibit the rapid saturation of Pd-H that provokes α -to- β phase transition and possible film damages as a consequence of the internal mechanical stresses. This may explain why our bimetallic Pd₉₀/Pt₁₀ material enhances the hydrogen sensor response.

4.3.3 Palladium/Silver Bimetallic Films

Similar results were obtained by Pd₉₀/Ag₁₀, but this material detects hydrogen concentrations only up to 5% without signal instability on the first run (Figure 4.17). This membrane was not pretreated with hydrogen, thus the first increment occurs as consequence of the reduction of PdO after first exposition of hydrogen.

The in situ XRD results at different hydrogen concentrations of Pd₉₀/Ag₁₀ are presented in Figure 4.18. It shows that at 1.0 %v/v H₂ the phase transition has started and at 2.0% v/v it has apparently been completed. This behavior is similar to the one observed in the pure Pd sample suggesting that the Pd₉₀/Ag₁₀ as obtained by SSR does not help delay the phase transition. In addition, as similar to Pd₉₀/Pt₁₀, the final position of the beta structure is at higher angles than for pure Pd, suggesting a strong alloy-like interaction between the two metals.

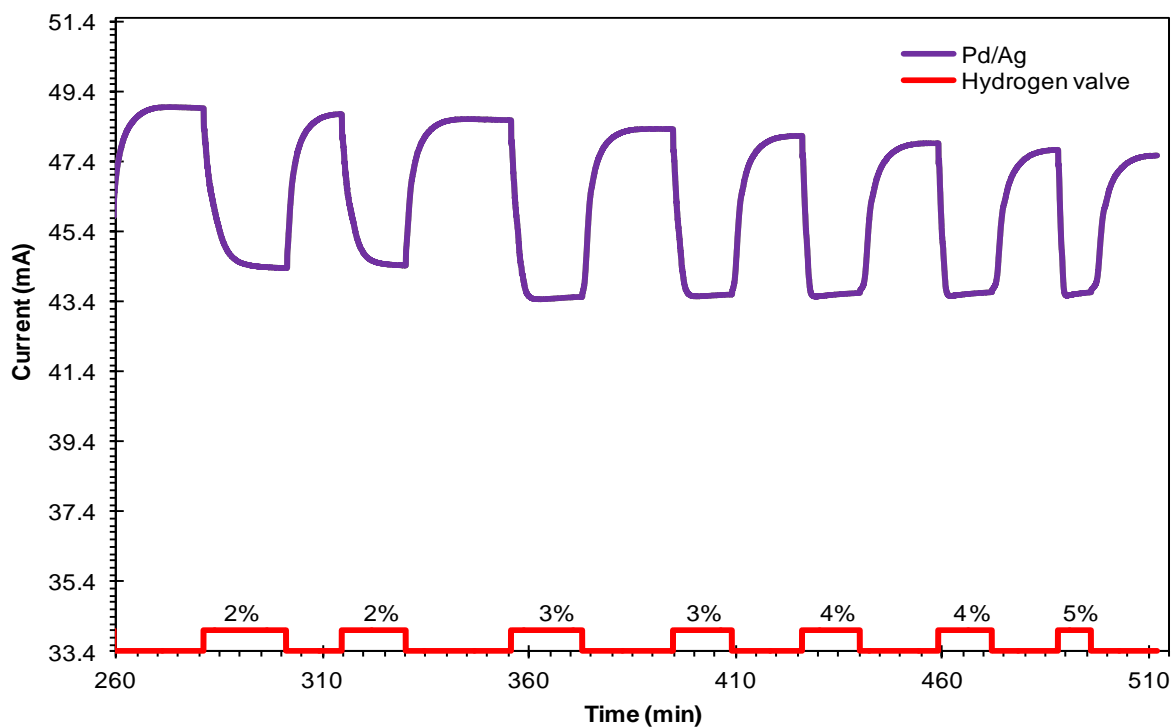
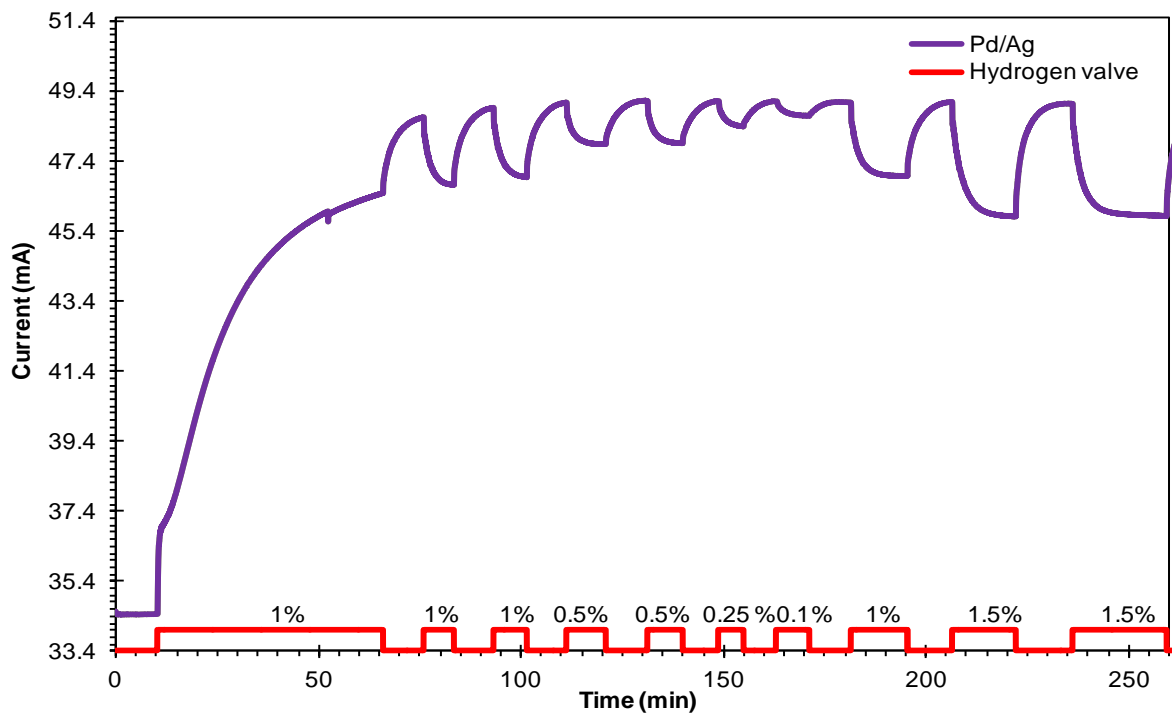


Figure 4. 17 Sensing Response to Hydrogen detection using the first Pd₉₀/Ag₁₀ film synthesized by SSR (A. First 10 cycles, B. Last 7 cycles)

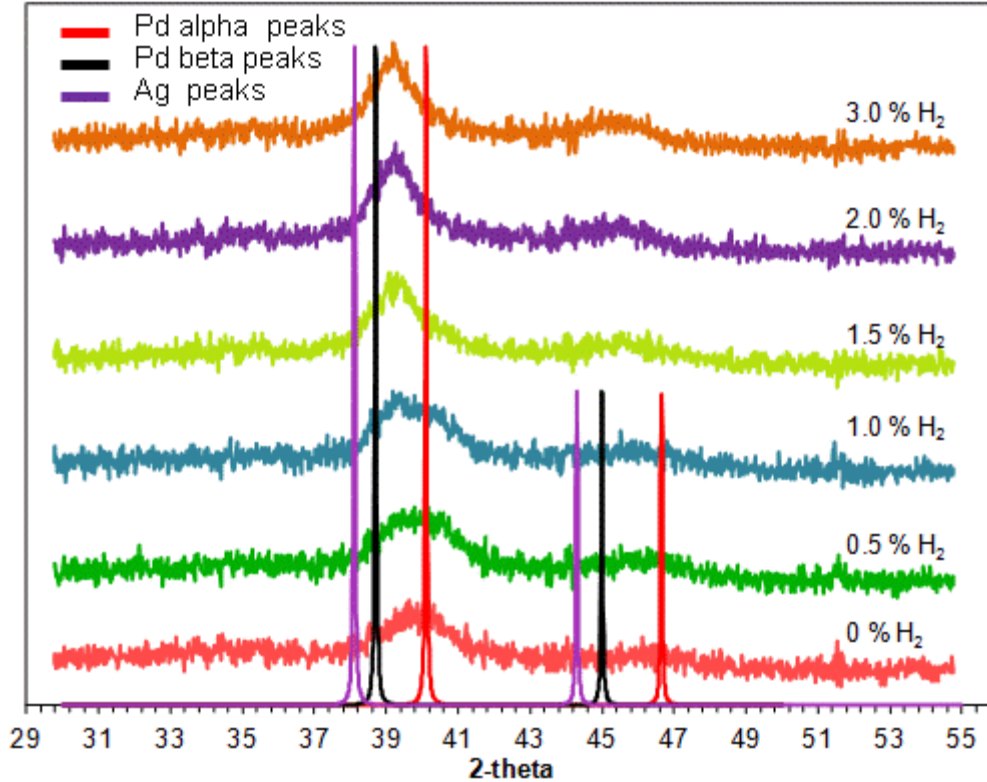


Figure 4.18 In situ XRD patterns of Pd₉₀/Ag₁₀ at different [H₂]

Figures 4.19 – 4.20 show the relation between [H₂], sensitivity, and response time. Similar to Pd₉₀/Pt₁₀ bimetallic film the sensitivity of Pd₉₀/Ag₁₀ increases as the hydrogen concentration increases from 0.1% to 3% and then decreases. As obtained by Pd/Pt film, a linear relationship was observed for concentrations between 0.1% - 1% with a R² of 0.9984, further by a second linear relation between 1% - 2% with a R² of 1 and a decrease at higher concentrations.

Similar to the Pd₉₀/Pt₁₀ results, the response time shows a small reduction on the response time (tr) at the alpha structure followed by an increase at hydrogen concentrations corresponding to the phase transition, and finally a decrease at concentrations where the Pd's structure approaches to the beta structure (Figure 4.20).

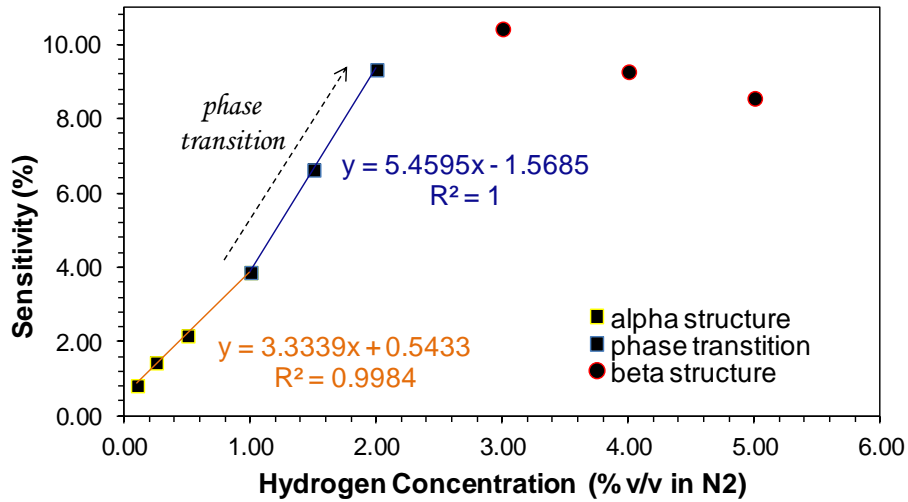


Figure 4. 19 Sensitivity (%) vs. [H₂] detected by Pd₉₀/Ag₁₀ bimetallic film

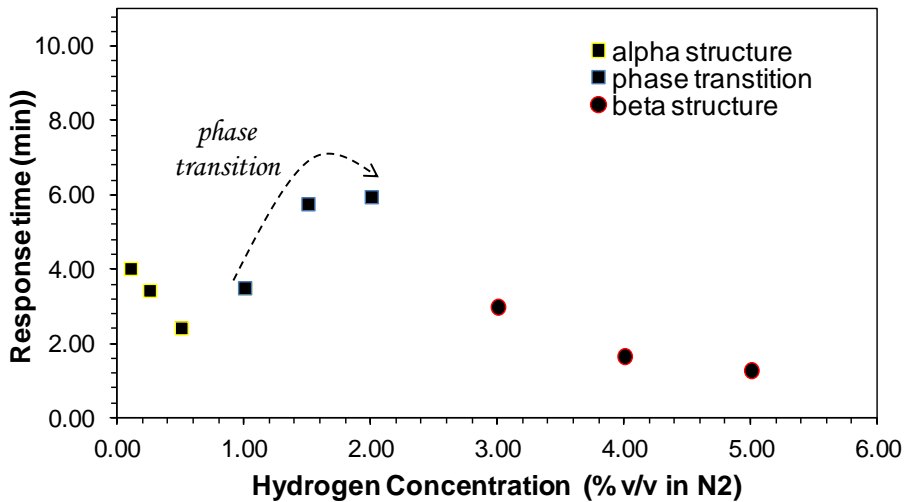


Figure 4. 20 Response time (min) vs. hydrogen concentration detected by Pd₉₀/Ag₁₀ bimetallic film

Figure 4.21 shows S vs $[H_2]^{1/2}$ and it shows similar trends as Pd/Pt. Also, when the sensitivity was normalized by the response time (S/t_r) it also exhibited two different linear relationships (Figure 4.22). The first linear relationship was at $[H_2] \leq 1.0\%$ (α phase) with a R^2 of 0.9520, and the second after the phase transition to the beta phase with a R^2 of 0.9839.

The reutilization also shifts the instability in the sensing response to lower hydrogen concentration and at 2%v/v H₂ there was a signal instability the first time it was reused (Appendix D3). However, the sensitivity didn't decrease in the recuperation at 1% v/v H₂.

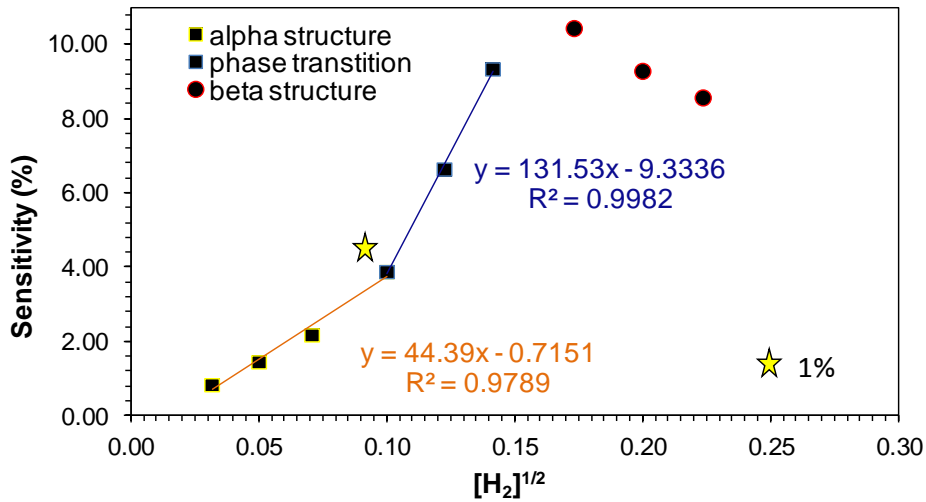


Figure 4. 21 Sensitivity vs. [H₂]^{1/2} detected by Pd₉₀/Ag₁₀ bimetallic film

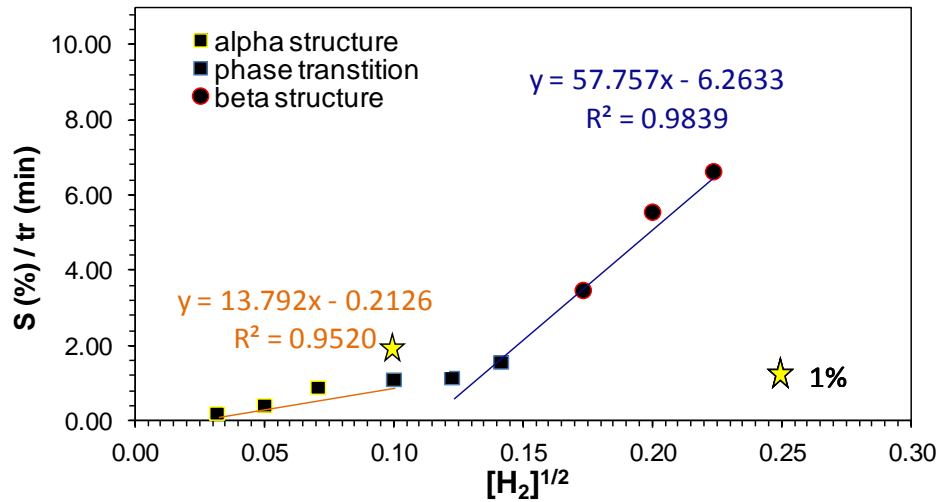


Figure 4. 22 Sensitivity/Response time (S/tr) vs. [H₂]^{1/2} detected by Pd₉₀/Ag₁₀ bimetallic film.

4.3.4 Palladium/Nickel Bimetallic Films

$\text{Pd}_{90}/\text{Ni}_{10}$ film was also synthesized by SRR Method but the results were not reproducible. The first synthesized film detected hydrogen and the results are presented in Figure 4.23. The other synthesized films were not able to detect hydrogen and similar problems shown in Figure 4.24 were obtained. As previously discussed the $\text{Ni}(\text{NO}_3)_2 \cdot 6\text{H}_2\text{O}$ salts were highly hydrated and did not reduce well by our SSR method. XPS show the presence of the nickel precursor salt in both films which should interfere with the chemisorptions of H_2 with palladium. The presence of this non reduced metal and internal water avoid the correct detection of hydrogen and at the same time decrease the active sites in the sensing material.

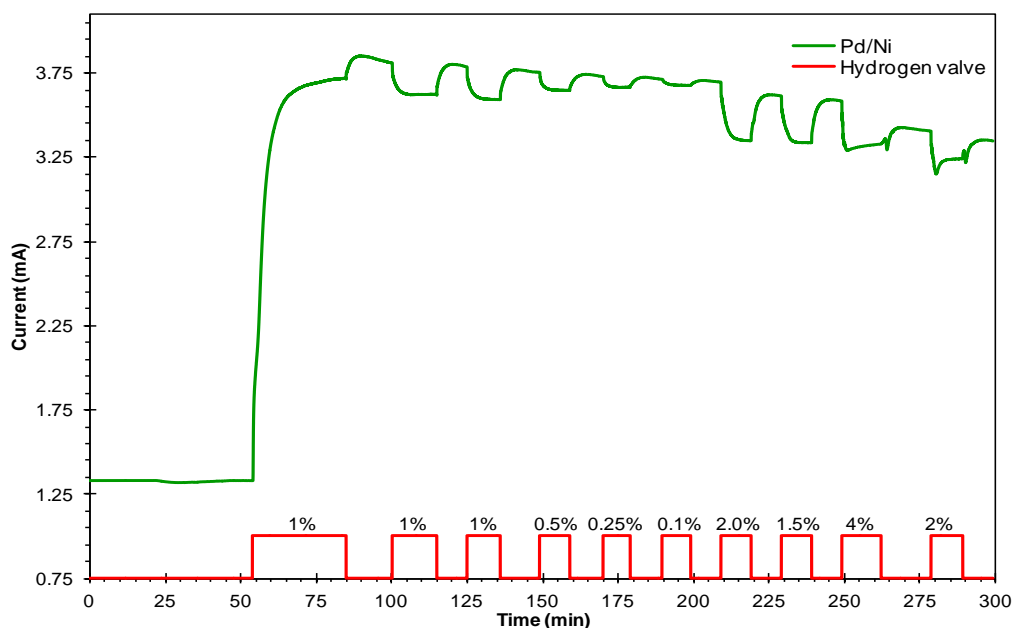


Figure 4. 23 Sensing Response to Hydrogen detection using the second $\text{Pd}_{90}/\text{Ni}_{10}$ membrane synthesized by SSR Method.

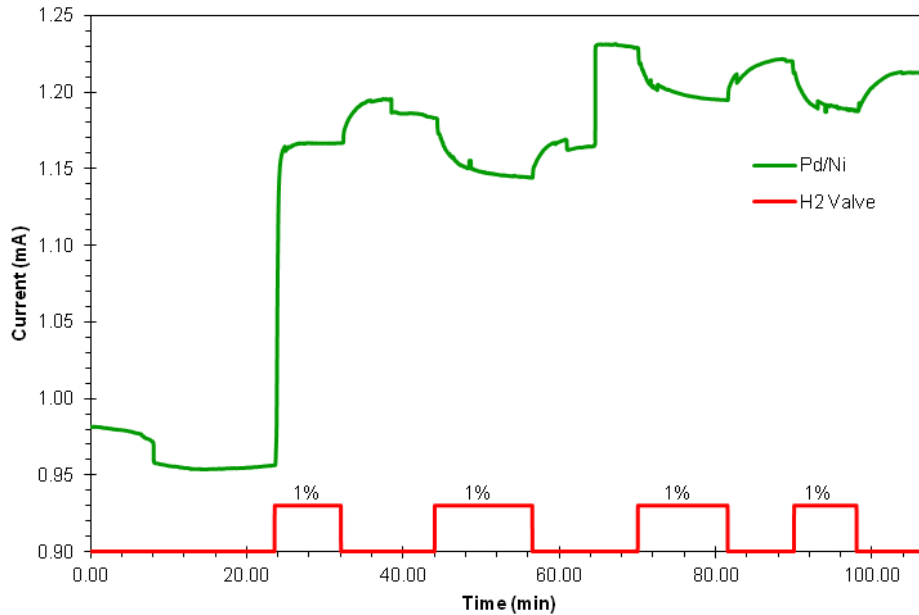


Figure 4. 24 Example of the sensing response obtained for the other synthesized Pd₉₀/Ni₁₀ membranes.

4.3.5 Palladium/Chromium Bimetallic Films

Pd₉₀/Cr₁₀ membranes were also synthesized using the modification of the SSR Method. Figures 4.25-4.26 show that Pd₉₀/Cr₁₀ didn't detect hydrogen concentrations. Results reported in the literature and in NASA reports drove the interest to synthesize these materials. However as a result of the poor hydrogen sensing performance, this membrane was not further characterized. The absence of bimetallic films in the Pd/Cr/AAM material may provoke the poor hydrogen response. The SEM images (Figure 3.3) in Chapter 3 showed the absence of a film in the reduction side and that the film in the precursor side was not as rough as the other bimetallic materials. All these facts suggest that the difference in the Pd/Cr/AMM material morphology, compared with the other bimetallic material, limits the use of these bimetallic films as a sensing

material. Also the limitations of detection could be as a consequence of the unreduced chromium hydrated precursor salt which affects the interaction of Pd with H₂,

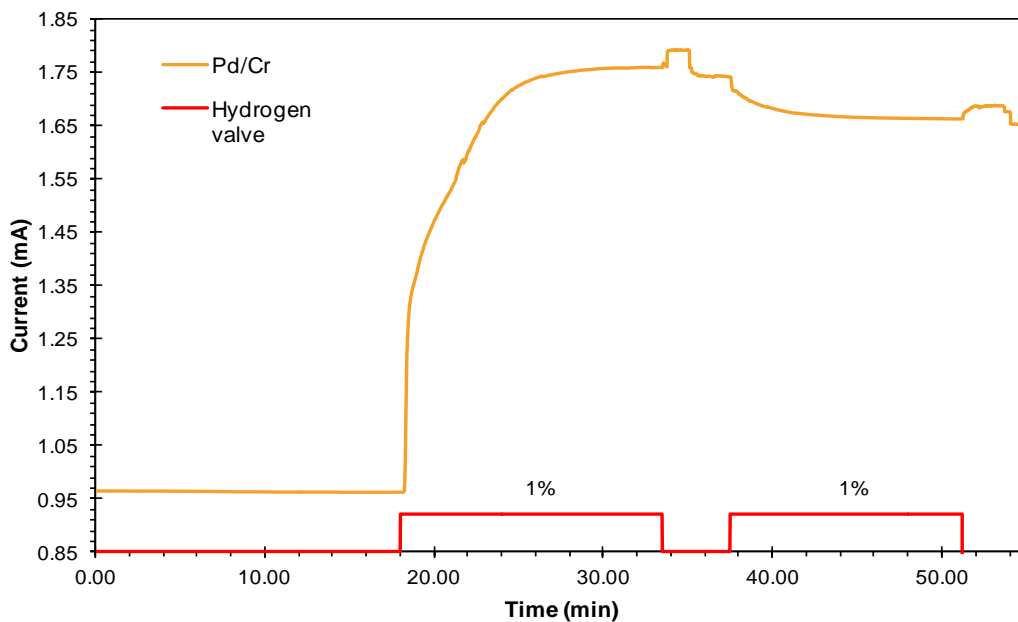


Figure 4. 25 Sensing response results using Pd₉₀/Cr₁₀ membrane synthesized by the SSR Method.

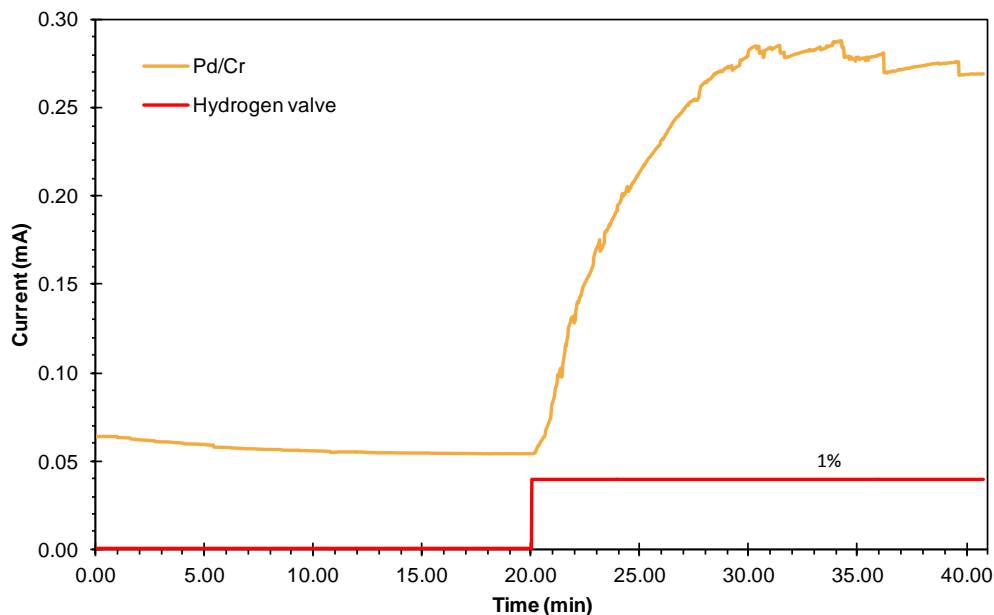


Figure 4. 26 Sensing Response using other Pd₉₀/Cr₁₀ membrane synthesized by the SSR Method.

4.4 Bimetallic and pure palladium comparison

Table 4.1 shows that Pd/Pt and Pd/Ag detected higher hydrogen concentrations than pure Pd, but with a decrease in sensitivity. Both bimetallic materials detected $[H_2]$ over the LEL. The reduction in sensitivity was expected because we reduce the Pd concentrations which is the metal that suffer changes in its physical properties when interacts with hydrogen. The response time does not change significantly and only Pd/Pt delayed the alpha to beta phase transition to higher concentrations. These results suggest that both bimetallic films show a homogenous and less abrupt unit cell expansion upon hydrogen adsorption which allows the detection of higher $[H_2]$ than pure Pd without failure.

Table 4. 1 Results summary

$[H_2]$	<i>Pure Pd</i>		<i>Pd/Pt</i>		<i>Pd/Ag</i>	
	<i>Sensitivity (%)</i>	<i>Resp time min (t 90%)</i>	<i>Sensitivity (%)</i>	<i>Resp time min (t 90%)</i>	<i>Sensitivity (%)</i>	<i>Resp time min (t 90%)</i>
0.10%	1.1	4.0	0.7	4.6	0.8	4.0
0.25%	2.0	3.9	1.3	4.2	1.5	3.4
0.50 %	3.1	3.7	2.0	4.4	2.2	2.4
1.00%	4.9	4.0	3.1	4.2	4.3	4.2
1.50 %	-	-	4.3	5.3	6.6	5.8
<i>Max. $[H_2]$ detection (1st run)</i>	1.0 %		10.0 %		5.0 %	
<i>Phase transition (H_2 range)</i>	1.0-2.0 %		1.5-3.0 %		1.0% - 2.0 %	

4.5 Conclusions

Our results show that the synthesis of bimetallic films by the modified Solid State Reduction method is a good alternative for the design of materials that can be used as hydrogen sensors but a hydrogen pretreatment is required in order to eliminate possible oxidized species. The morphology of our materials allows its facile implementation as a sensor for hydrogen detection.

The incorporation of Pt and Ag as second metal in the palladium film by our method enhanced the palladium sensing properties. The Pd₉₀Pt₁₀ sample delayed the phase transition to higher concentrations and both Pd₉₀Pt₁₀ and Pd₉₀Ag₁₀ detected [H₂] over the LEL on the first run. The XRD results showed a shift in the beta phase angle in both of these materials suggesting an alloy like interaction that maybe enhancing the detection limits.

Apparently the incorporation of a second metal to the palladium film supported on AAM template causes two different interstitial sites in the film with different activation energies. These differences in activation energies provoke the jumps of the H atom between the different active sites after H-H bond dissociation. Therefore these differences in activation energies inhibit the rapid saturation of Pd-H which provokes α -to- β phase transition and possible film damages. This might explain why our bimetallic material enhances the hydrogen sensor response.

Moreover, and contrary to pure Pd, no sensitivity decrease was detected during the recuperation from higher concentrations to 1% v/v in these two bimetallic materials. This suggests that the hysteresis effect in pure Pd at this concentration was avoided in the bimetallic films.

Our bimetallic samples show that the sensitivity normalized by the response time (S/t_r) shows a linear relationship with $[H_2]_5^{1/2}$ which can be used to calibrate the sensors. This occurs because S and t_r change as a function of the M-H structure.

In general Pd/Pt showed better sensing response than the other studied mixtures allowing the detection of higher concentrations without signal instability and more material reutilization. In this sample the delay in the alpha to beta phase transition may allow the detection of higher concentrations. Despite this, the decrease in the efficiency when the films were reused suggests that some film damage is happening. The film damage probably occurs as a result of internal mechanical stress.

Chapter 5

CONCLUSIONS AND RECOMMENDATIONS

The aim of this thesis was to synthesize Pd bimetallic films as a sensing material to detect hydrogen concentrations above the hydrogen low explosion limit of 4% v/v H₂ in air overcoming the limitations observed in pure Pd films. As part of our objectives, the Solid State Reduction (SSR) method was modified to synthesize our bimetallic materials. The conclusions and recommendations related with the use of SSR method to synthesize bimetallic films and its effect in the hydrogen sensing response are presented below.

5.1 Bimetallic film synthesized by the modified SSR Method

The SSR is an easy, fast and non expensive technique which requires the use of small amount of reagents and does not use organic solvents. This method does not need external energy sources to complete the reaction occurring at room temperature without current or voltage changes. Therefore the SSR complies several of the principles of green chemistry.

This method was developed to synthesize monometallic nanowires and then it was modified to synthesize pure palladium films. To achieve our objectives, this method was further modified and bimetallic films were synthesized. The optimal synthesis conditions studied to synthesize our bimetallic material include the addition of 2 μ L of deionized water during the reduction process and drying in air at room temperature. This allows to obtained rougher films avoiding cracks in the films' surfaces.

SEM and EDS results show the formation of bimetallic film on both sides of the AAM support with homogenous metal distribution for all the bimetallic mixtures except the Pd/Cr/AMM material. The XRD evidenced the crystalline structures of Pd and Ag which suggested that both metal were reduced. Platinum and nickel peaks were not detected by this technique, but the XPS results show that the platinum was also reduced. XPS results showed that our water washing removed all traces of the reducing agent and byproducts from our material. The oxidation state analysis using XPS showed that the silver salt (AgNO_3) was completely reduced whereas the palladium salt ($\text{Pd(NO}_3)_2 \cdot \text{H}_2\text{O}$) and the platinum salt ($\text{Pt(NH)}_4(\text{NO}_3)_2$) were only partially reduced with presence of palladium oxidized species and platinum interacting with some element in the films. XPS also showed that the nickel salt ($\text{Ni(NO}_3)_2 \cdot 6\text{H}_2\text{O}$) was not reduced by our method. The $\text{Cr(NO}_3)_3 \cdot 9\text{H}_2\text{O}$ salt was not studied with XPS but the results obtained suggest that it was not reduced either.

The complete reduction of silver salt is because, in addition to be an anhydrous salt, it was the only metal with partial charge +1 and because silver has a positive standard reduction potential.

As conclusion the SSR method works to form bimetallic films and nanowires supported on AAM if anhydrous salts of metals with positive standard reduction potentials are used.

As a recommendation other anhydrous or less hydrated metal salts with other ligands, such as: Rhodium(III) nitrate [$\text{Rh(NO}_3)_3 \cdot \text{H}_2\text{O}$], Palladium(II) chloride [PdCl_2], Platinum(II) chloride [PtCl_2], Chromium(II) chloride [CrCl_2], Gold(III) chloride [AuCl_3], Nickel(II) chloride [NiCl_2], Ruthenium(III) chloride [RuCl_3], and Rhodium(III) chloride [RhCl_3], can be used to promote the reduction of the desired metals by SSR. All considered metals are noble metals

which are resistant to corrosion and oxidation in air. In addition, Rh and Ru, similar to Pt, are part of the platinum group metals (PGM) which have similar physical and chemical properties to Pd. Also the analysis of the oxidation states of the metals by XPS after the reduction with H₂ should be studied to corroborate if the reduction was completed with the H₂ pretreatment. Also the synthesis should be modified and the use of a metal loading lower than 5 wt % should be considered in order to obtain the thinner films.

Despite the mentioned limitations, the fact that the SSR is an easy, fast, and not expensive method in which is not necessary the control of difficult parameters makes our method a good alternative for the synthesis of sensing materials.

5.2 Bimetallic films as a sensing material for hydrogen detection

Our results show that the synthesis of bimetallic films by the modified Solid State Reduction method is a good alternative for the design of materials that can be used as hydrogen sensors. The morphology of our materials allows its facile implementation as a sensor for hydrogen detection. But the presence of partial oxidized species requires a material pretreatment with hydrogen to promote the complete metal reduction.

Our material satisfies several specifications required to be an efficient hydrogen sensing material. Our bimetallic Pd/Pt/AAM and Pd/Ag/AAM detect hydrogen concentration over the LEL. This detection overcomes the limitation obtained with pure Pd film which detects hydrogen concentrations up to 1.5% - 2.0%. In addition these sensors are small size and light weight. In addition it is a cost effective as it doesn't require energy and the reaction is instantaneous. Also this material can be operated at 25°C avoiding the need to use higher temperatures.

Similar to pure Pd results, long response time were obtain with our bimetallic films, but current research studies that are being performed in our laboratory have shown that the response time can be enhanced optimizing the sensing test conditions. For example the chamber size where the tests were performed affects the time need to detect hydrogen, e.g. a smaller chamber shows faster response times.

The incorporation of Pt and Ag enhanced the palladium properties. Comparing with pure palladium, the addition of Pt allows the delay of the alpha to beta phase transition to higher concentrations and detected $[H_2]$ over the LEL. In general Pd/Pt material showed better sensing response than the other studied mixtures and allows the detection of higher concentrations without signal instability and more material reutilization. Therefore, Pd/Pt results showed great potential as a sensing material for hydrogen detection, even though it is not very studied and not considered by NASA. Add silver does not show a delay of the phase transition, but allow the detection of $[H_2]$ over the LEL. These results suggest that the enhancement of the sensors designed by SSR when a second metal is added occurs as a consequence of better hydrogen diffusion and not necessarily to the delay of the phase transition.

Our samples show that the sensitivity normalized by the response time (S/t_r) shows two linear relationships with $[H_2]^{1/2}$ not previously reported. Then our results, in addition to evidence an enhancement in the properties of Pd₉₀/Pt₁₀ compared with pure Pd, demonstrate that the sensitivity and response time results can be related in order to quantify the hydrogen concentrations. This allows the efficient use of our Pd₉₀/Pt₁₀ film as a sensing material for hydrogen detection at a wider range of concentrations.

However the sensing results showed a possible film damage when the material was reutilized. It can be as a result of internal mechanical stress which can provoke hysteresis, embrittlement, delamination or other film damage. SEMs after reutilization should be performed in order to study or identify cracks and film damage. In order to avoid this film damage, our synthesis should be modified to obtain thinner films. As mentioned in Chapter 1, reported results demonstrated that thin films can be strongly confined to the substrate, and other absorption of H atoms and the lattice expansion was restricted. Also, this strong interaction between the films and the substrate avoid mechanical stress which therefore avoid further film damage. Finally, the displays in the baseline can be a consequence of not efficient electrodes connections. This should be corroborated but in overall, it is evidenced that the use of our SSR method allows the synthesis of bimetallic material which can be used in different applications such as an efficient hydrogen sensors, but its require the use of anhydrous precursors salts.

Appendix

Appendix A

Elements identification by XPS Technique

The full scan XPS spectrums for all the samples are presented in Figures A1-A6 . Sodium and boron elements are not detected in 95% of our spectrums (17 out of 18) suggesting that the cleaning process after the reduction is efficient. These spectrums were analyzed to obtain the surface elemental composition using CasaXPS Software. Results are presented in Appendix B.

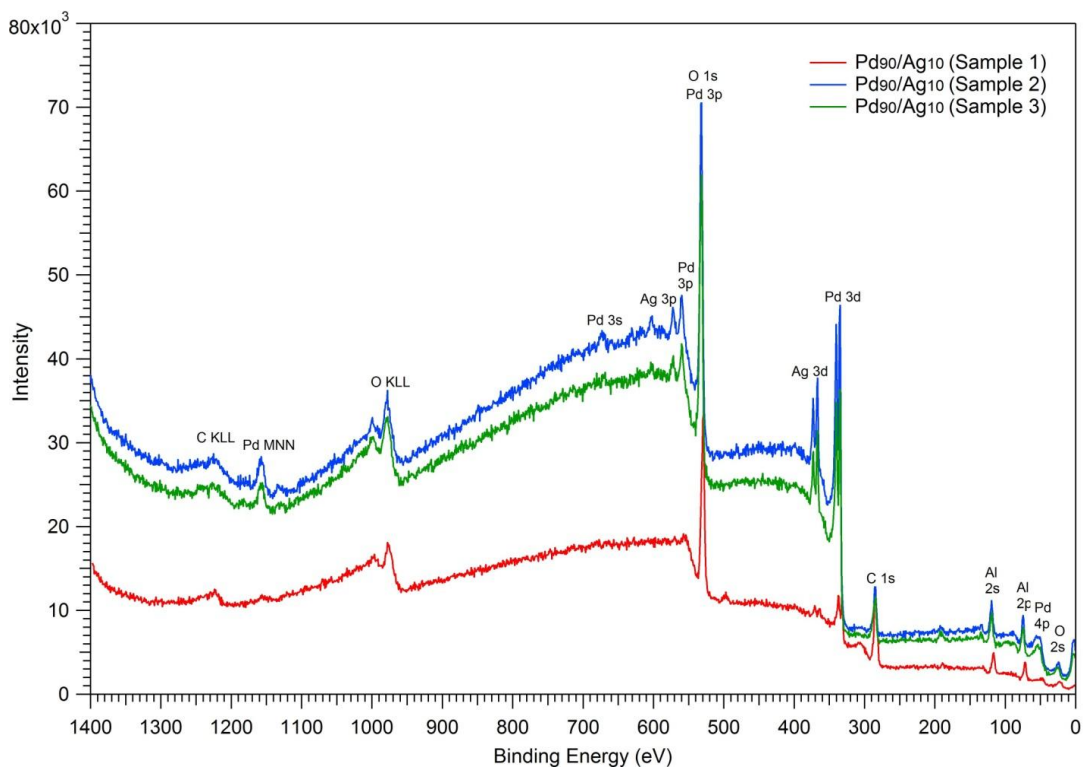


Figure A. 1 XPS spectra of Pd₉₀/Ag₁₀ Impregnation Side

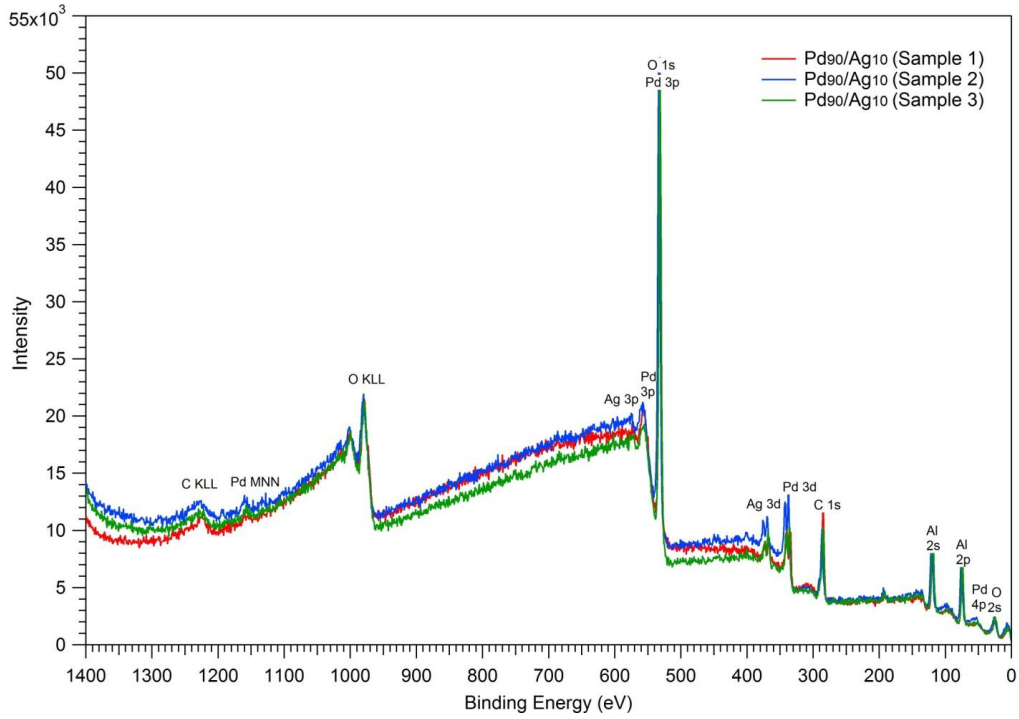


Figure A. 2 XPS spectra of Pd₉₀/Ag₁₀ Reduction Side

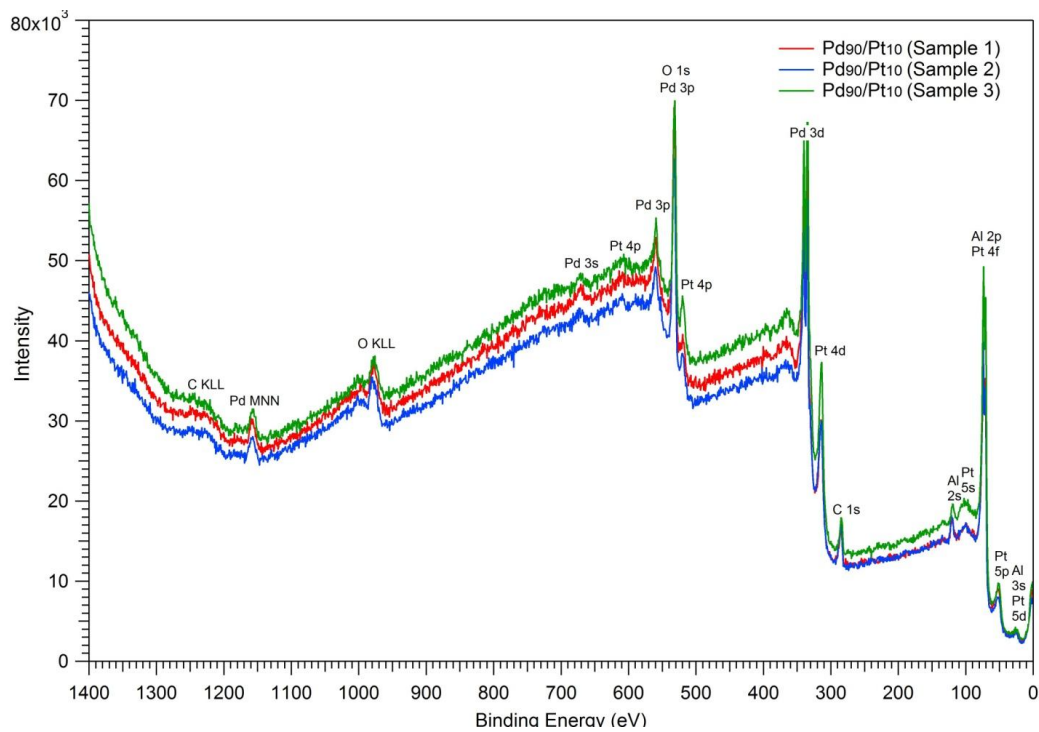


Figure A. 3 XPS spectra of Pd₉₀/Pt₁₀ Impregnation Side

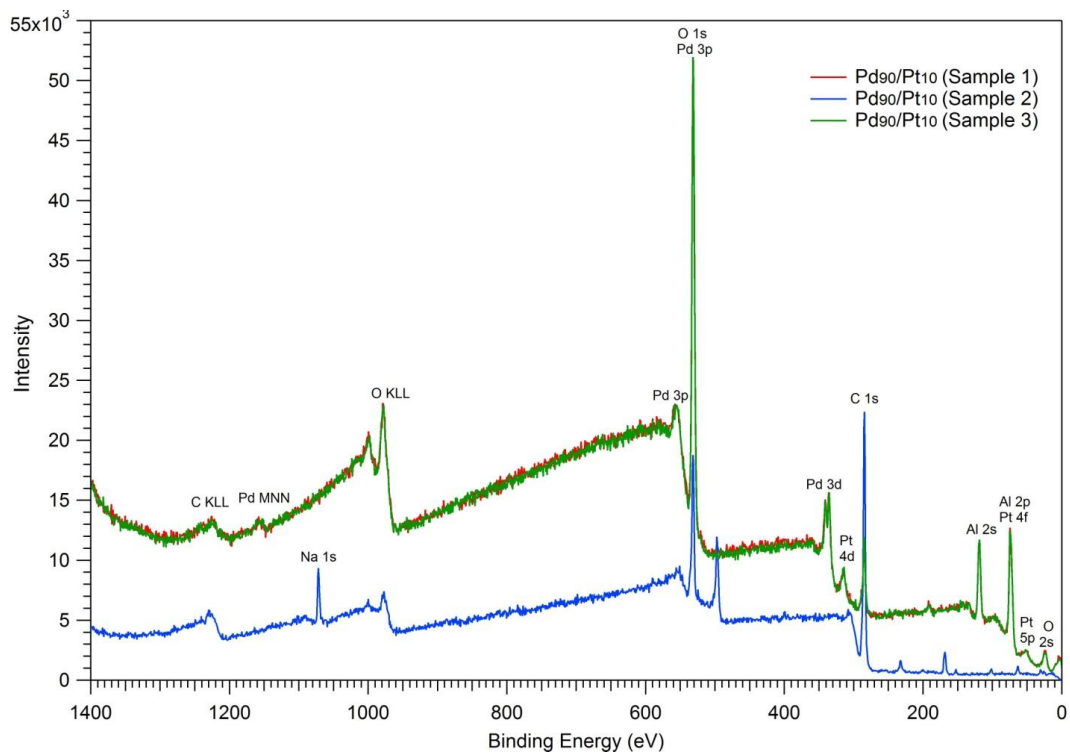


Figure A. 4 XPS spectra of Pd₉₀/Pt₁₀ Reduction Side

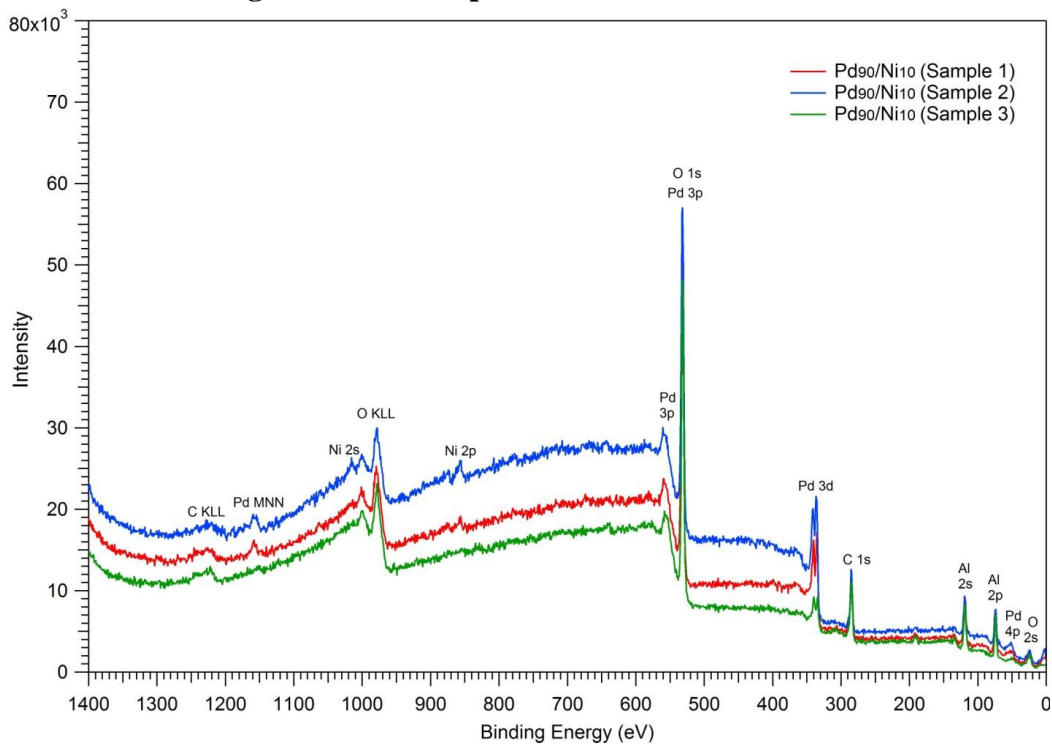


Figure A. 5 XPS spectra of Pd₉₀/Ni₁₀ Impregnation Side

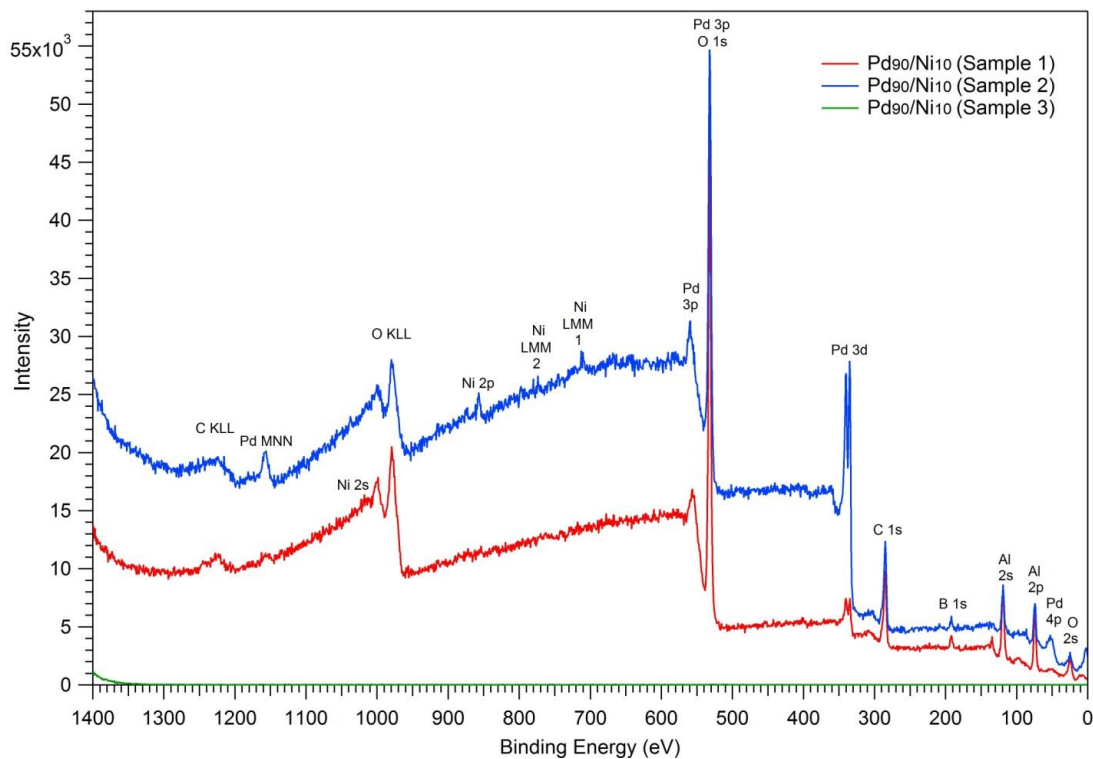


Figure A. 6 XPS spectra of Pd₉₀/Ni₁₀ Reduction Side

Appendix B

Metal Elemental Analysis obtained with CasaXPS Software

Elemental metal compositional data of the bimetallic films was obtained by analyzing the XPS spectra with Casa XPS Software. These results were summarized in Table 3.1. The Pt 4d peaks were used to quantify the metal composition but in the case of the oxidation states the analysis was performed using Pt 4f orbital.

B.1 Pd₉₀/Ag₁₀ membrane

B.1.1 Membrane side where the precursors were added

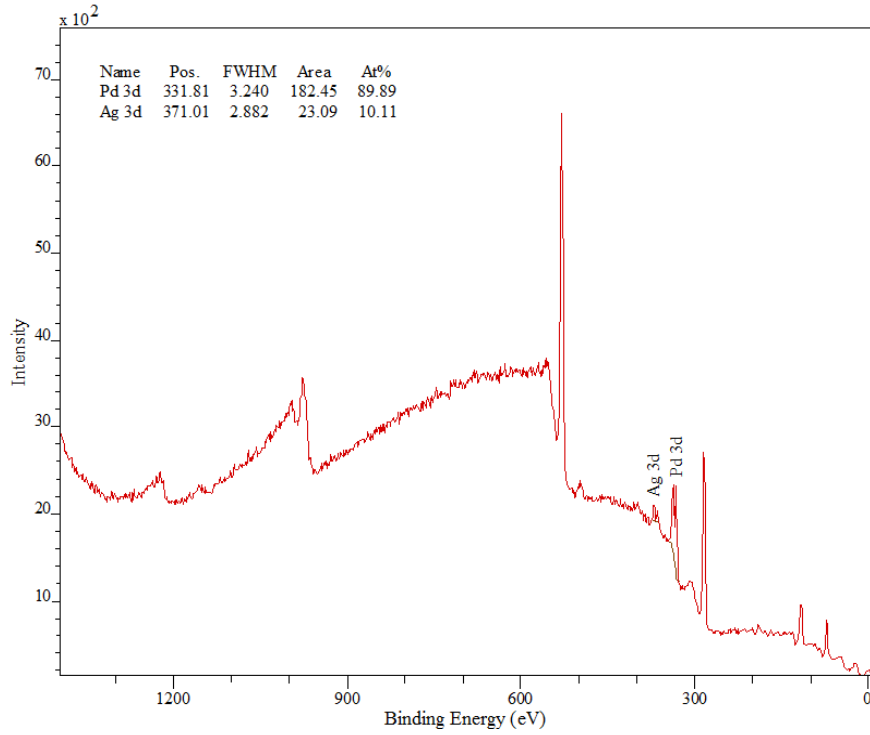


Figure B. 1 Impregnation side of Pd₉₀/Ag₁₀ (Sample 1)

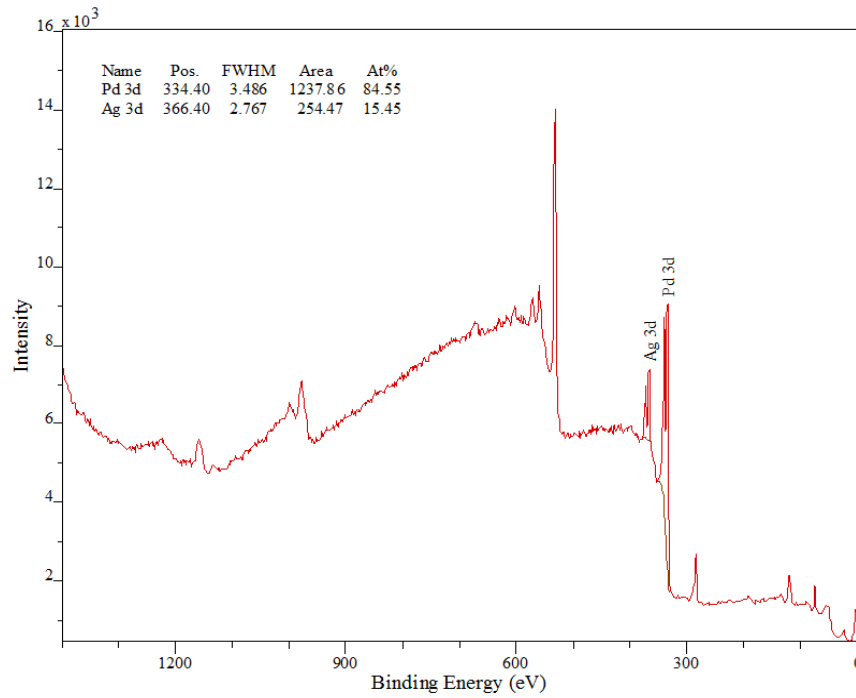


Figure B. 2 Impregnation side of Pd₉₀/Ag₁₀ (Sample 2)

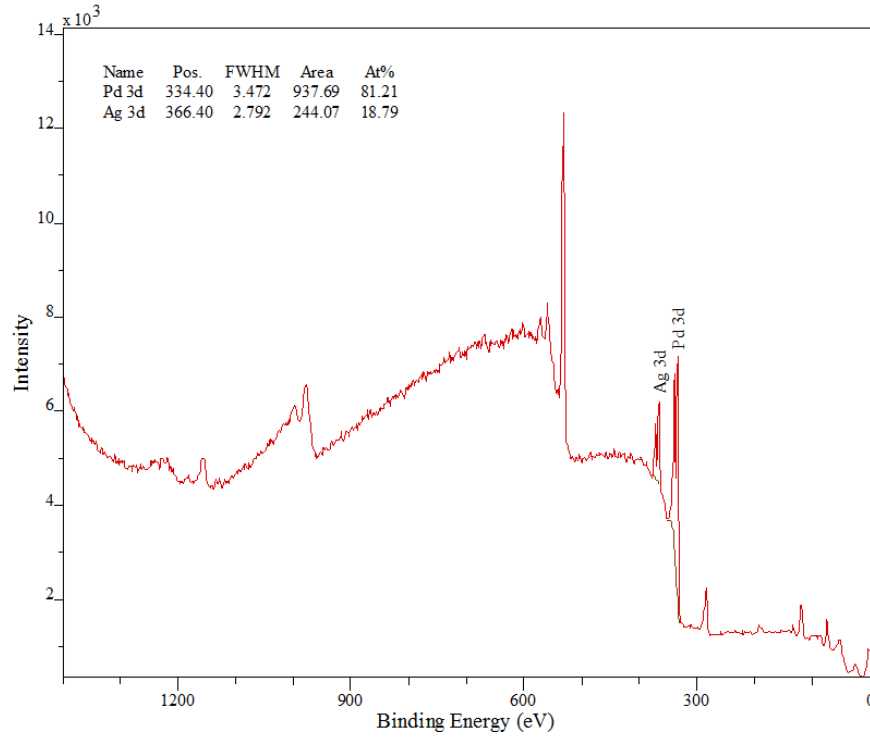


Figure B. 3 Impregnation side of Pd₉₀/Ag₁₀ (Sample 3)

B.1.2 Membrane side where the reduction agent was spread

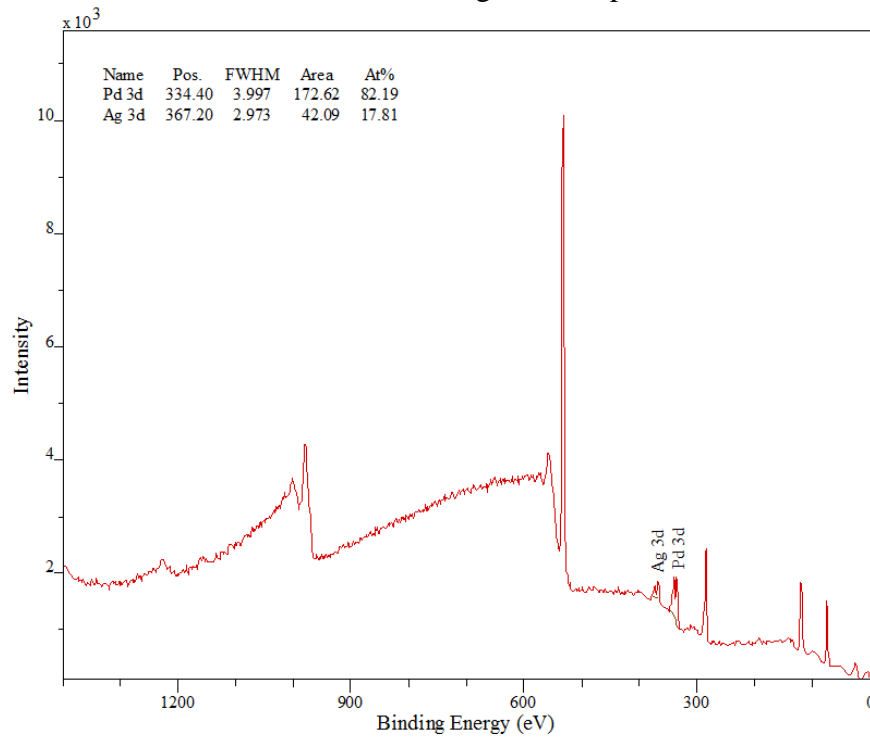


Figure B. 4 Reduction side of Pd₉₀/Ag₁₀ (Sample 1)

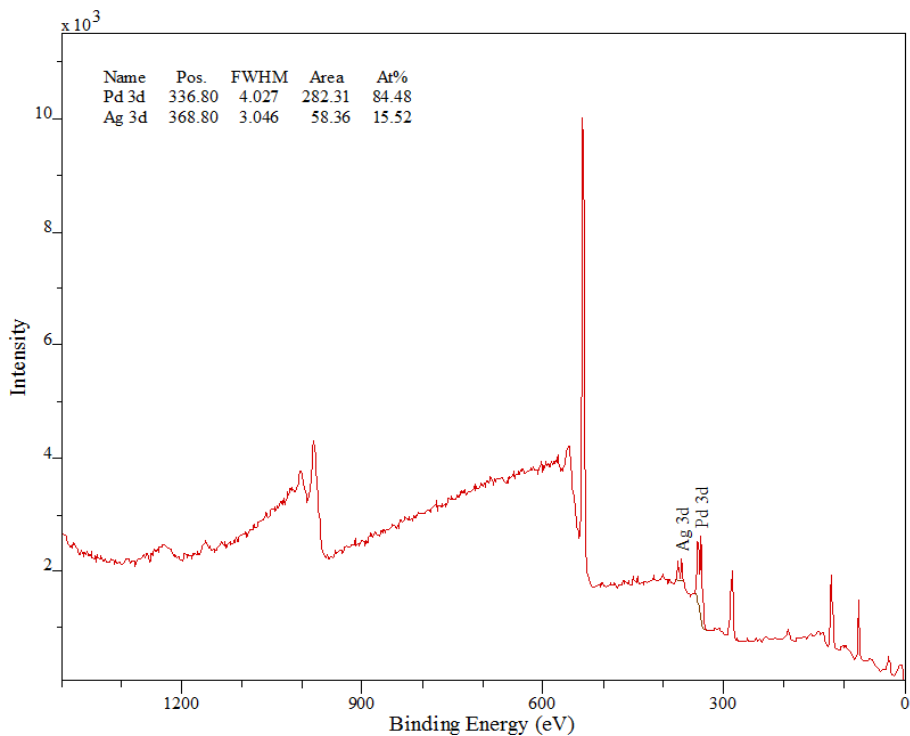


Figure B. 5 Reduction side of Pd₉₀/Ag₁₀ (Sample 2)

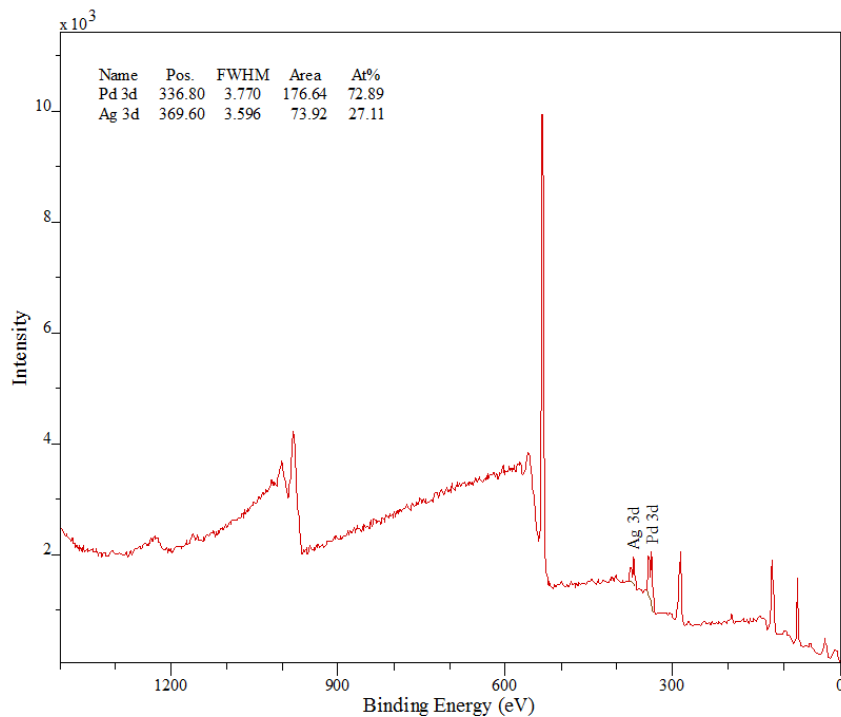


Figure B. 6 Reduction side of Pd₉₀/Ag₁₀ (Sample 3)

B.2 Pd₉₀/Pt₁₀ membrane

B.2.1 Membrane side where the precursors were added

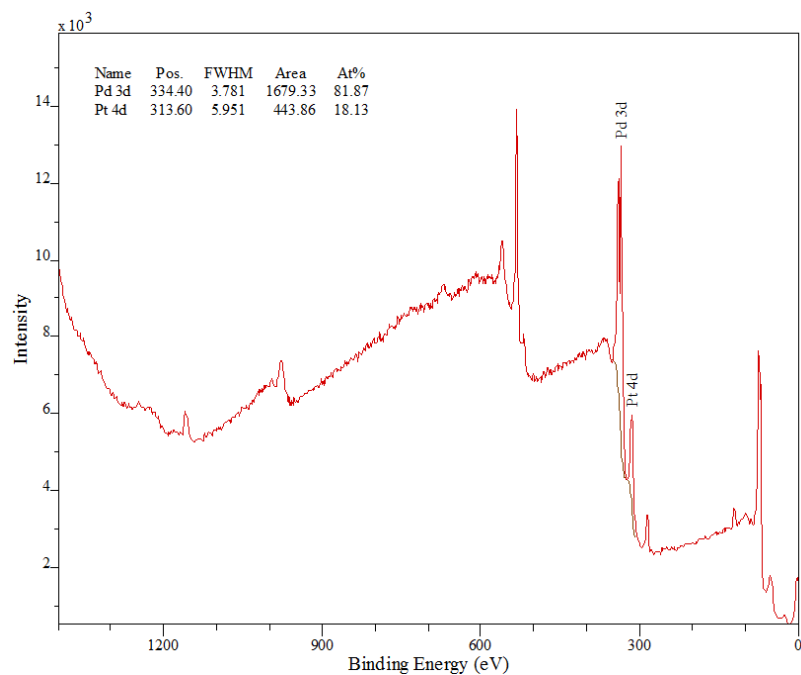


Figure B. 7 Impregnation side of Pd₉₀/Pt₁₀ (Sample 1)

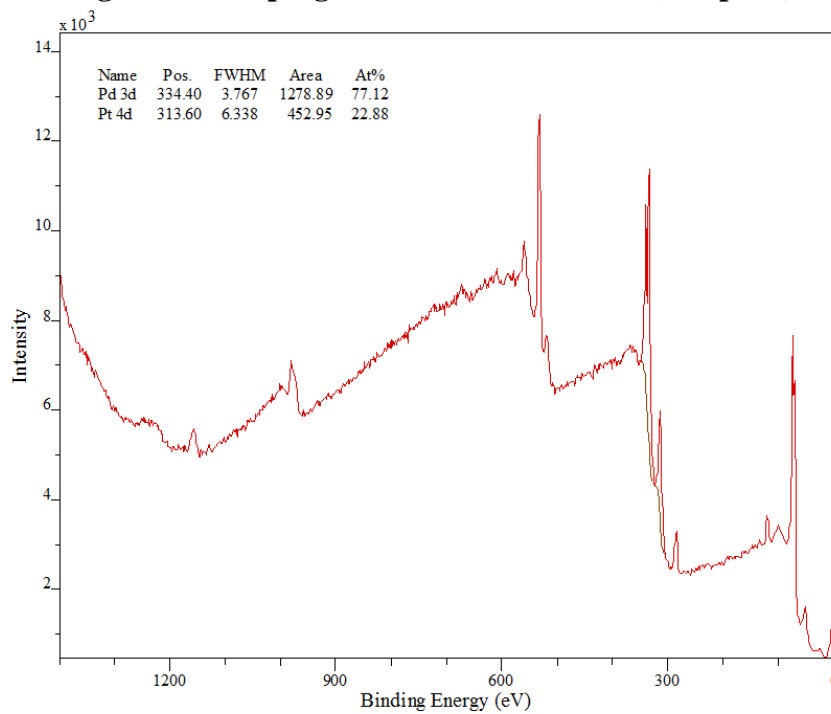


Figure B. 8 Impregnation side of Pd₉₀/Pt₁₀ (Sample 2)

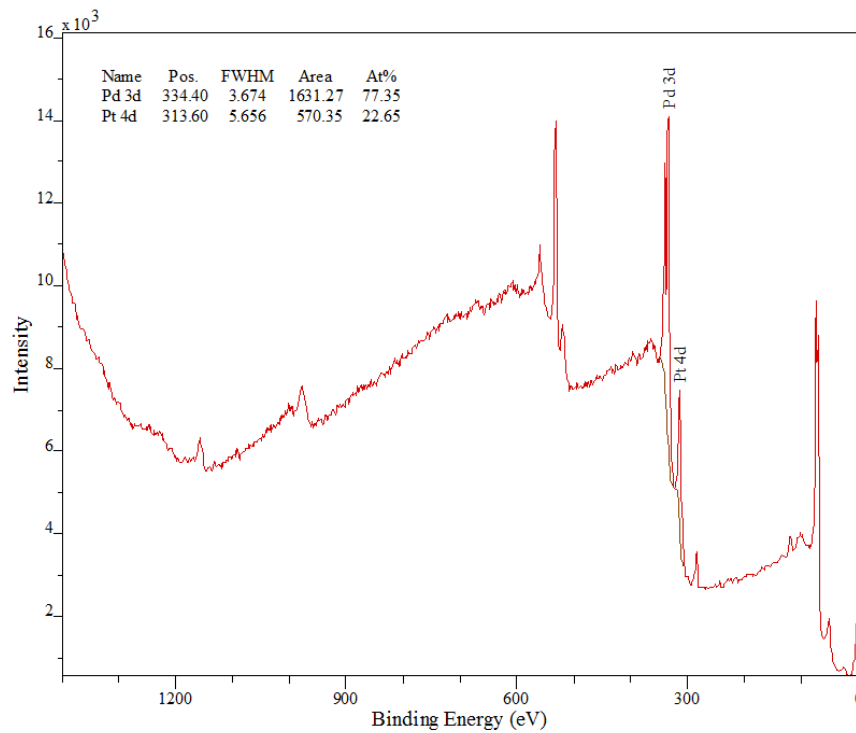


Figure B. 9 Impregnation side of Pd₉₀/Pt₁₀ (Sample 3)

B.2.2 Membrane side where reduction agent was spread

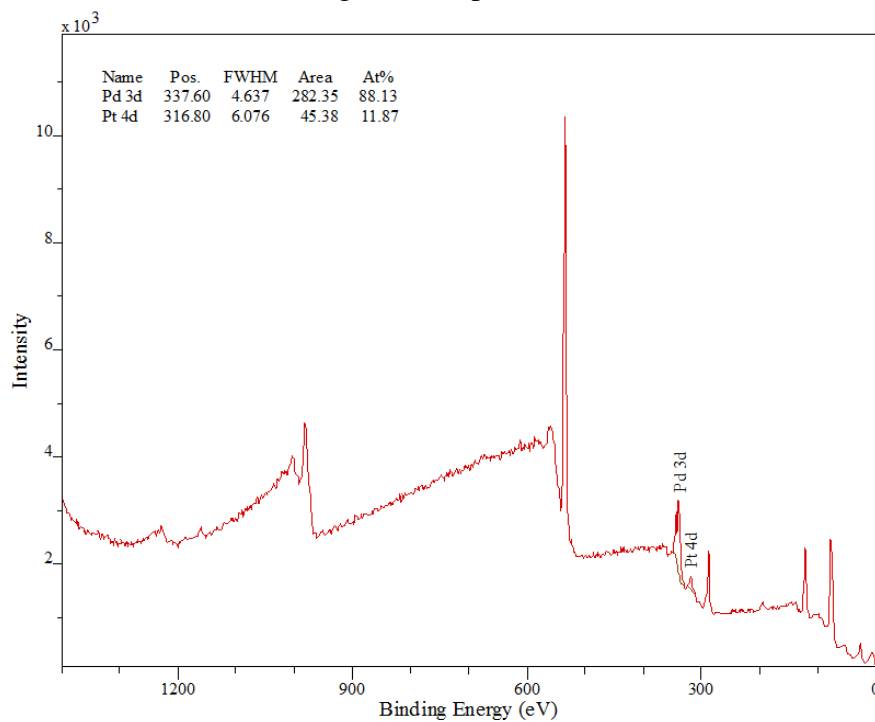


Figure B. 10 Reduction side of Pd₉₀/Pt₁₀ (Sample 1)

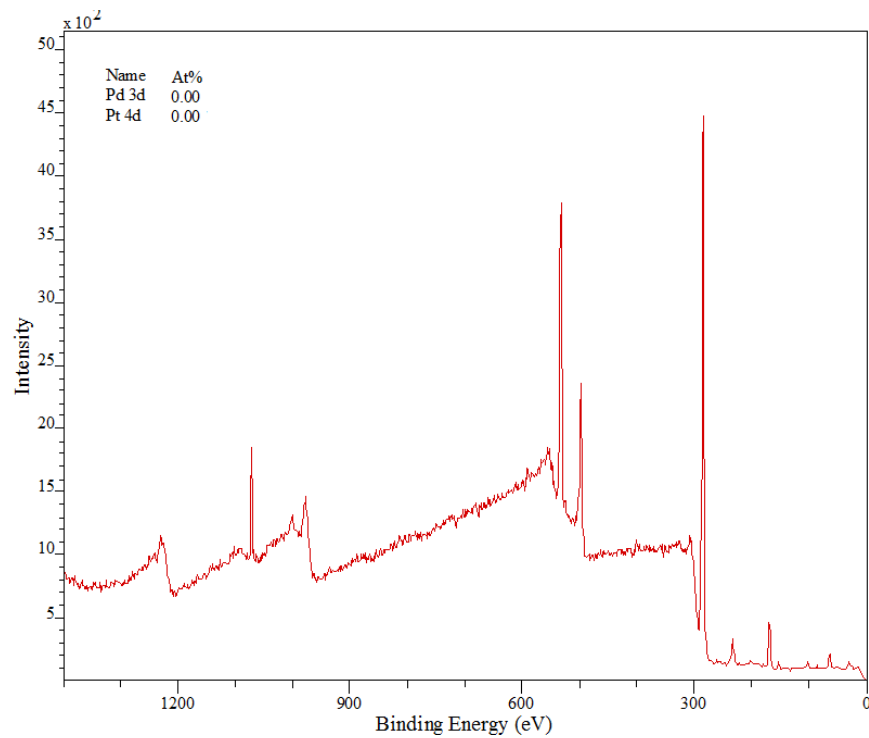


Figure B. 11 Reduction side of Pd₉₀/Pt₁₀ (Sample 2)

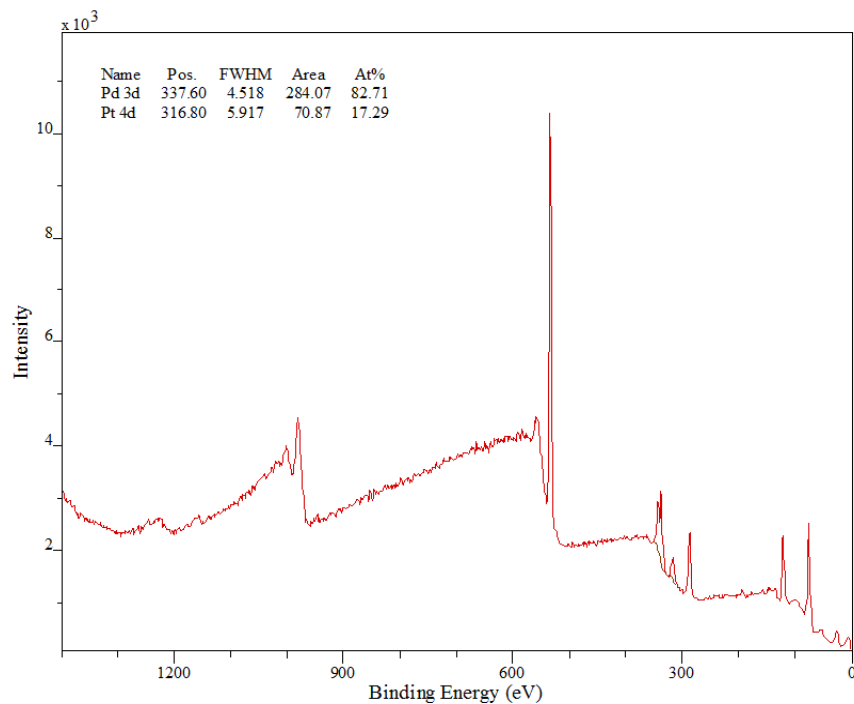


Figure B. 12 Reduction side of Pd₉₀/Pt₁₀ (Sample 3)

B.3 Pd₉₀/Ni₁₀ membrane

B.3.1 Membrane side where the precursors were added

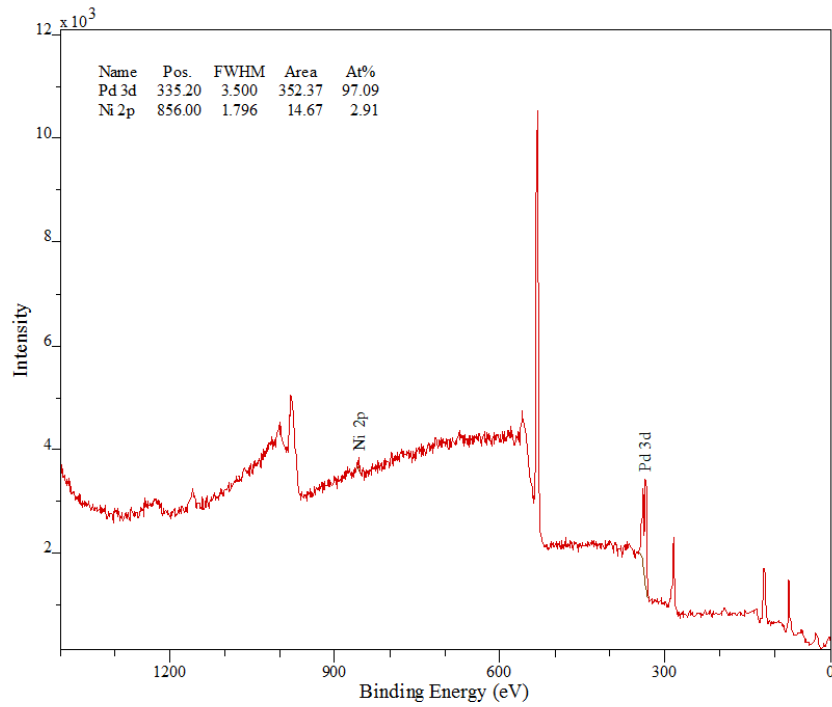


Figure B. 13 Impregnation side of Pd₉₀/Ni₁₀ (Sample 1)

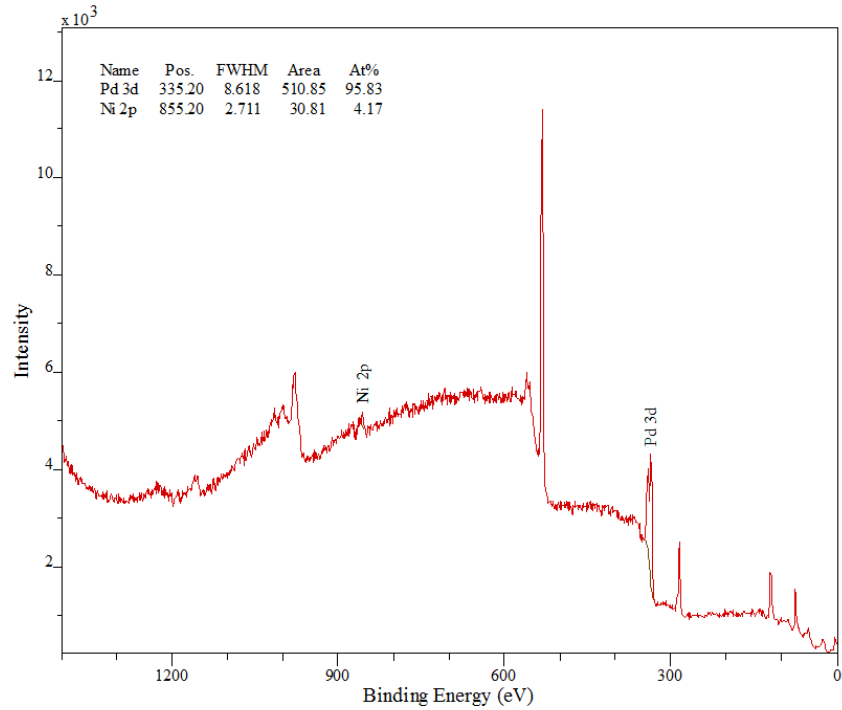


Figure B. 14 Impregnation side of Pd₉₀/Ni₁₀ (Sample 2)

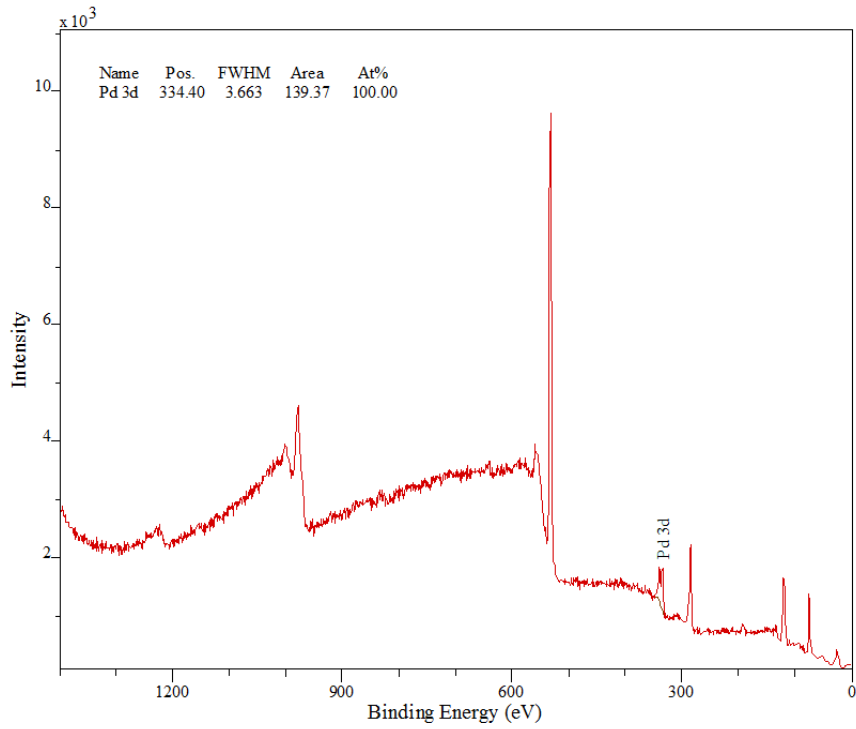


Figure B. 15 Impregnation side of Pd₉₀/Ni₁₀ (Sample 3)

B.3.2 Membrane side where the reduction agent was spread

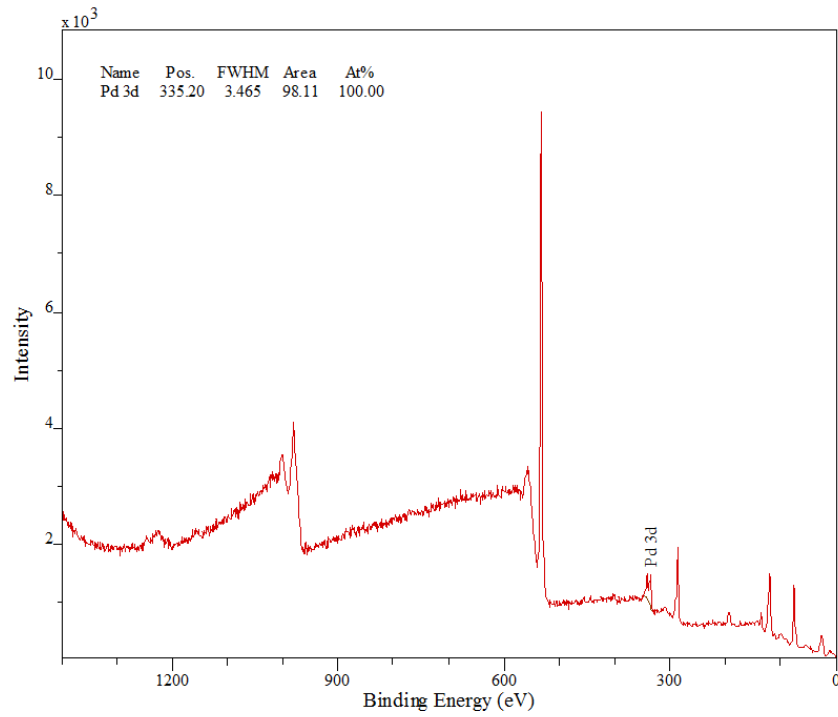


Figure B. 16 Reduction side of Pd₉₀/Ni₁₀ (Sample 1)

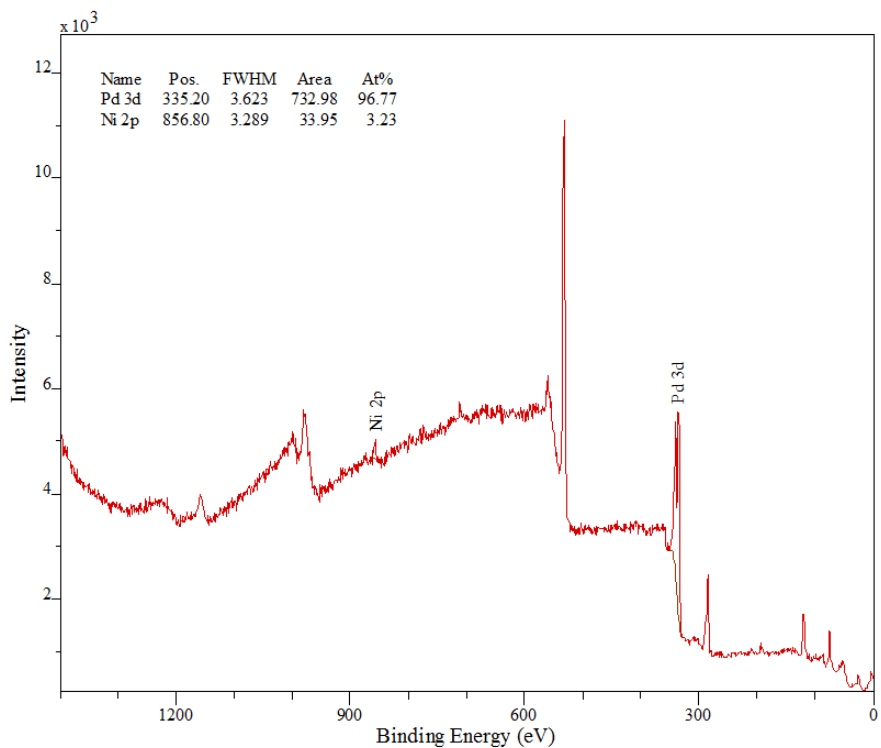


Figure B. 17 Reduction side of Pd₉₀/Ni₁₀ (Sample 2)

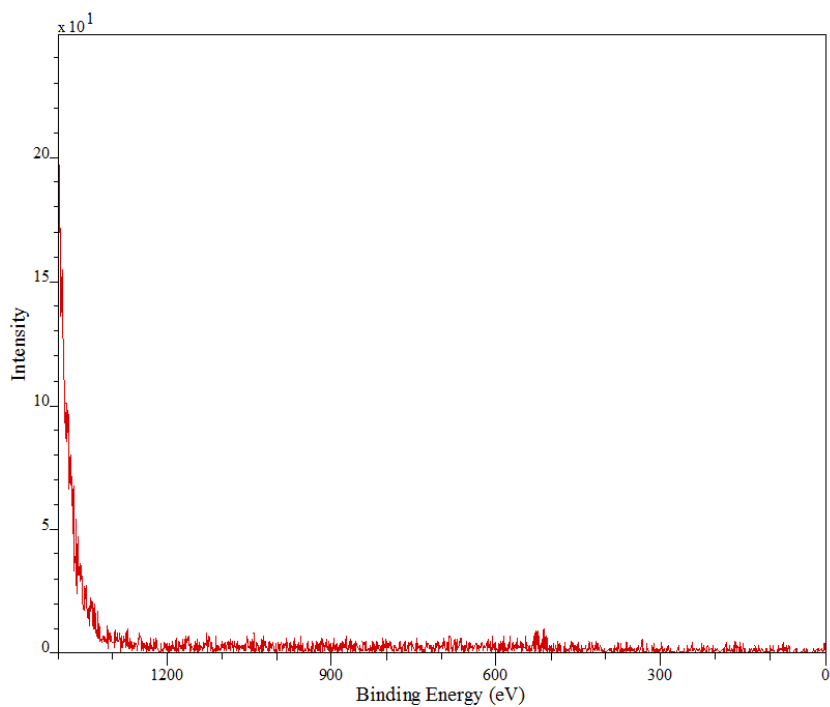


Figure B. 18 Reduction side of Pd₉₀/Ni₁₀ (Sample 3)

* NOTE: Elements were not detected on this run.

Appendix C

Analysis of the Metal Oxidation States obtained with CasaXPS Software

X-Ray Photoelectron Spectroscopy Analysis was also used to study the metals' chemical states. The XPS results were analyzed using the Casa XPS Software. Peaks deconvolution was performed in order to determine the chemical environment and chemical state of each metal in each bimetallic film. In this section the deconvolution of the peaks are presented. The binding energies and the classification of each peak are reported in Tables C.1 – C.3 for Pd₉₀/Ag₁₀, Pd₉₀/Pt₁₀, and Pd₉₀/Ni₁₀ respectively. The orbital 3d was used for the oxidation states analysis of palladium and silver, orbital 4f for platinum and 2p for nickel. The averages of these results were calculated and discussed in Chapter 3 (Tables 3.3, 3.4, and 3.5)

C.1 Pd₉₀/Ag₁₀ membrane

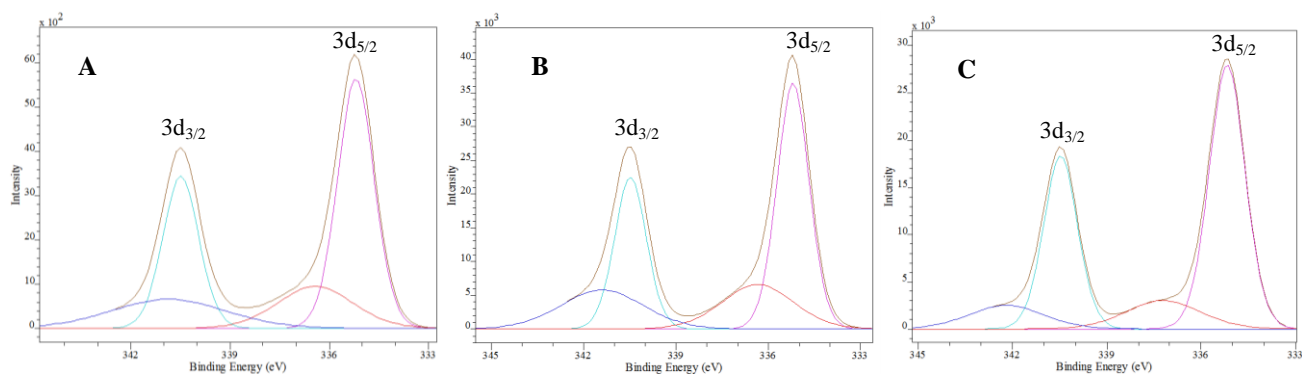


Figure C. 1 Peaks deconvolution of Pd's 3d orbitals in Pd₉₀/Ag₁₀ bimetallic film formed in the impregnation side. (A: sample 1, B: sample 2, C: sample 3)

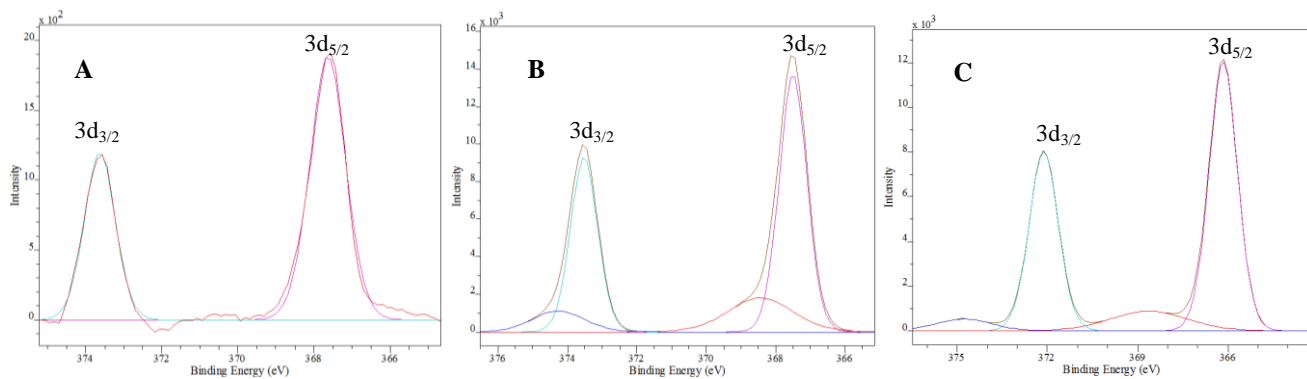


Figure C. 2 Peaks deconvolution of Ag's 3d orbitals in Pd₉₀/Ag₁₀ bimetallic film formed in the impregnation side. (A: sample 1, B: sample 2, C: sample 3)

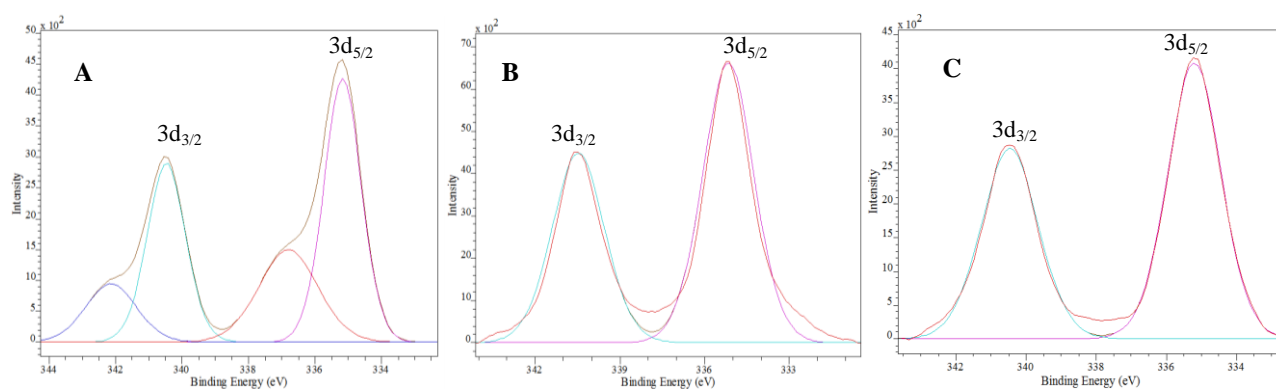


Figure C. 3 Peaks deconvolution of Pd's 3d orbitals in Pd₉₀/Ag₁₀ bimetallic film formed in the reduction side. (A: sample 1, B: sample 2, and C: sample 3)

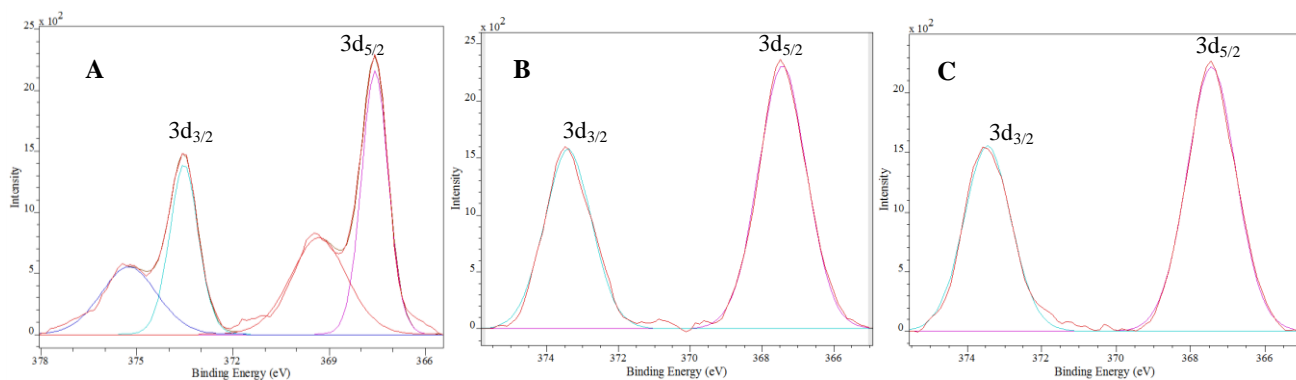


Figure C. 4 Peaks deconvolution of Ag's 3d orbitals in Pd₉₀/Ag₁₀ bimetallic film formed in the reduction side. (A: sample 1, B: sample 2, and C: sample 3)

C.2 Pd₉₀/Pt₁₀ membrane

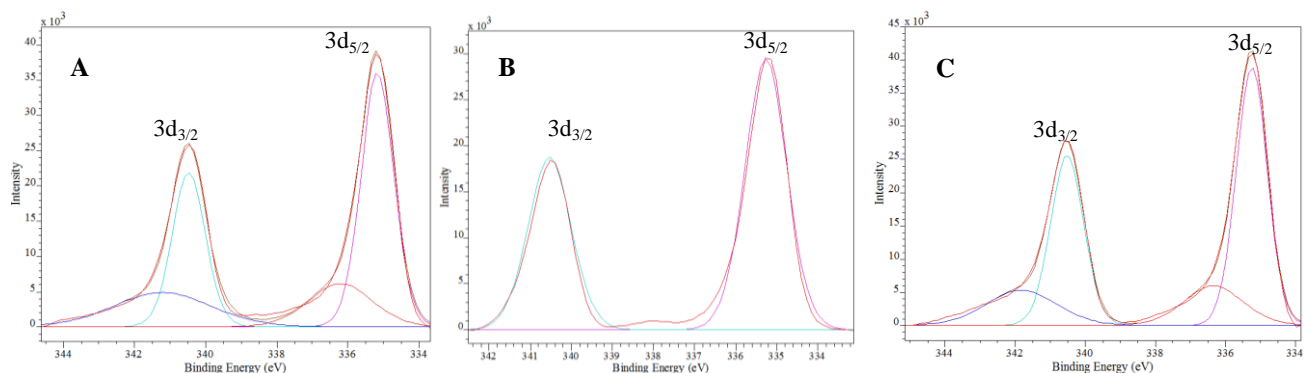


Figure C. 5 Peaks deconvolution of Pd's 3d orbitals in Pd₉₀/Pt₁₀ bimetallic film formed in the impregnation side. (A: sample 1, B: sample 2, and C: sample 3)

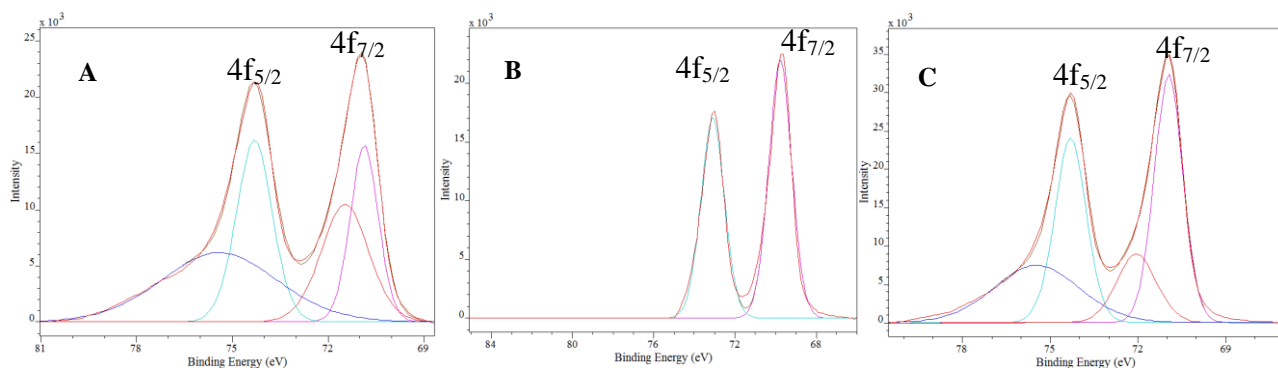


Figure C. 6 Peaks deconvolution of Pt's 4f orbitals in Pd₉₀/Pt₁₀ bimetallic film formed in the impregnation side. (A: sample 1, B: sample 2, and C: sample 3)

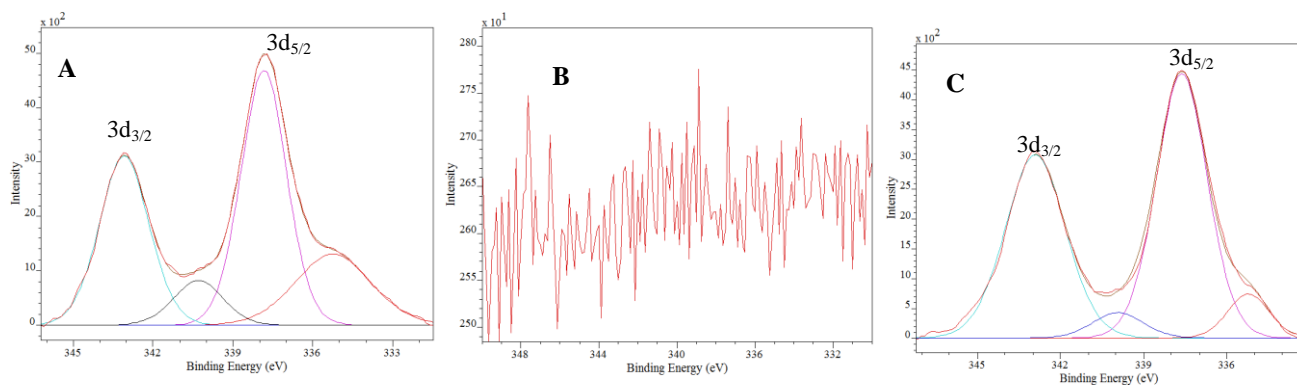


Figure C. 7 Peaks deconvolution of Pd's 3d orbitals in Pd₉₀/Pt₁₀ bimetallic film formed in the reduction side. Pd was not detected in sample 2. (A: sample 1, B: sample 2, and C: sample 3)

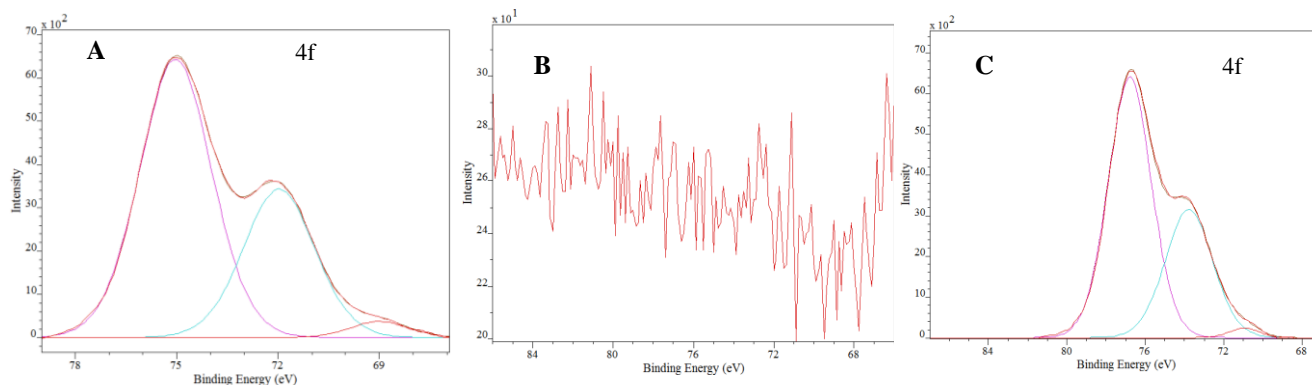


Figure C. 8 Peaks deconvolution of Pt's 4f orbitals in Pd₉₀/Pt₁₀ bimetallic film formed in the reduction side. Pt was not detected in Sample 2. (A: sample 1, B: sample 2, and C: sample 3)

C.3 Pd₉₀/Ni₁₀ membrane

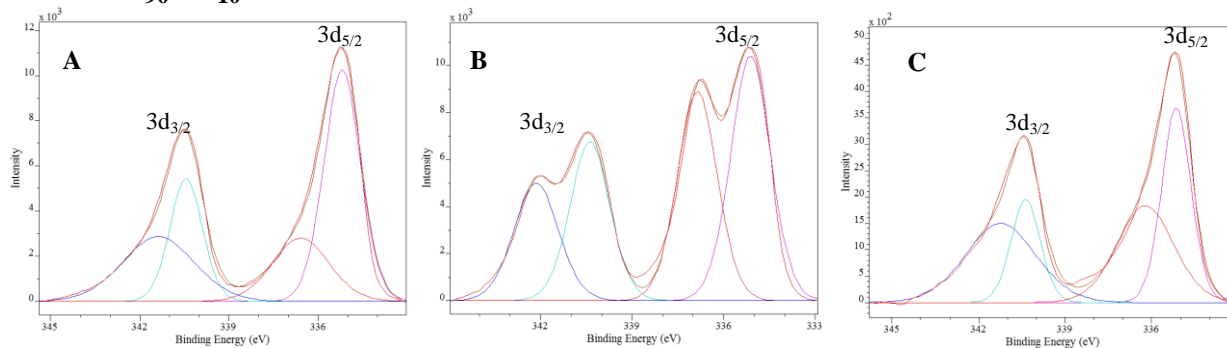


Figure C. 9 Peaks deconvolution of Pd's 3d orbitals in Pd₉₀/Ni₁₀ bimetallic film formed in the impregnation side. (A: sample 1, B: sample 2, and C: sample 3)

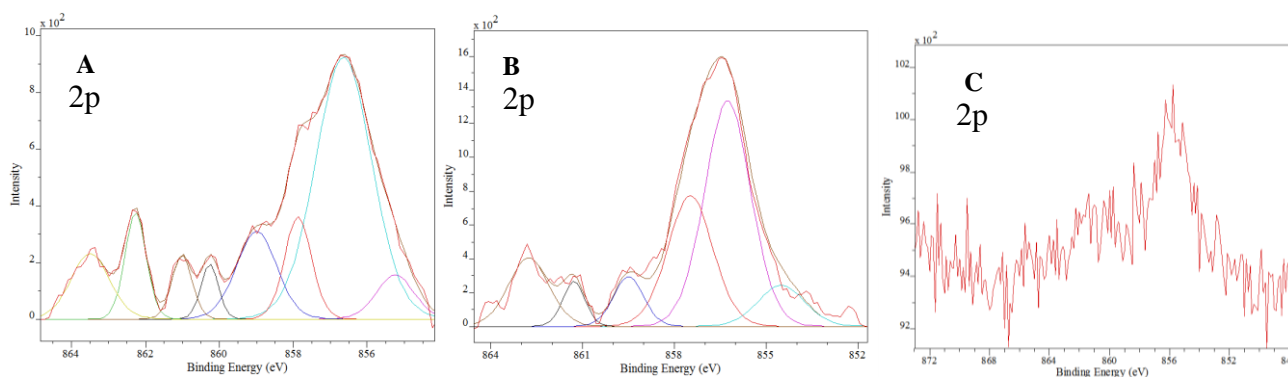


Figure C. 10 Peaks deconvolution of Ni's 2p orbitals in Pd₉₀/Ni₁₀ bimetallic film formed in the impregnation side. Ni can't be differentiated in the analyzed area presented in C. (A: sample 1, B: sample 2, and C: sample 3)

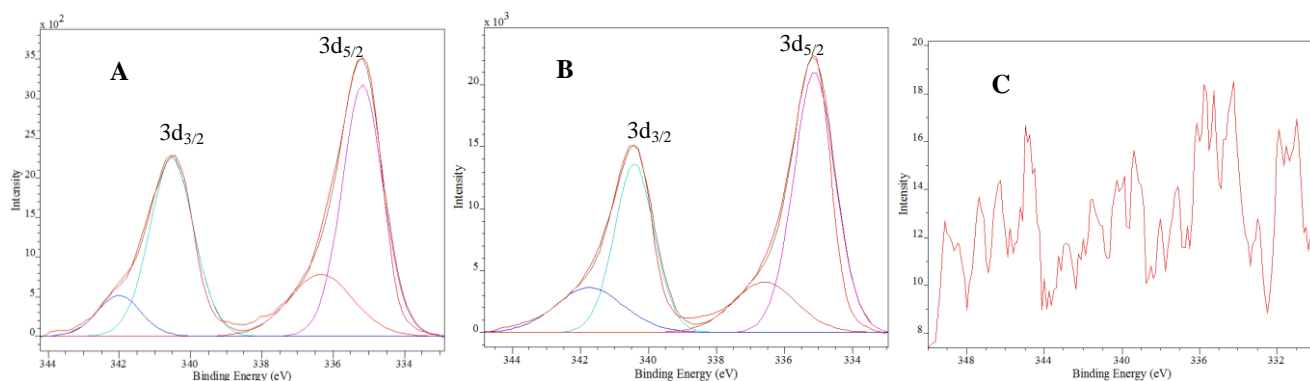


Figure C. 11 Peaks deconvolution of Pd's 3d orbitals in Pd₉₀/Ni₁₀ bimetallic film formed in the reduction side. Pd was not detected in sample 3. (A: sample 1, B: sample 2, and C: sample 3)

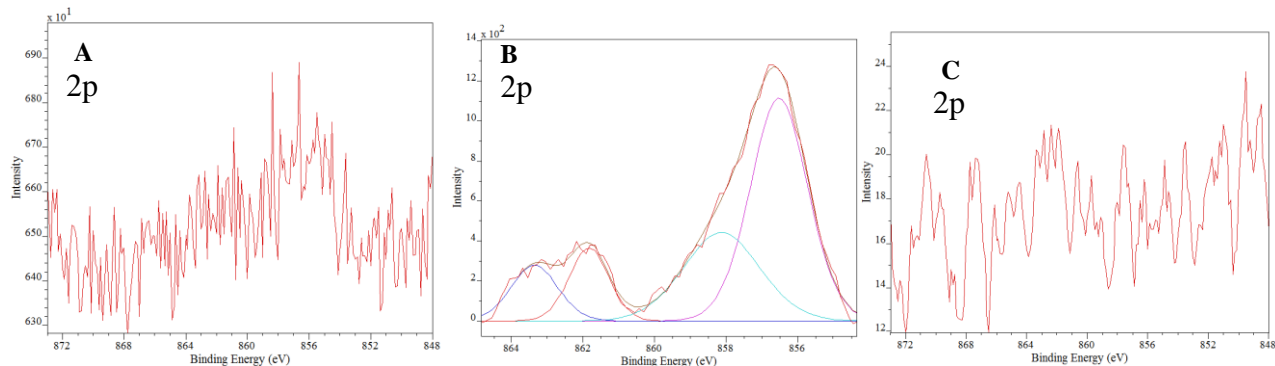


Figure C. 12 Peaks deconvolution of Ni's 2p orbitals in Pd₉₀/Ni₁₀ bimetallic film formed in the reduction side. Ni can't be differentiated in the analyzed areas presented in A and C. A: sample 1, B: sample 2, and C: sample 3)

Table C. 1 XPS results of Pd₉₀/Ag₁₀ after peaks deconvolution using CASA-XPS

Sample	Metal	Precursors Side				Reduction Side			
		Peak	%	FWHM	Description	Peaks	%	FWHM	Description
1	Pd	335.201	40.36	1.299	Pd(0) 3d _{5/2} ^A	335.205	38.17	1.297	Pd(0) 3d _{5/2} ^A
		336.914	14.67	2.863	PdO 3d _{5/2} ^B Pd(2+)	336.816	23.39	2.246	PdO 3d _{5/2} ^B Pd(2+)
		340.473	30.85	1.451	Pd(0) 3d _{3/2}	340.501	26.45	1.357	Pd(0) 3d _{3/2}
		342.446	14.12	4.075	PdO 3d _{3/2} Pd(2+)	342.176	13.55	2.020	PdO 3d _{3/2} Pd(2+)
	Ag	367.569	61.42	1.060	Ag(0) 3d _{5/2} ^C (interacting with Pd)	367.571	35.04	0.973	Ag(0) 3d _{5/2} ^C (interacting with Pd)
		-	-	-	-	369.418	23.99	1.775	Unknown 369.0 eV for Ag ₅ Al ₉₅ ^A
		373.557	38.58	1.007	Ag(0) 3d _{3/2} (interacting with Pd)	373.536	21.75	0.971	Ag(0) 3d _{3/2} (interacting with Pd)
-	-	-	-	375.249	19.21	2.124	Unknown		
2	Pd	335.204	39.42	1.212	Pd(0) 3d _{5/2} ^A	335.200	59.43	1.900	Pd(0) 3d _{5/2} ^A
		336.239	18.92	2.735	PdO 3d _{5/2} ^{A,B} Pd(2+)				
		340.487	25.06	1.216	Pd(0) 3d _{3/2}	340.514	40.57	1.900	Pd(0) 3d _{3/2}
		341.428	16.60	3.137	PdO 3d _{3/2} Pd(2+)				
	Ag	367.519	45.46	0.928	Ag(0) 3d _{5/2} ^C (interacting with Pd)	367.446	60.83	1.561	Ag(0) 3d _{5/2} ^C
		368.324	15.77	2.177	Ag(0) 3d _{5/2} ^{A,C} (Pure)	-	-	-	-
		373.509	29.03	0.905	Ag(0) 3d _{3/2} (interacting with Pd)	373.426	39.17	1.490	Ag(0) 3d _{3/2}
374.087	9.74	1.753	Ag(0) 3d _{3/2} (Pure)	-	-	-	-		
3	Pd	335.198	42.38	1.229	Pd(0) 3d _{5/2} ^A	335.198	57.5	1.700	Pd(0) 3d _{5/2} ^A
		336.425	16.18	2.782	PdO 3d _{5/2} ^{A,B} Pd(2+)	-	-	-	-
		340.494	31.69	1.290	Pd(0) 3d _{3/2}	340.463	42.5	1.900	Pd(0) 3d _{3/2}
		342.431	9.74	2.791	PdO 3d _{3/2} Pd(2+)				
	Ag	367.505	50.07	1.098	Ag(0) 3d _{5/2} ^C (interacting with Pd)	367.481	59.73	1.541	Ag(0) 3d _{5/2} ^C
		369.847	10.89	3.119	Unknown 369.0 eV for Ag ₅ Al ₉₅ ^A	-	-	-	-
		373.593	34.35	1.124	Ag(0) 3d _{3/2} (interacting with Pd)	373.494	40.27	1.484	Ag(0) 3d _{3/2}
376.287	4.70	2.159	Unknown	-	-	-	-		

- A. Φ Handbook of X-Ray photoelectron Spectroscopy
 B. Data obtain from [99,104]
 C. Data obtained from [95,100]. Ag shifts -0.7 eV when interacts with Pd in a molar ratio of Pd₉₀:Ag₁₀

Table C. 2 XPS results of Pd₉₀/Pt₁₀ after peaks deconvolution using CASA-XPS

Sample	Metal	Precursors Side				Reduction Side			
		Peak	%	FWHM	Description	Peak	%	FWHM	Description
1	Pd	335.20	42.74	1.09	Pd(0) 3d _{5/2} ^A	335.20	18.62	3.25	Pd(0) 3d _{5/2} ^A
		336.24	14.04	2.11	PdO 3d _{5/2} ^A Pd(2+)	337.91	42.30	1.09	PdO ₂ 3d _{5/2} ^A Pd(4+)
		340.50	26.01	1.09	Pd(0) 3d _{3/2}	340.35	8.25	2.15	Pd(0) 3d _{3/2}
		341.25	17.18	3.22	PdO 3d _{3/2} Pd(2+)	343.18	30.83	2.27	PdO ₂ 3d _{3/2} Pd(4+)
	Pt	70.89	19.74	1.03	Pt (0) 4f _{7/2} ^A	70.96	2.93	1.99	Pt (0) 4f _{7/2} ^A
		71.50	22.32	1.76	Pt (δ+) 4f _{7/2}	73.93	33.61	2.48	Al ₂ O ₃ ^A
		74.34	25.99	1.32	Pt(0) 4f _{5/2}	74.98	63.46	2.48	Unknown
		75.44	31.96	4.26	Pt (δ+) 4f _{5/2}	-	-	-	-
2	Pd	335.20	60.33	1.19	Pd(0) 3d _{5/2} ^A	-	-	-	-
		340.46	39.67	1.23	Pd(0) 3d _{3/2}	-	-	-	-
		-	-	-	-	-	-	-	-
		-	-	-	-	-	-	-	-
	Pt	70.97	55.64	55.64	Pt (0) 4f _{7/2} ^A	-	-	-	-
		74.29	44.36	1.35	Pt(0) 4f _{5/2}	-	-	-	-
		-	-	-	-	-	-	-	-
		-	-	-	-	-	-	-	-
3	Pd	335.25	43.26	1.03	Pd(0) 3d _{5/2} ^A	335.20	6.65	1.75	Pd(0) 3d _{5/2} ^A
		336.23	12.83	1.97	PdO 3d _{5/2} ^A Pd(2+)	337.59	49.03	2.16	PdO ₂ 3d _{5/2} ^A Pd(4+)
		340.72	30.33	1.09	Pd(0) 3d _{3/2}	339.91	4.68	2.13	Pd(0) 3d _{3/2}
		341.82	13.58	2.36	PdO 3d _{3/2} Pd(2+)	342.87	39.64	2.52	PdO ₂ 3d _{3/2} Pd(4+)
	Pt	71.00	39.88	1.23	Pt (0) 4f _{7/2} ^A	70.94	1.65	1.79	Pt (0) 4f _{7/2} ^A
		72.38	9.02	1.28	Pt (δ+) 4f _{7/2}	73.77	34.62	2.83	Al ₂ O ₃ ^A
		74.28	30.29	1.27	Pt(0) 4f _{5/2}	76.76	63.74	2.57	Unknown
		75.75	20.81	2.87	Pt (δ+) 4f _{5/2}	-	-	-	-

A. Φ Handbook of X-Ray photoelectron Spectroscopy

Table C. 3 XPS results of Pd₉₀/Ni₁₀ after peaks deconvolution using CASA-XPS

Sample	Metal	Precursors Side				Reduction Side			
		Peak	%	FWHM	Description	Peaks	%	FWHM	Description
1	Pd	335.20	33.77	1.27	Pd(0) 3d _{5/2} ^A	335.17	43.24	1.35	Pd(0) 3d _{5/2} ^A
		336.30	23.78	2.22	PdO 3d _{5/2} ^A	336.34	16.53	2.09	PdO 3d _{5/2} ^A
		340.49	19.92	1.27	Pd(0) 3d _{3/2}	340.53	32.81	1.44	Pd(0) 3d _{3/2}
		341.40	22.53	2.79	PdO 3d _{3/2}	342.01	7.42	1.42	PdO 3d _{3/2}
	Ni	855.25	5.60	1.18	<i>Not identified</i>	-	-	-	
		856.64	49.43	1.77	[Ni(NO ₃) ₂]•6H ₂ O ^A	-	-	-	
		857.87	9.36	0.86	<i>Not identify</i>	-	-	-	
		859.00	11.89	1.27	<i>Not identify</i>	-	-	-	
		860.26	3.20	0.55	<i>Not identify</i>	-	-	-	
		861.01	4.41	0.65	<i>Not identify</i>	-	-	-	
2	Pd	335.12	32.86	1.53	Pd(0) 3d _{5/2} ^A	335.12	45.56	1.43	Pd(0) 3d _{5/2} ^A
		336.86	28.11	1.53	PdO 3d _{5/2} ^A	336.58	13.47	2.18	PdO 3d _{5/2} ^A
		340.39	21.34	1.53	Pd(0) 3d _{3/2}	340.42	28.14	1.37	Pd(0) 3d _{3/2}
		342.15	17.69	1.53	PdO 3d _{3/2}	341.73	12.83	2.34	PdO 3d _{3/2}
	Ni	854.51	8.21	1.80	<i>Not identify</i>	856.53	50.86	1.88	[Ni(NO ₃) ₂]•6H ₂ O ^A
		856.26	44.24	1.77	[Ni(NO ₃) ₂]•6H ₂ O ^A	861.84	11.63	1.31	<i>Not identify</i>
		857.49	25.13	1.73	<i>Not identify</i>	858.13	26.97	2.50	<i>Not identify</i>
		859.50	6.38	1.16	<i>Not identify</i>	863.37	10.53	1.55	<i>Not identify</i>
		861.29	4.24	0.85	<i>Not identify</i>	-	-	-	<i>Not identify</i>
		862.77	11.80	1.56	<i>Not identify</i>	-	-	-	<i>Not identify</i>
3	Pd	335.15	29.30	1.18	Pd(0) 3d _{5/2} ^A	-	-	-	
		336.22	27.35	2.30	PdO 3d _{5/2} ^A	-	-	-	
		340.42	15.58	1.1831	Pd(0) 3d _{3/2}	-	-	-	
		341.24	27.77	2.85	PdO 3d _{3/2}	-	-	-	
	Ni	-	-	-		-	-	-	
		-	-	-		-	-	-	
		-	-	-		-	-	-	
		-	-	-		-	-	-	

A. Φ Handbook of X-Ray photoelectron Spectroscopy

Appendix D

Sensitivity and Response Time Calculations and Additional Sensing Results

The sensitivity of a material with which detect some species related the signal before and after the exposition of the species of interest. As mention in Chapter 1 the sensitivity is calculated using the equation 1.1

$$S = \frac{|I_j - I_o|}{I_o}$$

where I_j represents the plateau value of the current under H_2 exposure and I_o represents the current plateau value under N_2 exposure. The response time (t_r) is defined as the time required to reaches 90% of the maximum change in the electrical resistance for a given H_2 concentration. The response time is calculated subtracting the time when this 90% of the maximum change is reached to the time when the H_2 valve is open (Equation D.1). The time at the 90% is determined by the equation shown below and correspond to the time where $AP = 90\%$ (Equation D.2).

$$t_r = t_{90} = t_{(AP=90\%)} - t_{(H_2 \text{ is on})} \quad \text{Equation D.1}$$

$$AP = \frac{|I_o - I_i|}{|I_o - I_j|} * 100$$

Equation D.2

Figure D.1 show the previously mentioned.

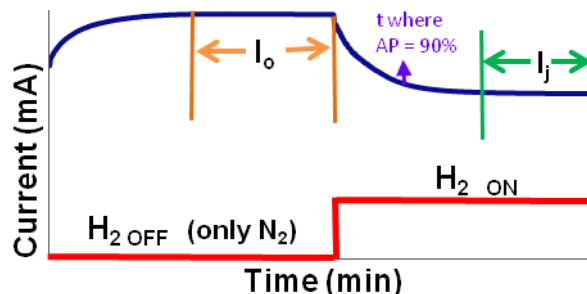


Figure D. 1 Sensitivity and Response Time Determination

Additional Hydrogen Sensing Results

The sensitivity and response time for all studied hydrogen concentrations detected by our synthesized films are tabulated in this section. This data was presented in the Chapter 4 in plots of Sensitivity (S) vs. Hydrogen Concentration, Response Time (t_r) vs. Hydrogen Concentration, and S/t_r vs. Hydrogen Concentration. In addition, the plots corresponding to the second Pd₉₀/Ag₁₀ bimetallic film results, mentioned in Chapter 4, are presented in this section.

D.1 Pure Palladium

Table D. 1 Sensitivity and Sensor Response Time using Pure Palladium Film (Figure 4.3)

Concentration	Cycle: [H ₂]	Sensitivity (%)	Resp time min ($t_{90\%}$)
1.00 %	1 : 1.00	-	-
1.00 %	2 : 1.00	4.81	3.84
	3 : 1.00	4.76	4.06
0.50 %	4 : 0.50	3.07	3.72
	5 : 0.50	3.14	3.94
0.25%	6 : 0.25	2.00	3.86
0.10%	7 : 0.10	1.14	4.08
1.00%	8 : 1.00	4.90	4.08
1.50 %	9 : 2.00	-	-
1.00 %	10 : 1.50	4.17	4.14

D.2 Pd₉₀/Pt₁₀ membrane

Table D.2 shows the results of sensitivity and response time calculated for the run presented in Figure 4.8. These results were used to graph Figures 4.10-4.13 in which the relation of [H₂] with S and t_r was presented. This Pd₉₀/Pt₁₀ film was used three consecutive times to study its reusability. The sensing response for the run # 2 and run # 3 were discussed in Chapter 4 (Figures 4.14 – 4.16) but the complete runs were not presented. Therefore, the runs #2 and #3 are presented in Figures D.2 and D.3 although the data are tabulated in Tables D.3 and D.4. Figures

D.2 and D.3 (compared with Figure 4.8) show a significant change in the hydrogen detection in which the film detects lower concentrations when was reused.

Table D. 2 Sensitivity and Sensor Response Time of the run presented in Figure 4.8 using Pd₉₀/Pt₁₀ Film (first run)

Concentration	Cycle : [H ₂]	Sensitivity (%)	Resp Time min (<i>t</i> 90 %)
1.00%	1 : 1.00	-	-
1.00%	2 : 1.00	3.20	3.92
	3 : 1.00	3.15	4.30
0.50%	4 : 0.50	1.95	4.39
	5 : 0.50	1.96	4.22
0.25%	6 : 0.25	1.31	4.17
0.10%	7 : 0.15	0.74	4.62
1.00%	8 : 1.00	3.09	4.23
	9 : 1.00	3.06	4.43
1.50%	10: 1.50	4.33	5.30
	11 : 1.50	4.21	5.02
2.00%	12 : 2.00	6.10	6.92
	13 : 2.00	5.82	5.74
3.00%	14 : 3.00	10.79	5.88
	15 : 3.00	9.26	4.20
4.00%	16 : 4.00	9.84	3.47
	17 : 4.00	8.98	2.98
5.00%	18 : 5.00	8.76	2.34
	19 : 5.00	8.08	2.24
6.00%	20 : 6.00	7.70	1.82
	21 : 6.00	7.13	1.72
10.00%	22 : 10.00	6.85	1.00

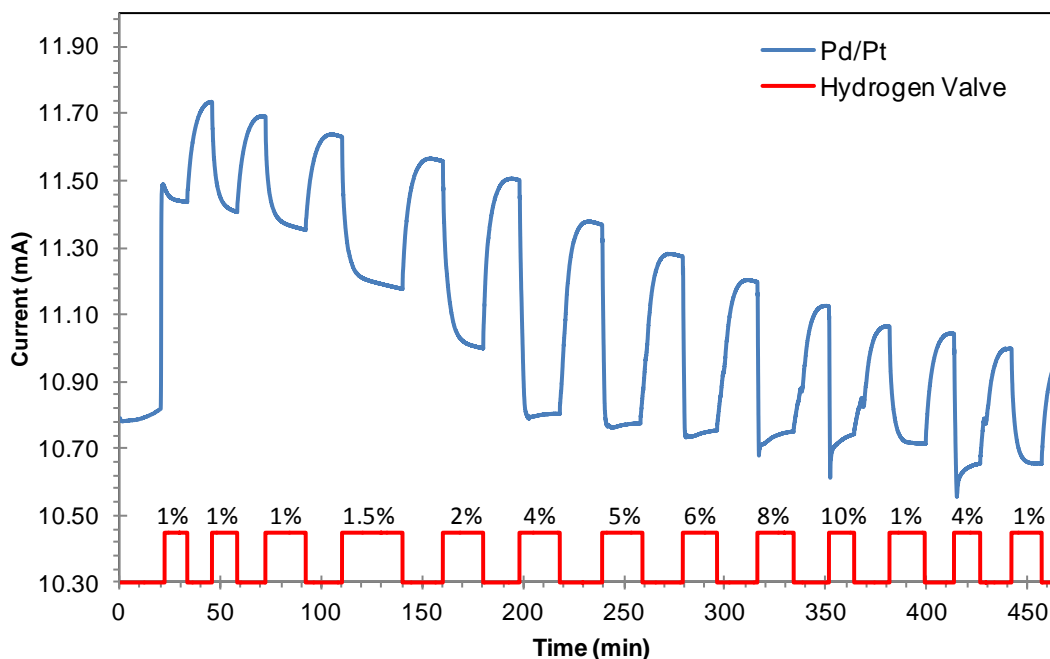


Figure D. 2 Sensing Response to Hydrogen detection using the second Pd₉₀/Pt₁₀ film synthesized by SSR Method (second run). The first run was presented in Figure 4.10.

Table D. 3 Sensitivity and Sensor Response Time of the run presented in Figure D.2 using Pd₉₀/Pt₁₀ Film (second film – second run)

Concentration	Cycle : [H₂]	Sensitivity (%)	Resp Time min (t 90 %)
1.00%	1 : 1.00	-	-
1.00%	2 : 1.00	2.77	4.9129
	3 : 1.00	2.86	5.9841
1.50%	4 : 1.50	3.85	6.2371
2.00%	5 : 2.00	4.83	1.8774
4.00%	6 : 4.00	6.10	2.2429
5.00%	7 : 5.00	5.29	1.2739
6.00%	8 : 6.00	4.67	0.8417
8.00%	9 : 8.00	4.05	0.5334
10.00%	10: 10.00	-	-
1.00%	11 : 1.00	3.15	4.2484
4.00%	12 : 4.00	-	-
1.00%	13 : 1.00	3.11	4.0873

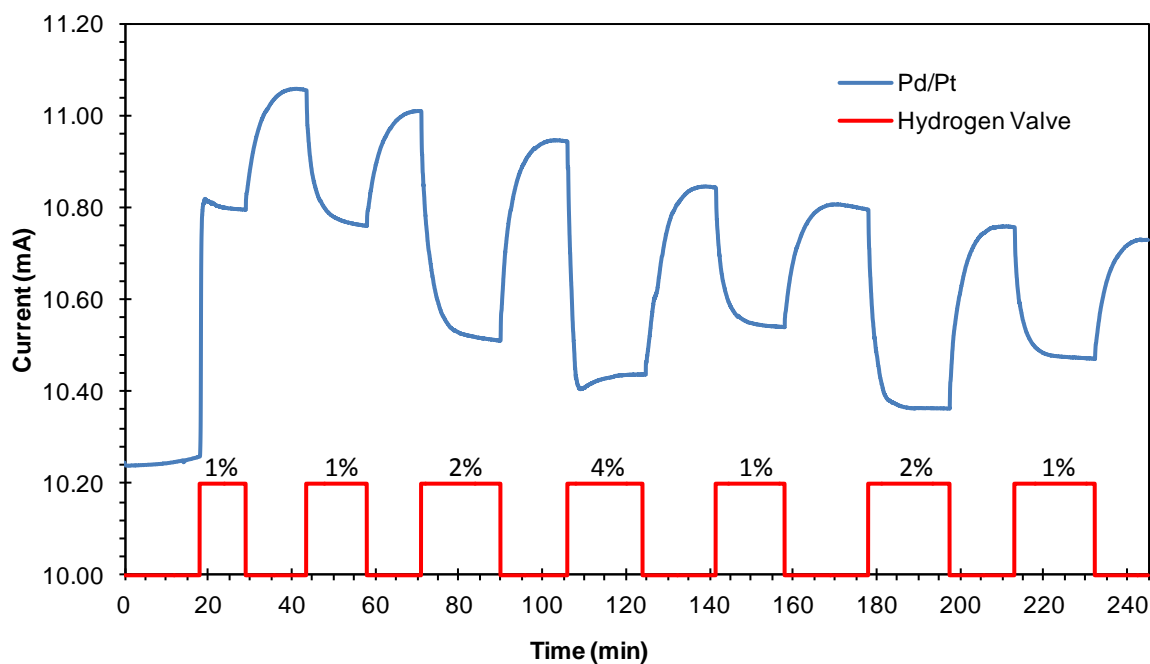


Figure D. 3 Sensing Response to Hydrogen detection using the second Pd₉₀/Pt₁₀ film synthesized by SSR Method (third run). The first run was presented in Figure 4.10 and the second run in Figure D.2.

Table D. 4 Sensitivity and Sensor Response Time of the run presented in Figure D.3 using Pd₉₀/Pt₁₀ Film (second film – third run)

Concentration	Cycle : [H ₂]	Sensitivity (%)	Resp Time min (<i>t</i> 90 %)
1.00%	1 : 1.00	-	-
1.00%	2 : 1.00	2.64	4.8385
2.00%	3 : 2.00	4.48	5.2693
4.00%	4 : 4.00	4.65	1.6600
1.00%	5 : 1.00	2.77	4.3624
2.00%	6 : 2.00	4.06	3.4983
1.00%	7 : 1.00	2.64	4.5308

D.3 Pd₉₀/Ag₁₀ membrane

Table D.5 shows the results of sensitivity and response time calculated for the run presented in Figure 4.17. These results were used to graph Figures 4.19 – 4.22 in which the relation of [H₂] with S and t_r was presented. A second Pd₉₀/Ag₁₀ material synthesized by SSR was used two consecutive times to study its reusability. The sensitivity and response time of the second Pd₉₀/Ag₁₀ material were generally discussed in Chapter 4 but the Figures were not presented. Therefore, these results are shown in Figures D.4-D.11 and reported in Tables D.6 and D.7. As mentioned in Chapter 4 the reutilization also shifts the instability in the sensing response to lower hydrogen concentration.

Table D. 5 Sensitivity and Sensor Response Time of the run presented in Figure 4.17 using Pd₉₀/Ag₁₀ Membrane (first membrane)

Concentration	Cycle : [H ₂]	Sensitivity (%)	Resp Time min (<i>t</i> 90 %)
1.00%	1 : 1.00	-	-
1.00%	2 : 1.00	3.88	3.51
	3 : 1.00	3.98	3.86
0.50%	4 : 0.50	2.18	2.43
	5 : 0.50	2.47	3.53
0.25%	6 : 0.25	1.45	3.44
0.10%	7 : 0.15	0.83	4.03
1.00%	8 : 1.00	4.29	4.24
1.50%	9 : 1.00	6.64	5.77
	10 : 1.50	6.53	5.52
2.00%	11 : 1.50	9.34	5.96
	12 : 2.00	8.85	4.92
3.00%	13 : 2.00	10.44	3.00
	14 : 3.00	9.81	2.57
4.00%	15 : 3.00	9.29	1.67
	16 : 4.00	8.92	1.64
5.00%	17 : 4.00	8.57	1.29

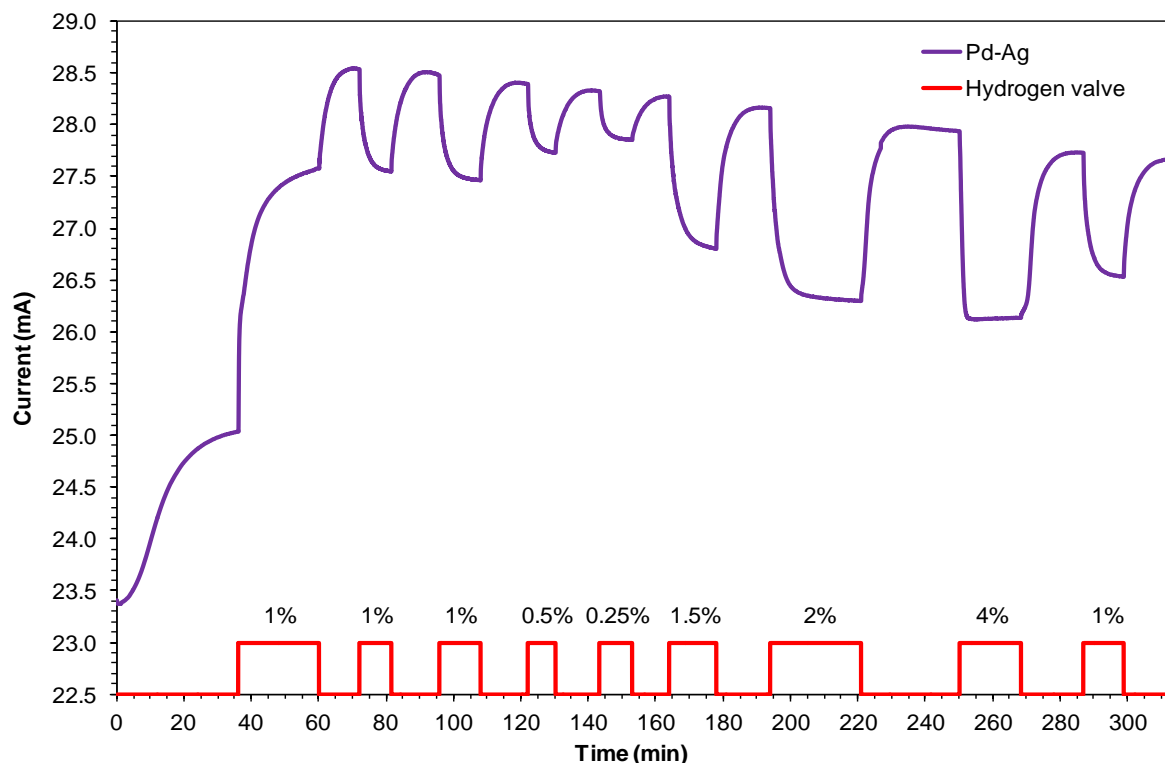


Figure D. 4 Sensing Response to Hydrogen detection using the second Pd₉₀/Ag₁₀ membrane synthesized by SSR Method (first run)

Table D. 6 Sensitivity and Sensor Response Time of the run presented in Figure D.4 using Pd₉₀/Ag₁₀ Membrane (second membrane - first run)

Concentration	Cycle : [H ₂]	Sensitivity (%)	Resp Time min (<i>t</i> 90 %)
1.00%	1 : 1.00%	-	-
1.00%	2 : 1.00%	3.44	3.46
	3 : 1.00%	3.61	3.84
0.50%	4 : 0.50%	2.35	3.22
0.25%	5 : 0.25%	1.66	3.36
1.5%	6 : 1.25%	5.15	5.42
2.00%	7 : 2.00%	6.59	5.18
4.00%	8 : 4.00%	6.55	1.43
1.00%	9 : 1.00%	4.29	3.99

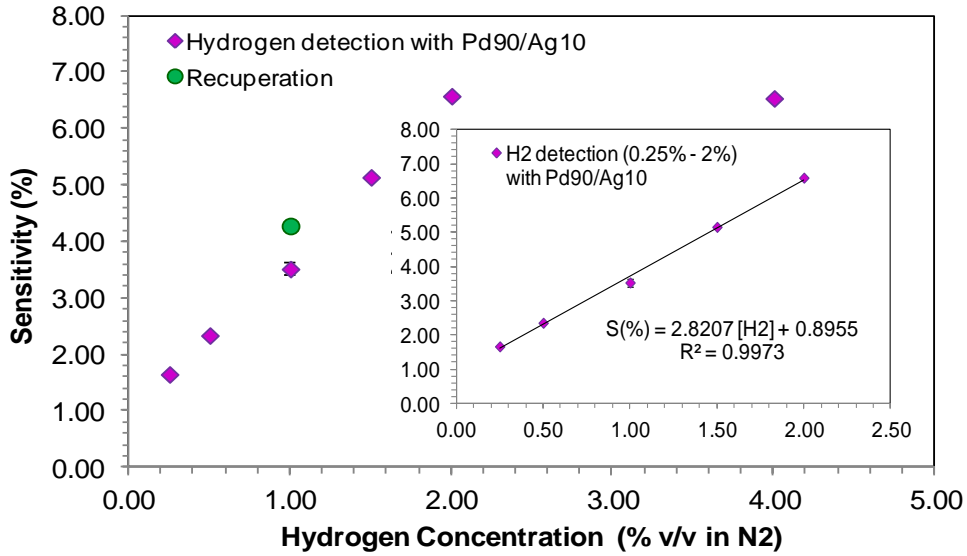


Figure D. 5 Sensitivity (%) vs. hydrogen concentration detected by Pd₉₀/Ag₁₀ bimetallic film. Run presented in Figure D.4.

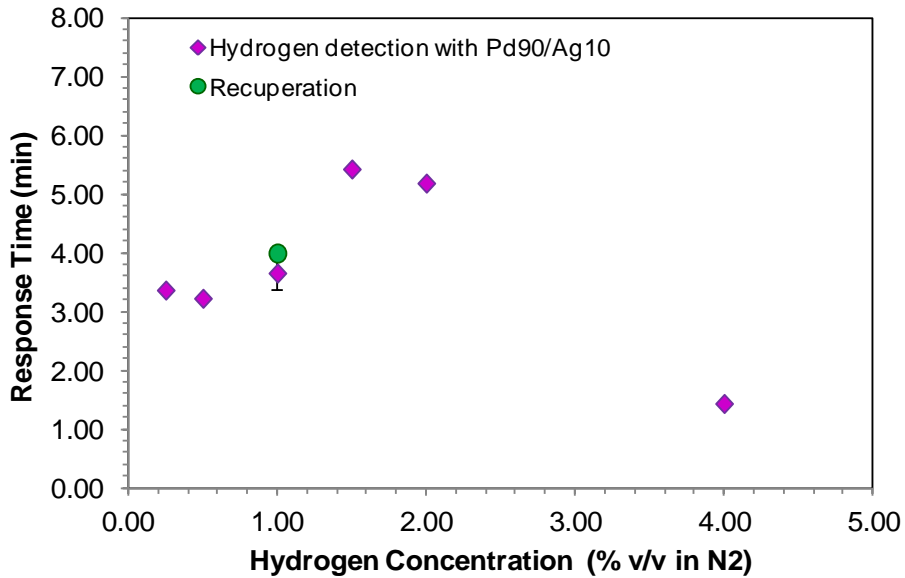


Figure D. 6 Response time (t_r) vs. hydrogen concentration detected by Pd₉₀/Ag₁₀ bimetallic film. Run presented in Figure D.4.

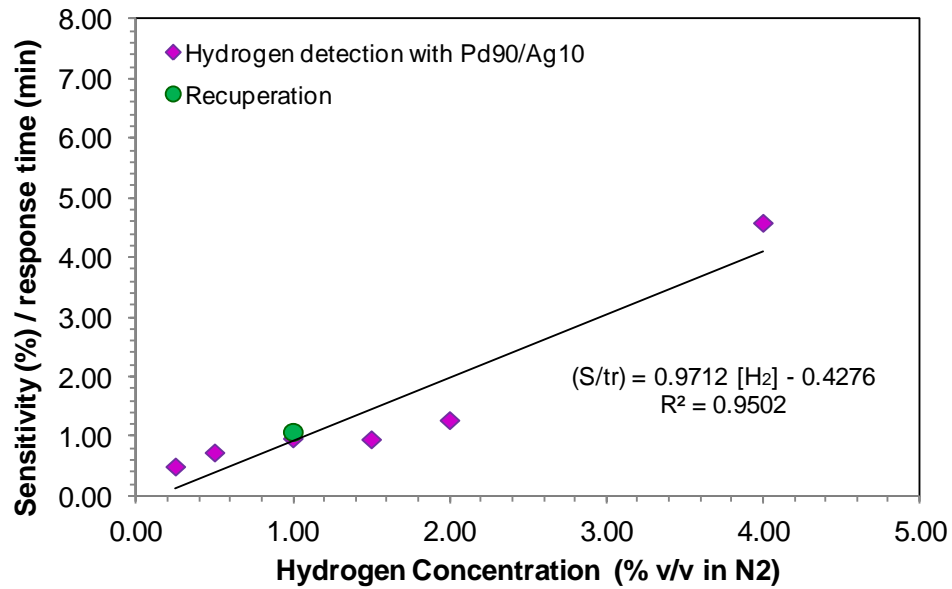


Figure D. 7 Sensitivity/Response time (S/t_r) vs. hydrogen concentration detected by Pd₉₀/Ag₁₀ bimetallic film. Run presented in Figure D.4.

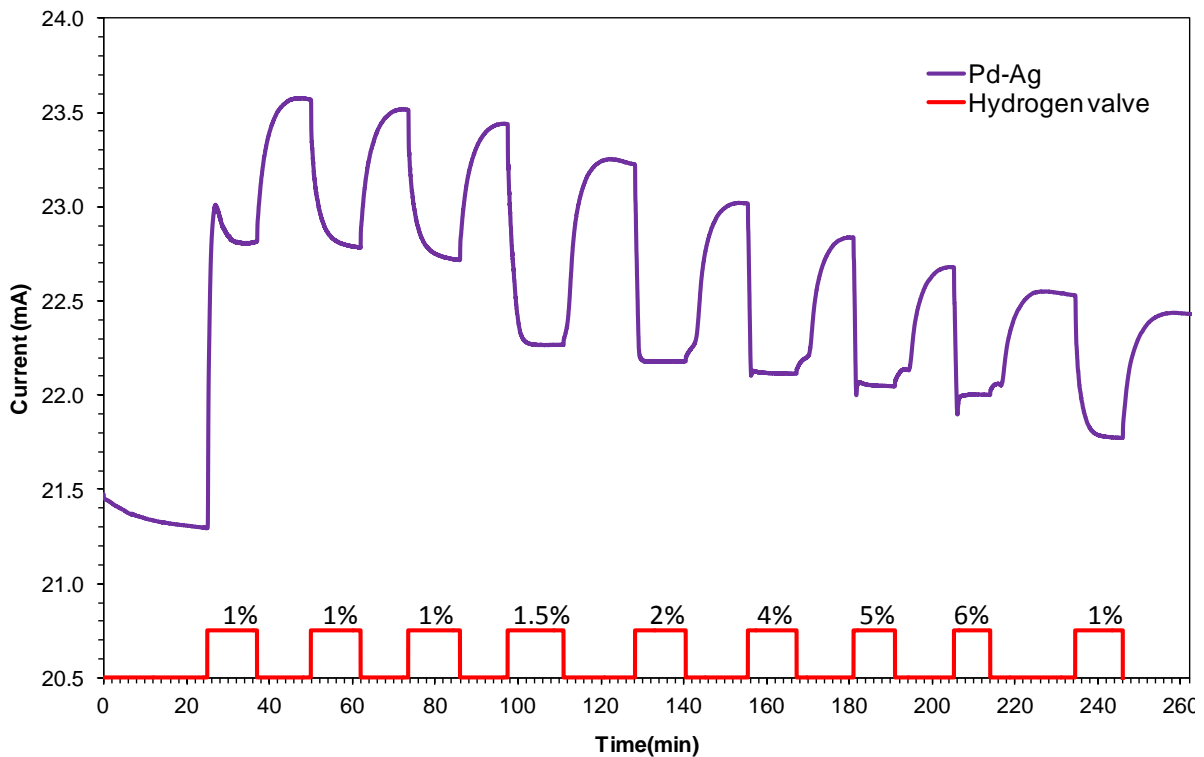


Figure D. 8 Sensing Response to Hydrogen detection using the second Pd₉₀/Ag₁₀ membrane synthesized by SSR Method (second run)

Table D. 7 Sensitivity and Sensor Response Time of the run presented in Figure D.8 using Pd₉₀/Ag₁₀ Membrane (second membrane - second run)

Concentration	Cycle : [H ₂]	Sensitivity (%)	Resp Time min (t 90 %)
1.00%	1 : 1.00%	-	-
1.00%	2 : 1.00%	3.33	3.03
	3 : 1.00%	3.34	3.96
1.50%	4 : 1.50%	4.99	2.60
2.00%	5 : 2.00%	4.58	0.88
4.00%	6 : 4.00%	3.93	0.61
5.00%	7 : 5.00%	-	-
6.00%	8 : 6.00%	-	-
1.00%	9 : 1.00%	3.41	2.91

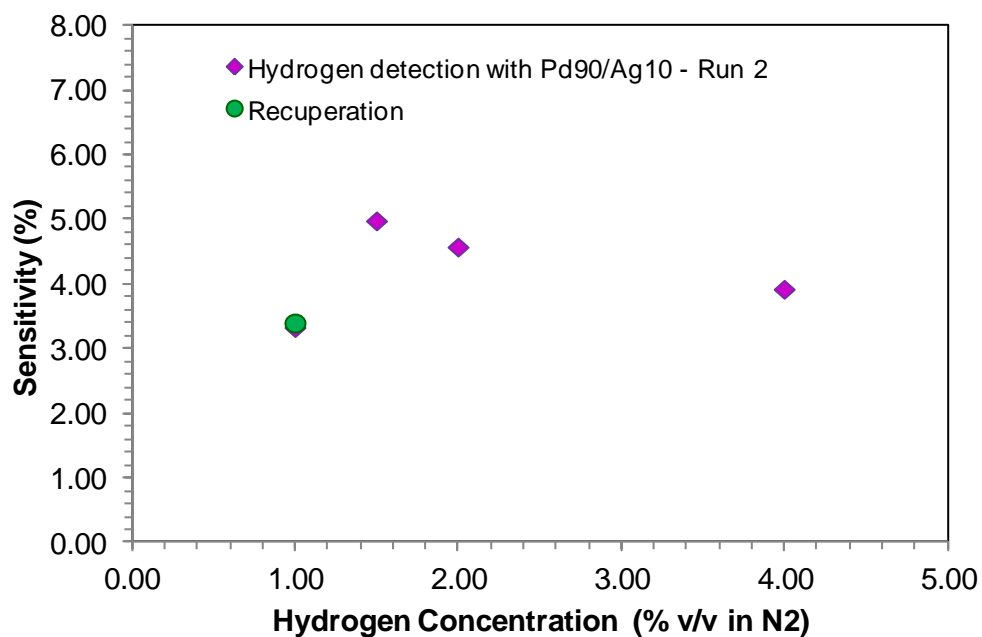


Figure D. 9 Sensitivity (%) vs. hydrogen concentration detected by the reused Pd₉₀/Ag₁₀ bimetallic film. Run presented in Figure D.8.

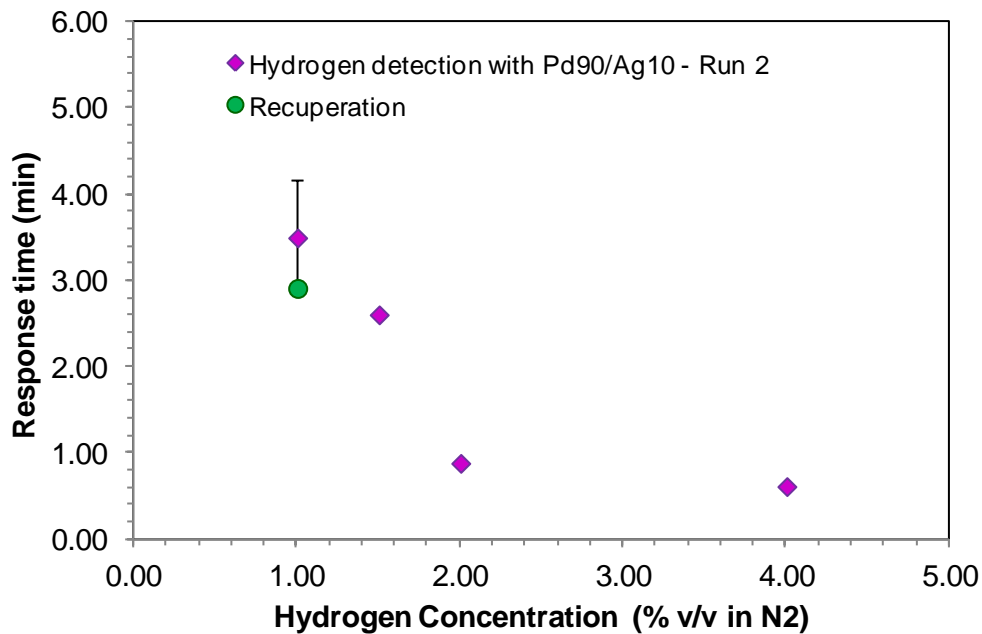


Figure D. 10 Response Time (min) vs. hydrogen concentration detected by the reused Pd₉₀/Ag₁₀ bimetallic film. Run presented in Figure D.8.

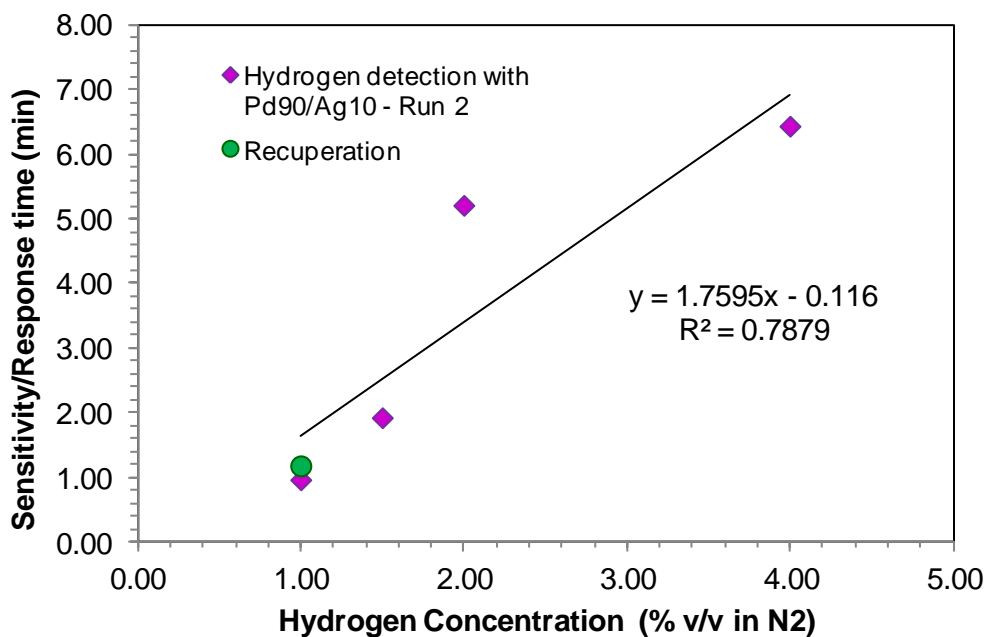


Figure D. 11 Sensitivity/Response Time (S/t_r) vs. hydrogen concentration detected by the reused Pd₉₀/Ag₁₀ bimetallic film. Run presented in Figure D.8.

D.3 Pd₉₀/Ni₁₀ membrane

Table D.8 shows the results of sensitivity and response time calculated for the run presented in Figure 4.23.

Table D. 8 Sensitivity and Sensor Response Time of the run presented in Figure 4.23 using Pd₉₀/Ni₁₀ Membrane

Concentration	Cycle : [H ₂]	Sensitivity (%)	Resp Time min (<i>t</i> 90 %)
1.00%	1 : 1.00%	-	-
1.00%	2 : 1.00%	5.17	2.7020
	3 : 1.00%	5.35	1.0760
0.50%	4 : 0.50%	2.91	2.4770
0.25%	5 : 0.25%	1.82	2.1030
0.10%	6 : 0.10%	1.11	3.3400
2.00%	7 : 2.00%	9.48	3.2060
1.50%	8 : 1.50%	7.76	2.7560
4.00%	-	-	-
2.00%	-	-	-

REFERENCES

- (1) Taşaltın, N.; Öztürk, S.; Kılınc, N.; Öztürk, Z. Z. Investigation of the Hydrogen Gas Sensing Properties of Nanoporous Pd Alloy Films Based on AAO Templates. *J. Alloys Compd.* **2011**, *509*, 4701–4706.
- (2) Hunter, G. W.; Neudeck, P. G.; Chen, L. Y. A Hazardous Gas Detection System for Aerospace and Commercial Applications. *Natl. Aeronaut. Sp. Adm.* **1998**.
- (3) Lu, Y.; Jin, R.; Chen, W. Highly Efficient Hydrogen Storage with PdAg Nanotubes. *Nanoscale* **2011**, *3*, 2476–2480.
- (4) Hyeonsik, C.; Jae, Y. S.; Jae, D. L.; Jung, M. J.; So-Hee, L. Comparison of Pd, Pt and Pt/Pd as Catalysts for Hydrogen Sensor Films. *J. Korean Phys. Soc.* **2009**, *55*, 2693.
- (5) Zeng, X.-Q.; Wang, Y.-L.; Deng, H.; Latimer, M. L.; Xiao, Z.-L.; Pearson, J.; Xu, T.; Wang, H.-H.; Welp, U.; Crabtree, G. W.; *et al.* Networks of Ultrasmall Pd/Cr Nanowires as High Performance Hydrogen Sensors. *ACS Nano* **2011**, *5*, 7443–7452.
- (6) Weng, Y.-C.; Hsieh, C.-T. Scanning Electrochemical Microscopy Characterization of Bimetallic Pt–M (M=Pd, Ru, Ir) Catalysts for Hydrogen Oxidation. *Electrochim. Acta* **2011**, *56*, 1932–1940.
- (7) Zhao, Z.; Carpenter, M. a.; Xia, H.; Welch, D. All-Optical Hydrogen Sensor Based on a High Alloy Content Palladium Thin Film. *Sensors Actuators B Chem.* **2006**, *113*, 532–538.
- (8) Peters, T. A.; Kaleta, T.; Stange, M.; Bredesen, R. Development of Thin Binary and Ternary Pd-Based Alloy Membranes for Use in Hydrogen Production. *J. Memb. Sci.* **2011**, *383*, 124–134.
- (9) Hunter, G. W.; Neudeck, P. G.; Liu, C. C.; Wu, Q. H. Advances in Hydrogen Sensor Technology for Aerospace Applications. *Natl. Aeronaut. Sp. Adm.* **1994**.
- (10) Hunter, G. W. Patent Number 5,520,753. 5,520,753, 1996.
- (11) Timeline of all Hydrogen Vehicles Worldwide www.netinform.net (accessed Jan 14, 2014).
- (12) Tollefson, J. Hydrogen Vehicles: Fuel of the Future? *Nature News*, 2010, *464*, 1262–1264.
- (13) Hydrogen and fuel cells <http://energy.gov/eere/transportation/hydrogen-and-fuel-cells> (accessed Jan 15, 2014).

- (14) Transportation Fuel Basics - Hydrogen <http://energy.gov/eere/energybasics/articles/transportation-fuel-basics-hydrogen> (accessed Jan 15, 2014).
- (15) Fuel Cell Vehicle - Toyota http://www.toyota-global.com/innovation/environmental_technology/fuelcell_vehicle/ (accessed Jan 15, 2014).
- (16) Fuel Cell Electric Vehicles - Nissan http://www.nissan-global.com/EN/ENVIRONMENT/CAR/FUEL_BATTERY/DEVELOPMENT/FCV/ (accessed Jan 15, 2014).
- (17) Hydrogen Fueling Station Locations http://www.afdc.energy.gov/fuels/hydrogen_locations.html (accessed Jan 15, 2014).
- (18) Hydrogen Uses <http://www.usesof.net/uses-of-hydrogen.html>.
- (19) Hydrogen Uses <http://www.uigi.com/hydrogen.html> (accessed May 19, 2004).
- (20) Morreale, B. D.; Ciocco, M. V.; Enick, R. M.; Morsi, B. I.; Howard, B. H.; Cugini, A. V.; Rothenberger, K. S. The Permeability of Hydrogen in Bulk Palladium at Elevated Temperatures and Pressures. *J. Memb. Sci.* **2003**, *212*, 87–97.
- (21) Duan, S.; Wang, R. Bimetallic Nanostructures with Magnetic and Noble Metals and Their Physicochemical Applications. *Prog. Nat. Sci. Mater. Int.* **2013**, *23*, 113–126.
- (22) Sun, Y.; Tao, Z.; Chen, J.; Herricks, T.; Xia, Y. Ag Nanowires Coated with Ag/Pd Alloy Sheaths and Their Use as Substrates for Reversible Absorption and Desorption of Hydrogen. *J. Am. Chem. Soc.* **2004**, *126*, 5940–5941.
- (23) Hughes, R. C.; Schubert, W. K. Thin Films of Pd/Ni Alloys for Detection of High Hydrogen Concentrations. *J. Appl. Phys.* **1992**, *71*, 542.
- (24) Kajita, S.; Yamaura, S.; Kimura, H.; Inoue, A. Hydrogen Sensing Ability of Pd-Based Amorphous Alloys. *Sensors Actuators B Chem.* **2010**, *150*, 279–284.
- (25) Burkhanov, G. S.; Gorina, N. B.; Kolchugina, N. B.; Roshan, N. R.; Slovetsky, D. I.; Chistov, E. M. Palladium-Based Alloy Membranes for Separation of High Purity Hydrogen from Hydrogen-Containing Gas Mixtures. *Platin. Met. Rev.* **2011**, *55*, 3–12.
- (26) David, E.; Kopac, J. Development of Palladium/ceramic Membranes for Hydrogen Separation. *Int. J. Hydrogen Energy* **2011**, *36*, 4498–4506.
- (27) Crouch-Baker, S.; McKubre, M. C. H.; Tazella, F. L. Variation of Resistance with Composition in the B-Phase of H-Pd System at 298 K. **1998**, *204*, 247–254.
- (28) Boon-Brett, L.; Bousek, J.; Black, G.; Moretto, P.; Castello, P.; Hübert, T.; Banach, U. Identifying Performance Gaps in Hydrogen Safety Sensor Technology for Automotive and Stationary Applications. *Int. J. Hydrogen Energy* **2010**, *35*, 373–384.

- (29) *Hydrogen Fuel: Production, Transport, and Storage*; Gupta, R. B., Ed.; CRC Press: Boca Raton, 2009; p. 611.
- (30) Ramanathan, M.; Skudlarek, G.; Wang, H. H.; Darling, S. B. Crossover Behavior in the Hydrogen Sensing Mechanism for Palladium Ultrathin Films. *Nanotechnology* **2010**, *21*, 125501.
- (31) Hunter, G. W.; Xu, J. C.; Evans, L.; Biaggi-Labiosa, A.; Ward, B. J.; Rowe, S.; Makel, D. B.; Liu, C. C.; Dutta, P.; Berger, G. M.; *et al.* The Development of Micro/Nano Chemical Sensor Systems for Aerospace Applications. **2010**.
- (32) Kumar, R.; Varandani, D.; Mehta, B. R.; Singh, V. N.; Wen, Z.; Feng, X.; Müllen, K. Fast Response and Recovery of Hydrogensensing in Pd–Pt Nanoparticle–graphene Composite Layers. *Nanotechnology* **2011**, *22*, 275719.
- (33) Bangar, M. A.; Ramanathan, K.; Yun, M.; Lee, C.; Hangarter, C.; Myung, N. V. Controlled Growth of a Single Palladium Nanowire between Microfabricated Electrodes. *Chem. Mater.* **2004**, 4955–4959.
- (34) Khanuja, M.; Mehta, B. R.; Agar, P.; Kulriya, P. K.; Avasthi, D. K. Hydrogen Induced Lattice Expansion and Crystallinity Degradation in Palladium Nanoparticles: Effect of Hydrogen Concentration, Pressure, and Temperature. *J. Appl. Phys.* **2009**, *106*, 093515.
- (35) Lee, E.; Lee, J. M.; Koo, J. H.; Lee, W.; Lee, T. Hysteresis Behavior of Electrical Resistance in Pd Thin Films during the Process of Absorption and Desorption of Hydrogen Gas. *Int. J. Hydrogen Energy* **2010**, *35*, 6984–6991.
- (36) Chen, S.; Adams, B. D.; Chen, A. Synthesis and Electrochemical Study of Nanoporous Pd–Ag Alloys for Hydrogen Sorption. *Electrochim. Acta* **2010**, *56*, 61–67.
- (37) Zhao, Z.; Sevryugina, Y.; Carpenter, M. a; Welch, D.; Xia, H. All-Optical Hydrogen-Sensing Materials Based on Tailored Palladium Alloy Thin Films. *Anal. Chem.* **2004**, *76*, 6321–6326.
- (38) Lewis, F. A. Solubility of Hydrogen in Metals. *Pure Appl. Chem.* **1990**, *62*, 2091–2096.
- (39) Brittle Fracture Surface http://www.hsctut.materials.unsw.edu.au/Crack_Theory/crack_theory3a.htm (accessed May 18, 2014).
- (40) Zeng, X. Q.; Latimer, M. L.; Xiao, Z. L.; Panuganti, S.; Welp, U.; Kwok, W. K.; Xu, T. Hydrogen Gas Sensing with Networks of Ultrasmall Palladium Nanowires Formed on Filtration Membranes. *Nano Lett.* **2011**, *11*, 262–268.
- (41) Ma, Y. H.; Engwall, E. E.; Mardilovich, I. P. Composite Palladium and Palladium-Alloy Membranes for High Temperature Hydrogen Separations. **2003**, *48*, 333–334.

- (42) Hughes, R. C.; Schubert, W. K.; Zipperian, T. E.; Rodriguez, J. L.; Plut, T. A. Thin-Film Palladium and Silver Alloys and Layers for Metal-Insulator-Semiconductor Sensors. *J. Appl. Phys.* **1987**, *62*, 1074.
- (43) Smith, B.; Loganathan, M.; Shekhar, M. A Review of the Water Gas Shift Reaction Kinetics. *Int. J. Chem. React. Eng.* **2010**, *8*, 1–32.
- (44) Sánchez Hervás, J. M.; Maroño, M.; Cabanillas, A. *Clean Hydrogen-Rich Synthesis Gas*; 2005.
- (45) Koenigsmann, C.; Tan, Z.; Peng, H.; Sutter, E.; Jacobskind, J.; Wong, S. S. Multifunctional Nanochemistry: Ambient, Electroless, Template-Based Synthesis and Characterization of Segmented Bimetallic Pd/Au and Pd/Pt Nanowires as High-Performance Electrocatalysts and Nanomotors. *Isr. J. Chem.* **2012**, *52*, 1090–1103.
- (46) Cheng, Y.-T.; Li, Y.; Lisi, D.; Wang, W. M. Preparation and Characterization of Pd/Ni Thin Films for Hydrogen Sensing. *Sensors Actuators B Chem.* **1996**, *30*, 11–16.
- (47) Guo, S.; Zhang, S.; Sun, X.; Sun, S. Synthesis of Ultrathin FePtPd Nanowires and Their Use as Catalysts. **2011**, 15354–15357.
- (48) Zhou, Y.; Yu, G.; Chang, F.; Hu, B.; Zhong, C.-J. Gold-Platinum Alloy Nanowires as Highly Sensitive Materials for Electrochemical Detection of Hydrogen Peroxide. *Anal. Chim. Acta* **2012**, *757*, 56–62.
- (49) Ferrando, R.; Jellinek, J.; Johnston, R. L. Nanoalloys: From Theory to Applications of Alloy Clusters and Nanoparticles. *Chem. Rev.* **2008**, *108*, 845–910.
- (50) Chen, C.-K.; Chang, S.-C. An Investigation of the Internal Temperature Dependence of Pd–Pt Cluster Beam Deposition: A Molecular Dynamics Study. *Appl. Surf. Sci.* **2010**, *256*, 2890–2897.
- (51) Liu, Y.; Chi, M.; Mazumder, V.; More, K. L.; Soled, S.; Henao, J. D.; Sun, S. Composition-Controlled Synthesis of Bimetallic PdPt Nanoparticles and Their Electro-Oxidation of Methanol. *Chem. Mater.* **2011**, *23*, 4199–4203.
- (52) Zhang, B.; Guo, R.; Liu, X. Synthesis and Characterization of Nanostructured Bimetallic Films on A-Al₂O₃ Substrates Using Electroless Deposition. *Appl. Surf. Sci.* **2008**, *254*, 5394–5398.
- (53) RaviPrakash, J.; McDaniel, A. H.; Horn, M.; Piloni, L.; Sunal, P.; Messier, R.; McGrath, R. T.; Schweighardt, F. K. Hydrogen Sensors: Role of Palladium Thin Film Morphology. *Sensors Actuators B Chem.* **2007**, *120*, 439–446.
- (54) Rumiche, F.; Wang, H. H.; Hu, W. S.; Indacochea, J. E.; Wang, M. L. Anodized Aluminum Oxide (AAO) Nanowell Sensors for Hydrogen Detection. *Sensors Actuators B Chem.* **2008**, *134*, 869–877.

- (55) Jewell, L. L.; Davis, B. H. Review of Absorption and Adsorption in the Hydrogen-Palladium System. *Appl. Catal. A Gen.* **2006**, *310*, 1–15.
- (56) Tung, Y.-L.; Tseng, W.-C.; Lee, C.-Y.; Hsu, P.-F.; Chi, Y.; Peng, S.-M.; Lee, G.-H. Synthesis and Characterization of Allyl(β -ketoiminato)palladium(II) Complexes: New Precursors for Chemical Vapor Deposition of Palladium Thin Films. *Organometallics* **1999**, *18*, 864–869.
- (57) Elam, J. W.; Zinovev, A.; Han, C. Y.; Wang, H. H.; Welp, U.; Hryn, J. N.; Pellin, M. J. Atomic Layer Deposition of Palladium Films on Al₂O₃ Surfaces. *Thin Solid Films* **2006**, *515*, 1664–1673.
- (58) Hernández, S. C.; Yoo, B. Y.; Stefanescu, E.; Khizroev, S.; Myung, N. V. Electrodeposition of Iron–palladium Thin Films. *Electrochim. Acta* **2008**, *53*, 5621–5627.
- (59) Feliciano, J.; Martínez-Iñesta, M. M. Synthesis and Characterization of Pd, Cu, and Ag Nanowires in Anodic Alumina Membranes Using Solid State Reduction. *Mater. Lett.* **2012**, *82*, 211–213.
- (60) Quiñones, L.; Grazul, J.; Martínez-Iñesta, M. M. Synthesis of Platinum Nanostructures in Zeolite Mordenite Using a Solid-State Reduction Method. *Mater. Lett.* **2009**, *63*, 2684–2686.
- (61) Guo, S.; Wang, E. Functional Micro/nanostructures: Simple Synthesis and Application in Sensors, Fuel Cells, and Gene Delivery. *Acc. Chem. Res.* **2011**, *44*, 491–500.
- (62) Sharma, P. C.; Srinivasan, S. S.; Wilson, J. F. Nanomaterials Driven Energy, Environmental and Biomedical Research. *AIP Conf. Proc.* **2014**, *234*, 234–243.
- (63) Herrera, A. P.; Rodríguez, M.; Torres-Lugo, M.; Rinaldi, C. Multifunctional Magnetite Nanoparticles Coated with Fluorescent Thermo-Responsive Polymeric Shells. *J. Mater. Chem.* **2008**, *18*, 855–858.
- (64) Torres-Lugo, M.; Rinaldi, C. Thermal Potentiation of Chemotherapy by Magnetic Nanoparticles. *Nanomedicine (Lond)*. **2013**, *8*, 1689–1707.
- (65) Qian, H.; Pretzer, L. a.; Velazquez, J. C.; Zhao, Z.; Wong, M. S. Gold Nanoparticles for Cleaning Contaminated Water. *J. Chem. Technol. Biotechnol.* **2013**, *88*, 735–741.
- (66) Sreeprasad, T. S.; Maliyekkal, S. M.; Lisha, K. P.; Pradeep, T. Reduced Graphene Oxide-Metal/metal Oxide Composites: Facile Synthesis and Application in Water Purification. *J. Hazard. Mater.* **2011**, *186*, 921–931.
- (67) Fu, H.; Yang, X.; Jiang, X.; Yu, A. Bimetallic Ag-Au Nanowires: Synthesis, Growth Mechanism, and Catalytic Properties. *Langmuir* **2013**, *29*, 7134–7142.

- (68) Cheng, Y.; Yu, G.; Tang, L.; Zhou, Y.; Zhang, G. Self-Assembled Dendritic Nanowires of Au–Pt Alloy through Electrodeposition from Solution under AC Fields. *J. Cryst. Growth* **2011**, *334*, 181–188.
- (69) Rajan, A.; MeenaKumari, M.; Philip, D. Shape Tailored Green Synthesis and Catalytic Properties of Gold Nanocrystals. *Spectrochim. Acta. A. Mol. Biomol. Spectrosc.* **2014**, *118*, 793–799.
- (70) Zaheer Zoya, R. Silver Nanoparticles to Self-Assembled Films: Green Synthesis and Characterization. *Colloids Surf. B. Biointerfaces* **2012**, *90*, 48–52.
- (71) Guo, H.; Chen, Y.; Ping, H.; Jin, J.; Peng, D.-L. Facile Synthesis of Cu and Cu@Cu-Ni Nanocubes and Nanowires in Hydrophobic Solution in the Presence of Nickel and Chloride Ions. *Nanoscale* **2013**, *5*, 2394–2402.
- (72) Shi, X.; Wang, Y.; Wang, Z.; Sun, Y.; Liu, D.; Zhang, Y.; Li, Q.; Shi, J. High Performance Plasmonic Random Laser Based on Nanogaps in Bimetallic Porous Nanowires. *Appl. Phys. Lett.* **2013**, *103*, 023504.
- (73) Wang, M.; Feng, Y. Palladium–silver Thin Film for Hydrogen Sensing. *Sensors Actuators B Chem.* **2007**, *123*, 101–106.
- (74) Hoang, H. .; Tong, H. .; Gielens, F. .; Jansen, H. .; Elwenspoek, M. . Fabrication and Characterization of Dual Sputtered Pd–Cu Alloy Films for Hydrogen Separation Membranes. *Mater. Lett.* **2004**, *58*, 525–528.
- (75) Dittmeyer, R.; Höllein, V.; Daub, K. Membrane Reactors for Hydrogenation and Dehydrogenation Processes Based on Supported Palladium. *J. Mol. Catal. A Chem.* **2001**, *173*, 135–184.
- (76) Gimeno, M. P.; Wu, Z. T.; Soler, J.; Herguido, J.; Li, K.; Menéndez, M. Combination of a Two-Zone Fluidized Bed Reactor with a Pd Hollow Fibre Membrane for Catalytic Alkane Dehydrogenation. *Chem. Eng. J.* **2009**, *155*, 298–303.
- (77) Feng, D.; Wang, Y.; Wang, D.; Wang, J. Pd–Ag–Au–Ni Membrane Reactor for Methoxymethane Steam Reforming. *J. Chem. Eng. Data* **2009**, *54*, 2444–2451.
- (78) Tong, J.; Matsumura, Y.; Suda, H.; Haraya, K. Experimental Study of Steam Reforming of Methane in a Thin (6 μM) Pd-Based Membrane Reactor. *Ind. Eng. Chem. Res.* **2005**, *44*, 1454–1465.
- (79) Shi, L.; Goldbach, A.; Zeng, G.; Xu, H. Direct H₂O₂ Synthesis over Pd Membranes at Elevated Temperatures. *J. Memb. Sci.* **2010**, *348*, 160–166.
- (80) Dinh, D. a.; Hui, K. S.; Hui, K. N.; Cho, Y. R.; Zhou, W.; Hong, X.; Chun, H.-H. Green Synthesis of High Conductivity Silver Nanoparticle-Reduced Graphene Oxide Composite Films. *Appl. Surf. Sci.* **2014**, *298*, 62–67.

- (81) Glavee, G. N.; Klabunde, K. J.; Sorensen, C. M.; Hadjapanayis, G. C. Borohydride Reductions of Metal Ions. A New Understanding of the Chemistry Leading to Nanoscale Particles of Metals, Borides, and Metal Borates. *Langmuir* **1992**, *8*, 771–773.
- (82) Bentley, A. K.; Farhoud, M.; Ellis, A. B.; Nickel, A.-M. L.; Lisensky, G. C.; Crone, W. C. Template Synthesis and Magnetic Manipulation of Nickel Nanowires. *J. Chem. Educ.* **2005**, *82*, 765.
- (83) Solomon, S. D.; Bahadory, M.; Jeyarajasingam, A. V.; Rutkowsky, S. a.; Boritz, C. Synthesis and Study of Silver Nanoparticles. *J. Chem. Educ.* **2007**, *84*, 322.
- (84) Rashid, M. U.; Bhuiyan, K. H.; Quayum, M. E. Synthesis of Silver Nano Particles (Ag-NPs) and Their Uses for Quantitative Analysis of Vitamin C Tablets. *J. Pharm., Sci.* **2013**, *12*, 29–35.
- (85) Raj, J.; Viswanathan, B. Synthesis of Nickel Nanoparticles with Fcc and Hcp Crystal Structures. *Indian J. Chem.* **2011**, *50*, 176–179.
- (86) Sodium nitrate MSDS <http://www.sciencelab.com/msds.php?msdsId=9927271> (accessed May 7, 2014).
- (87) Sodium borate MSDS <http://www.sciencelab.com/msds.php?msdsId=9924969>.
- (88) Sodium borohydride MSDS <http://www.sciencelab.com/msds.php?msdsId=9924969> (accessed May 7, 2014).
- (89) Moulder, J. F.; Stickle, W. F.; Sobol, P. E.; Bomben, K. *Handbook of X-Ray Photoelectron Spectroscopy*; Chastain, J., Ed.; 2nd ed.; Perkin-Elmer Corporation, 1992.
- (90) NIST X-ray Photoelectron Spectroscopy Database <http://srdata.nist.gov/xps/Default.aspx> (accessed Apr 1, 2014).
- (91) XPS Spectra - CasaXPS Software Manual http://www.casaxps.com/help_manual/manual_updates/xps_spectra.pdf (accessed Mar 25, 2014).
- (92) A Beginners Guide To Casa XPS @ www.casaxps.com <http://www.casaxps.com/cam7/BeginnersGuide/ABeginnersGuideToCasaXPS.htm> (accessed Mar 25, 2014).
- (93) Chou, K.; Chang, S.; Huang, K. Study on The Characteristics of Nanosized Nickel Particles Using Sodium Borohydride to Promote Conversion Study on The Characteristics of Nanosized Nickel Particles Using Sodium Borohydride to Promote Conversion. *Azo J. Mater. Online* **2007**, *3*, 1–12.
- (94) He, Y.; Qiao, M.; Hu, H.; Pei, Y.; Li, H. Preparation of Amorphous Ni – B Alloy : The Effect of Feeding Order , Precursor Salt , pH and Adding Rate. **2002**, *56*, 952–957.

- (95) Khan, N. a.; Uhl, a.; Shaikhutdinov, S.; Freund, H.-J. Alumina Supported Model Pd–Ag Catalysts: A Combined STM, XPS, TPD and IRAS Study. *Surf. Sci.* **2006**, *600*, 1849–1853.
- (96) Harris, D. C. *Exploring Chemical Analysis*; 3rd ed.; Freeman, W. H. & Company: New York, 2005; pp. 549–552.
- (97) Corro, G.; Cano, C.; Peña, V.; Serkin, V.; Bañuelos, F.; Juárez, A.; Fierro, J. L. G. Un Estudio Por XPS Del Estado Electrónico de Las Nanopartículas de Pt Y Pd En Catalizadore Pt-Pd/ γ -Al₂O₃ Para La Oxidación de Metano. *Nanociencia et Moletrónica* **2010**, *8*, 1511–1530.
- (98) Dablemont, C.; Lang, P.; Mangeney, C.; Piquemal, J.-Y.; Petkov, V.; Herbst, F.; Viau, G. FTIR and XPS Study of Pt Nanoparticle Functionalization and Interaction with Alumina. *Langmuir* **2008**, *24*, 5832–5841.
- (99) Batista, J.; Pintar, A.; Mandrino, D.; Jenko, M.; Martin, V. XPS and TPR Examinations of γ -Alumina-Supported Pd-Cu Catalysts. *Appl. Catal. A Gen.* **2000**, *206*, 113–124.
- (100) Barbieri, P. .; de Siervo, a; Carazzolle, M. .; Landers, R.; Kleiman, G. . XPS and XAES Study of Ag–Pd and Cu–Ni Alloys: Spectra, Shifts and Electronic Structure Information. *J. Electron Spectros. Relat. Phenomena* **2004**, *135*, 113–118.
- (101) Biesinger, M. C.; Payne, B. P.; Grosvenor, A. P.; Lau, L. W. M.; Gerson, A. R.; Smart, R. S. C. Resolving Surface Chemical States in XPS Analysis of First Row Transition Metals, Oxides and Hydroxides: Cr, Mn, Fe, Co and Ni. *Appl. Surf. Sci.* **2011**, *257*, 2717–2730.
- (102) Zemlyanov, D. In Situ XPS Study of Pd (111) Oxidation . Part 1 : 2D Oxide Formation in 10 3 Mbar O₂. *Purdue Univ. - Purdue e-Pubs* **2006**.
- (103) Gabasch, H.; Unterberger, W.; Hayek, K.; Klötzer, B.; Kleimenov, E.; Teschner, D.; Zafeiratos, S.; Hävecker, M.; Knop-Gericke, A.; Schlögl, R.; *et al.* In Situ XPS Study of Pd(111) Oxidation at Elevated Pressure, Part 2: Palladium Oxidation in the 10–1mbar Range. *Surf. Sci.* **2006**, *600*, 2980–2989.
- (104) Kim, K. S.; Gossmann, a. F.; Winograd, N. X-Ray Photoelectron Spectroscopic Studies of Palladium Oxides and the Palladium-Oxygen Electrode. *Anal. Chem.* **1974**, *46*, 197–200.
- (105) Hara, S.; Ishitsuka, M.; Suda, H.; Mukaida, M.; Haraya, K. Pressure-Dependent Hydrogen Permeability Extended for Metal Membranes Not Obeying the Square-Root Law. *J. Phys. Chem. B* **2009**, *113*, 9795–9801.
- (106) Lee, Y. T.; Lee, J. M.; Kim, Y. J.; Joe, J. H.; Lee, W. Hydrogen Gas Sensing Properties of PdO Thin Films with Nano-Sized Cracks. *Nanotechnology* **2010**, *21*, 165503.